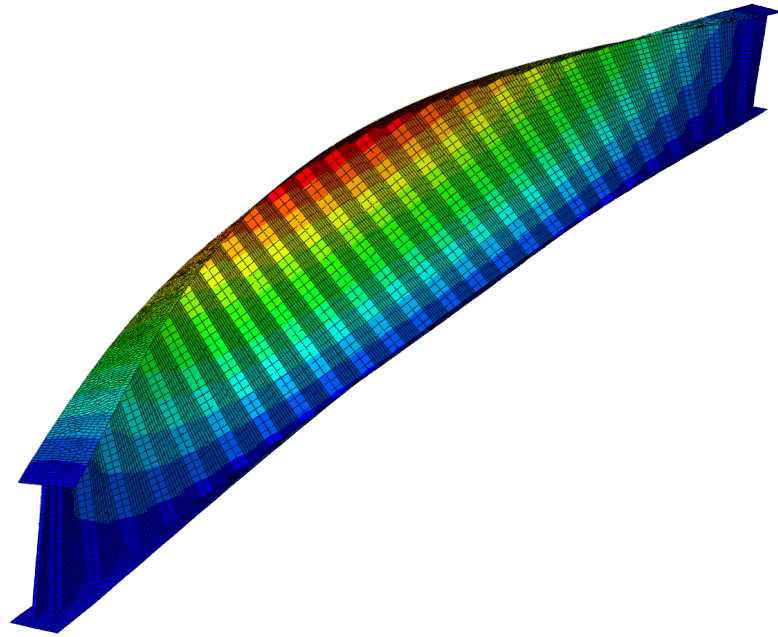


CHALMERS



Lateral-torsional buckling of steel girders with trapezoidally corrugated webs

Master of Science Thesis in the Master's Programme Structural Engineering and Building Technology

MATTIAS LARSSON
JOHN PERSSON

Department of Civil and Environmental Engineering
Division of Structural Engineering
Steel and Timber Structures
CHALMERS UNIVERSITY OF TECHNOLOGY
Göteborg, Sweden 2013
Master's thesis 2013:57

MASTER'S THESIS 2013:57

Lateral-torsional buckling of steel girders with trapezoidally
corrugated webs

*Master of Science Thesis in the Master's Programme Structural Engineering and Building
Technology*

MATTIAS LARSSON
JOHN PERSSON

Department of Civil and Environmental Engineering

Division of Structural Engineering

Steel and Timber Structures

CHALMERS UNIVERSITY OF TECHNOLOGY

Göteborg, Sweden 2013

Lateral-torsional buckling of steel girders with trapezoidally corrugated webs

Master of Science Thesis in the Master's Programme Structural Engineering and Building Technology

MATTIAS LARSSON

JOHN PERSSON

© MATTIAS LARSSON, JOHN PERSSON, 2013

Examensarbete/ Institutionen för bygg- och miljöteknik,
Chalmers tekniska högskola 2013:57

Department of Civil and Environmental Engineering
Division of Structural Engineering
Steel and Timber Structures
Chalmers University of Technology
SE-412 96 Göteborg
Sweden
Telephone: +46 (0)31-772 1000

Cover:

Global lateral-torsional buckling of a steel girder with trapezoidally corrugated web

Chalmers Reproservice
Göteborg, Sweden 2013

Lateral-torsional buckling of steel girders with trapezoidally corrugated webs

Master of Science Thesis in the Master's Programme Structural Engineering and Building Technology

MATTIAS LARSSON

JOHN PERSSON

Department of Civil and Environmental Engineering

Division of Structural Engineering

Steel and Timber Structures

Chalmers University of Technology

ABSTRACT

Steel girders with trapezoidally corrugated webs are structural members with high load-carrying capacity in relation to the material usage. The main advantage is that the corrugated web provides a high shear capacity for very thin web plates. Research on this type of girders has been conducted at Chalmers University of Technology since the 1980's, with the main focus on the shear capacity. It is also suspected that the lateral-torsional buckling capacity increases due to the corrugation of the web.

In this report, previous research on the subject of lateral-torsional buckling of steel girders with trapezoidally corrugated webs is presented and critically reviewed. The critical buckling moment is strongly influenced by the torsion and warping constants, which are not well established for girders with corrugated webs. Previous researchers state that there is an increased resistance against lateral-torsional buckling caused by the corrugated web, and that this resistance should be attributed only to an increased *warping* constant. By considering fundamental torsion theory and by studying the torsional response of girders with corrugated webs using finite element simulations conducted in ABAQUS CAE, the authors of this report conclude that the extra stiffness instead should be accounted for by an increased *torsion* constant.

In this report, a method is established for finding the torsion and warping constants of I-shaped girders with arbitrary web profiles using finite element simulations of cantilevers subjected to torsion. This method is verified by comparing the results to results from linear buckling finite element analyses and analytically calculated values of the torsion and warping constants of girders with flat webs.

The authors of this report suggest using a modified version of the expressions for the torsion and warping constants stated by Lindner in previous research. By reformulating the original expressions, the increased resistance can be attributed to the torsion constant instead of the warping constant, resulting in critical buckling moments and sectional constants which agree well with those obtained using the method proposed in this report.

Keywords: Lateral-torsional buckling, corrugated web, torsion constant, warping constant, steel girder, torsional response

Vippning av stålbalkar med trapetskorrugerade liv

Examensarbete inom Mastersprogrammet *Structural Engineering and Building Technology*

MATTIAS LARSSON
JOHN PERSSON

Institutionen för bygg- och miljöteknik
Avdelningen för konstruktionsteknik
Stål- och träbyggnad
Chalmers tekniska högskola

SAMMANFATTNING

Stålbalkar med trapetskorrugerade livplåtar har hög bärförmåga i förhållande till materialåtgång. Den största fördelen med denna typ av balk är att korrugeringen ger hög tvärkraftskapacitet även för mycket tunna livplåtar. Forskning kring denna typ av balkar har bedrivits vid Chalmers tekniska högskola sedan 1980-talet, med fokus på tvärkraftskapacitet. Mycket tyder på att även det kritiska vippningsmomentet ökar tack vare det korrugerade livet.

I detta examensarbete presenteras och granskas tidigare forskning kring vippning av stålbalkar med trapetskorrugerade liv. Det kritiska vippningsmomentet påverkas kraftigt av balkens vrid- och välvkonstanter. För balkar med korrugerade liv saknas väletablerade uttryck för att beräkna dessa tvärsnittskonstanter. Tidigare forskning visar att motståndet mot vippning ökar på grund av det korrugerade livet, och att denna ökning bör tillskrivas en ökad *välvkonstant*. Genom att beakta grundläggande vridteori och genom att studera vridresponsen av balkar med korrugerade livplåtar i finita element-simuleringar utförda med ABAQUS CAE, drar författarna av denna rapport slutsatsen att den extra styvheten istället skall tillskrivas en ökad *vridkonstant*.

I rapporten etableras en metod för att hitta vrid- och välvkonstanterna för I-balkar med godtycklig korrugeringsprofil för livplåten genom att använda finita element-simuleringar av vridbelastade konsoler. Denna metod verifieras genom att jämföra erhållna resultat med resultat från linjära instabilitetsanalyser samt med analytiskt beräknade vrid- och välvkonstanter för balkar med plana liv.

Författarna av denna rapport föreslår en modifierad version av uttrycken för att beräkna vrid- och välvkonstanter som presenterades av Lindner i tidigare forskning. Genom att omformulera dessa ursprungliga uttryck kan det ökade motståndet tillskrivas vridkonstanten istället för välvkonstanten, vilket resulterar i ett kritiskt vippningsmoment och tvärsnittskonstanter som stämmer väl överens med dem som erhålls från den metod som föreslås i denna rapport.

Nyckelord: Vippning, korrugerat liv, vridkonstant, välvkonstant, stålbalk, vridrespons

PREFACE

This master's thesis was carried out at the Division of Structural Engineering, department of Civil and Environmental Engineering at Chalmers University of Technology, Sweden, from January 2013 to June 2013.

First of all, we would like to thank our supervisors Professor Emeritus Bo Edlund at Chalmers University of Technology and Tobias Andersson at Borga Steel Buildings for their support during the project. We would also like to thank our examiner and supervisor Associate Professor Mohammad Al-Emrani for his invaluable guidance and commitment throughout the process.

Furthermore, we would like to express our gratitude towards our opponent group consisting of Mathias Wernborg and Magnús Heidar Björnsson for their interest in and comments on the thesis.

Finally, many thanks to all the students writing their theses at the division this semester for creating a good atmosphere at the office.

Mattias Larsson
John Persson

NOTATIONS

Upper case Roman letters

C_1, C_2	Correction factors accounting for boundary conditions and moment gradient
C_b	Equivalent moment factor
E	Modulus of elasticity
G	Shear modulus
G_{co}	Reduced shear modulus due to the corrugation of the web, used by Moon et al.
I_t	Torsion constant
I_t^e	Equivalent torsion constant from the method proposed in this report
I_t^*	Equivalent torsion constant used by Lindner
I_t'	Equivalent torsion constant from the modified Lindner method
I_w	Warping constant
I_w^e	Equivalent warping constant from the method proposed in this report
I_w^*	Equivalent warping constant used by Lindner
I_w'	Equivalent warping constant from modified Lindner method
\bar{I}_w	Equivalent warping constant used by Moon et al.
\hat{I}_w	Equivalent warping constant used by Zhang et al.
I_y	Moment of inertia about the strong axis
I_{y1}	Moment of inertia of upper flange about the strong axis
I_{y2}	Moment of inertia of lower flange about the strong axis
I_z	Moment of inertia about the weak axis
L	Girder length
L_{ij}	Length of the interconnected plate element between the nodes i and j
M_{cr}	Elastic critical bending moment for lateral-torsional buckling
M_{cr}^e	Elastic critical buckling moment obtained using the proposed method
M_{cr}^{FE}	Elastic critical buckling moment obtained using linear buckling analysis (ABAQUS CEA)
M_{cr}^L	Elastic critical buckling moment obtained using Lindner's method
M_f	Flange moment
$M_{f,0}$	Flange moment at the fixed end
M_{pl}	Plastic bending moment
$M_{R,LT}$	Moment resistance with respect to lateral-torsional buckling
T	Torsional moment, general
T_t	Saint-Venant torsional moment
T_w	Vlasov torsional moment
V_w	Warping shear force due to flange bending
W_{el}	Elastic section modulus
W_{pl}	Plastic section modulus
W_{ni}	Normalised unit warping at point i of an element ($i-j$)
W_{nj}	Normalised unit warping at point j of an element ($i-j$)
Q	Applied external torsional moment

Lower case Roman letters

a	Length of longitudinal panel
a	Torsion bending constant
b	Projected length of inclined panel
b_f	Flange width
c	Actual length of inclined panel
d	Maximum eccentricity of web
e	Eccentricity of web
e_{max}	Maximum eccentricity of web
h_m	Distance between centroids of flanges
h_r	Amplitude of corrugation
h_w	Web height
f_y	Yield limit
k, k_w	Effective length factors with regard to torsion and warping respectively
t_{ij}	Thickness of the interconnected plate element between the nodes i and j
t_f	Flange thickness
t_w	Web thickness
q	Wavelength of corrugation
q	Uniformly distributed transversal load
w	Transversal deflection
w_{0i}	Unit warping at point i of an element ($i-j$)
w_{0j}	Unit warping at point j of an element ($i-j$)
z_g	Distance between the point of load application and the shear centre

Lower case Greek letters

α	Angle of inclined web panel in relation to the longitudinal axis
α	Imperfection factor
α	Torsional parameter, describing the torsional response of a member
χ_{LT}	Reduction factor, reduction with respect to lateral-torsional buckling
γ_M	Material partial factor
γ	Addition to the warping constant, suggested by Lindner
δ	Addition to the torsion constant, modification to Lindner's expression
λ	Slenderness parameter
θ	Rotation of the cross-section about the longitudinal axis
θ_L	Total rotation of the cross-section about the longitudinal axis
θ'	First derivative of the rotation about the longitudinal axis
θ'''	Third derivative of the rotation about the longitudinal axis
ρ_{ij}	Perpendicular distance between the centroid and the shear centre of the section
$\sigma_x(x)$	Longitudinal flange stress, at the outermost fibre, along the member
$\sigma_{x,0}$	Longitudinal flange stress, at the outermost fibre, at the fixed end of a cantilever

CONTENTS

Abstract	i
Sammanfattning	ii
Preface	v
Notations	vii
Contents	ix
1 Introduction	1
1.1 Background	1
1.2 Aim	1
1.3 Approach	2
1.4 Limitations	2
1.5 Outline and contents of the report	3
2 Theory	4
2.1 Introduction to lateral-torsional buckling	4
2.2 Description of different types of torsional response	7
2.3 Influence of boundary conditions on torsional response	9
2.3.1 Unrestrained girder loaded in torsion	9
2.3.2 Cantilever loaded in torsion	9
3 Overview of existing approaches for lateral-torsional buckling of girders with trapezoidally corrugated webs	13
3.1 Approach suggested by Lindner	13
3.1.1 A proposed modified version of the approach suggested by Lindner	15
3.2 Approach suggested by Moon et al.	16
3.2.1 Comments	18
3.3 Approach suggested by Zhang et al.	18
3.4 Evaluation of assumptions used in existing research	19
3.4.1 Moment of inertia about the strong axis, I_y	19
3.4.2 Moment of inertia about the weak axis, I_z	20
3.4.3 Torsion constant, I_t	21
4 Torsional response of prismatic and non-prismatic members	22
4.1 Prismatic I-girder	22
4.2 Prismatic I-girder with one discrete partial warping restraint	23
4.3 Prismatic I-girder with several discrete warping restraints	24
4.4 I-girder with corrugated web	25

5	Derivation of method for obtaining torsion and warping constants of non-prismatic girders	27
5.1	Method for finding equivalent torsion and warping constants, I_t^e and I_w^e	27
5.2	Verification of the proposed method for finding equivalent cross-sectional constants, I_t^e and I_w^e	31
5.2.1	Torsion and warping constants of prismatic girders	32
5.2.2	Elastic critical buckling moment for girders with corrugated web	32
5.2.3	Influence of girder length	32
5.2.4	Torsion constant of girders subjected to uniform torsion	33
6	Finite Element models	34
6.1	Bending about the strong axis of a simply supported girder	35
6.2	Bending about the weak axis of a simply supported girder	35
6.3	Uniform torsion of an unrestrained girder	36
6.4	Non-uniform torsion of a cantilever	37
6.5	Critical lateral-torsional buckling moment of a simply supported girder	38
6.6	Convergence studies	39
7	Results and discussion	40
7.1	Parametric study for evaluating existing methods	40
7.2	Influence of girder length on the critical buckling moment	44
7.3	Accuracy of the modified Lindner method for arbitrary corrugation profiles . .	47
8	Conclusions	50
9	Suggestions for further research	51
	References	52
	Appendices	1
A	Evaluation of assumptions used in previous research	1
B	Torsional response of I-shaped girders	6
C	Implementation of the proposed method	12
D	Verification of the proposed method	16
E	Verifications of FE models	22
F	Convergence studies	26
G	Parametric study	32
H	Influence of girder length on the critical buckling moment	46
I	Different corrugation profiles evaluated using the modified Lindner method	64

1 Introduction

1.1 Background

As the demand for inexpensive structures increases, so do the incentives for optimizing building components. In order to create cheap and effective structural members, it is desirable to achieve a high load carrying capacity using as little material as possible. For steel members subjected to bending, this is achieved by creating cross-sections with large sectional depth, with a large distance between the majority of the material and the gravity center of the cross-section. A typical section of this type is an I-section, where a thin and high web creates a large distance between the flanges. These slender members are susceptible to instability phenomena such as local buckling of the web or global lateral-torsional buckling. In order to increase the resistance against local web buckling without adding extra web stiffeners or increasing the web thickness, a corrugated web can be used.

Research on steel girders with thin, corrugated webs has been conducted at Chalmers University of Technology since the 1980's [1]. The focus of this research has been the shear resistance of steel girders with corrugated webs and, to some extent, the patch load capacity. Internationally, some research has been carried out on the subject of lateral-torsional buckling of this type of girders, but no comprehensive methodology for the design has been established. Designers are currently forced to either use relatively complex and time consuming Finite Element models for each unique structure in order to capture the positive effects of the corrugated web, or to use the same approach as for girders with flat webs, thereby disregarding any extra resistance provided by the corrugated web in terms of lateral-torsional stability.

This master's thesis was initiated by Chalmers University of Technology and Borga Steel Buildings, a steel product manufacturer, which often uses girders with trapezoidally corrugated webs. One product that Borga Steel Buildings provides is prefabricated steel hall buildings, using girders with corrugated webs, and they want to investigate the effect from corrugated webs on the resistance against lateral-torsional buckling.

1.2 Aim

The aim of this master thesis is to find a method for calculating the resistance against lateral-torsional buckling of steel girders with trapezoidally corrugated webs subjected to bending, which could be used in the design process. The aim is to find a method which is easy to implement, captures the beneficial effects of the corrugated web and does not overestimate the capacity of the girders.

1.3 Approach

In order to reach the aim stated above, the project is divided into a number of steps:

- First of all, a literature study is performed in order to understand the phenomenon of lateral-torsional buckling and different types of torsional response. Previous research on lateral-torsional buckling of girders with corrugated webs is critically reviewed.
- A method for obtaining the equivalent cross-sectional constants of girders with corrugated webs is derived. These constants are used for calculating the critical lateral-torsional buckling moment in the same way as for girders with flat webs.
- A parametric study is then performed where the proposed method and the existing models are compared to each other and to results from FE-simulations performed in ABAQUS CAE, in order to investigate how different geometrical parameters of the girder affect the resistance against lateral-torsional buckling.

1.4 Limitations

This report is limited to consider:

- Members subjected to a uniform bending moment about the strong axis of the member, when considering lateral-torsional buckling.
- Linear elastic, homogeneous isotropic material.
- Girders with the same material properties for flanges and web.
- Thin-walled I-shaped girders with equal flanges.
- Prismatic steel girders and steel girders with trapezoidally corrugated webs.
- Webs with constant height over the length of the girder.
- Global lateral-torsional buckling. Local instability, such as web or flange buckling, has not been considered.

Note: In some literature, the word 'prismatic' is used to describe a girder which has the same cross-sectional depth and flange dimensions over the length of the girder, regardless of the shape of the web. In this report, the term prismatic girder refers to a girder with flat web. A prismatic girder should have the same cross-section in every section, which is not true for a girder with corrugated web.

1.5 Outline and contents of the report

Chapter 1 - Background to the subject as well as aim, approach and limitations of the project.

Chapter 2 - Introduction to theory on lateral-torsional buckling and different types of torsional response.

Chapter 3 - Overview of existing approaches for calculating the critical buckling moment of girders with corrugated webs.

Chapter 4 - Analysis of different types of torsional response of prismatic and non-prismatic members.

Chapter 5 - Derivation of the method used in this project for finding the equivalent torsion and warping constants I_t^e and I_w^e of girders with corrugated webs.

Chapter 6 - Description of the FE models used in the simulations included in the project.

Chapter 7 - Results and discussion.

Chapter 8 - Conclusions drawn from the results.

Chapter 9 - Suggestions for further research.

2 Theory

This chapter provides an overview of the theory on which the methods and analyses used in this report are based. An introduction to lateral-torsional buckling is given as well as a summary of different types of torsional response.

2.1 Introduction to lateral-torsional buckling

In order to get optimal use of material, girders with high load carrying capacity generally will have a high cross-sectional depth. Such slender cross-sections are susceptible to instability phenomena, and their full plastic capacity can not be utilized. An I-girder, for example, will carry the bending moment mainly as a force couple in the flanges, and at a certain load the compressive flange will become unstable and buckle laterally (the web prevents it from buckling transversally). The opposite flange will be subjected to tension, and will 'anchor' the lateral displacement of the cross-section. These actions combined will cause the whole cross-section to rotate about its longitudinal axis and translate in the lateral direction of the girder. This phenomenon is known as *lateral-torsional buckling*, and is illustrated in figure 2.1.

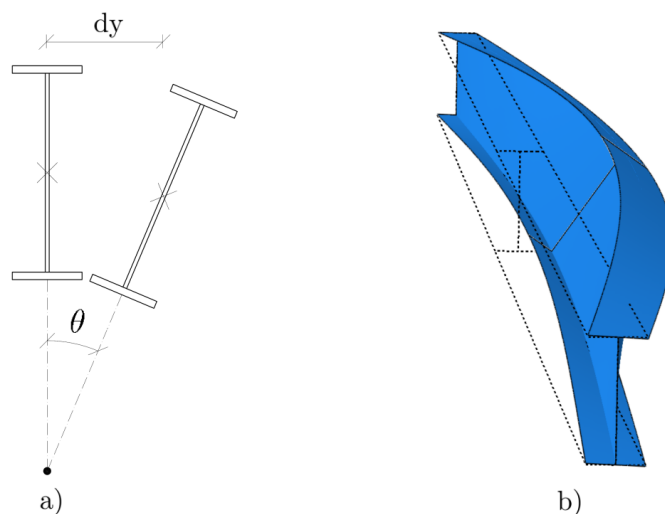


Figure 2.1: *Principle lateral-torsional buckling deformation of an I-girder subjected to bending about its strong axis. a) Displacement of the mid-section; b) Global instability mode.*

The susceptibility to lateral-torsional buckling of a member depends on the slenderness of the cross-section and the free length of the member, analogous to a column in compression. In order to take this instability phenomenon into account in the design process, the maximum bending moment capacity M_R of the section must be reduced. Eurocode 3 [2] provides two approaches for the design of members prone to lateral-torsional buckling; one more accurate method with specific buckling curves for lateral-torsional buckling, and one simplified method where the compression flange is seen as a column in compression. In this report, only the more accurate method will be considered. Both methods result in a reduction factor χ_{LT}

which is applied to the maximum bending moment capacity of the girder according to equation 2.1.

$$M_{R,LT} = \chi_{LT} \cdot M_R \quad (2.1)$$

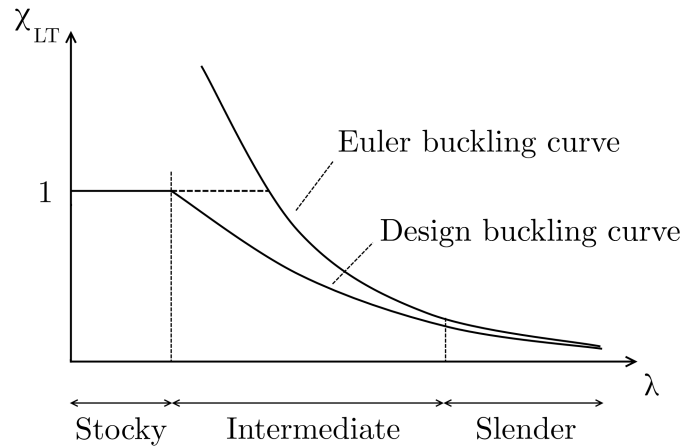


Figure 2.2: *Schematic buckling curve. Reduction factor taking into account lateral-torsional buckling as a function of the slenderness of the member.*

The reduction factor is based on the concept of buckling curves, applied in codes such as the Eurocode. A principle buckling curve is shown in figure 2.2. The starting point of the buckling curve is the Euler hyperbola. The background to the Euler hyperbola is entirely theoretical and holds true for a perfect, elastic girder, where the critical moment approaches infinity as the slenderness approaches zero. The shape of the buckling curve is governed by the yield stress of the material and the influence of initial stresses and imperfections. As shown in figure 2.2, the full plastic capacity can be utilized for members with low slenderness ('stocky' members), and for members with high slenderness the actual buckling load is very close to the theoretical elastic buckling load. The influence of the initial stresses and imperfections is greatest for members with intermediate slenderness, as illustrated by the difference between the Euler buckling curve and the design buckling curve in figure 2.2. The design buckling curve is defined by equations 2.2 and 2.3[2]. Since χ_{LT} is a reduction factor, its value should never be greater than 1.0.

$$\chi_{LT} = \frac{1}{\Phi_{LT} + \sqrt{\Phi_{LT}^2 - \lambda_{LT}^2}} \quad (2.2)$$

$$\Phi_{LT} = 0.5 \cdot [1 + \alpha_{LT} \cdot (\lambda_{LT} - 0.2) + \lambda_{LT}^2] \quad (2.3)$$

The imperfection factor α_{LT} , used in equation 2.3, is based on the geometry of the cross-section. The relative slenderness is generally defined as the square root of the maximum load carrying capacity divided by the elastic critical load. This definition is used regardless of what instability phenomenon is considered, whether it concerns buckling of columns, buckling of plates or lateral-torsional buckling of girders. The slenderness with regard to lateral-torsional buckling

λ_{LT} will simply be denoted λ since this report only considers lateral-torsional buckling and no other instability phenomena. In the case of lateral-torsional buckling, the slenderness is defined according to equation 2.4.

$$\lambda = \sqrt{\frac{M_R}{M_{cr}}} \quad (2.4)$$

The maximum bending moment capacity M_R (used in equation 2.4) is calculated according to equation 2.5

$$M_R = W_R \cdot f_y \quad (2.5)$$

where W_R is the section modulus. For cross-section classes 1 and 2, the section modulus is taken as the plastic section modulus W_{pl} . For cross-section class 3, the elastic section modulus W_{el} is used, and for cross-section class 4 the effective section modulus of the reduced cross-section W_{ef} is used [2].

The elastic critical bending moment M_{cr} is the theoretical maximum bending moment (Euler buckling moment) which can be resisted by the girder before lateral-torsional buckling occurs, where no initial stresses or imperfections are considered. The sectional properties which influence the resistance to lateral-torsional buckling are the moment of inertia about the weak axis I_z , the torsion constant I_t and the warping constant I_w . The moment of inertia I_z prevents lateral displacement, while the torsion and warping constants prevent rotation of the cross section. This report only considers *non-distorsional* buckling, meaning that the shape of the cross-section remains undeformed (as seen in figure 2.1a). The expression for the elastic critical buckling moment of a simply supported girder loaded in uniform bending is stated in equation 2.6.

$$M_{cr} = \frac{\pi^2 EI_z}{L^2} \sqrt{\frac{I_w}{I_z} + \frac{L^2 GI_t}{\pi^2 EI_z}} \quad (2.6)$$

This expression was derived analytically by Timoshenko [3] for a simply supported girder loaded by equal and opposite moments at the ends, meaning that the girder is subjected to a uniform bending moment. With this type of loading, no shear forces occur. In order to account for other boundary conditions, moment distributions and load applications, empirical modifications of that expression have been made, resulting in equation 2.7 [4].

$$M_{cr} = C_1 \cdot \frac{\pi^2 EI_z}{(kL)^2} \left\{ \sqrt{\left(\frac{k}{k_w}\right)^2 \cdot \frac{I_w}{I_z} + \frac{L^2 GI_t}{\pi^2 EI_z} + (C_2 z_g)^2} - C_2 z_g \right\} \quad (2.7)$$

The factor C_1 accounts for the moment distribution, allowing for different types of loading and boundary conditions. The term z_g is the vertical distance between the level of load application and the shear centre of the cross section and C_2 is a correction factor applied to z_g , governed

by the load distribution and the boundary conditions. The factors k and k_w are effective length factors, analogous to the ratio between buckling length and system length of a column subjected to normal buckling; k refers to the end rotation, while k_w refers to end warping [4]. Sayed-Ahmed [5] uses similar expression where the boundary conditions, moment distribution and load application are all accounted for in a single factor, the *equivalent moment factor* C_b . Sayed-Ahmed concludes that the same values of the factor C_b used for prismatic girders can be used for girders with corrugated webs as well. This factor replaces the factors C_1 and C_2 in equation 2.7. Based on this, the authors of this report assume that the values of C_1 and C_2 derived for prismatic girders can be used for girders with corrugated webs as well.

The focus of this report is the influence of the corrugated web on the resistance against lateral-torsional buckling. The influence from boundary conditions and moment distributions on the critical moment are not within the scope of the report, and therefore only equation 2.6 will be used.

2.2 Description of different types of torsional response

As seen in equation 2.6, the torsion and warping constants I_t and I_w govern the critical lateral-torsional buckling moment of a girder. In this section, the influence of these parameters on the torsional response of a girder is studied. When a girder is subjected to a torsional moment, the moment is resisted by shear stresses in the cross-section, which can be divided into two types of torsional response – *St. Venant torsion* and *Vlasov torsion* [6]. St. Venant torsion consists of shear stresses in the plane of the cross-section, without any out-of-plane stresses or deformations. This type of torsional response is found in cross-sections where the shear stresses mainly generate closed shear trajectories as seen in figure 2.3a, such as solid and circular sections. Vlasov torsion also has shear stresses in the plane of the cross-section, but these in-plane stresses are accompanied by out-of-plane deformations. Vlasov torsion dominates the torsional response of cross-sections where the shear trajectories are open, as seen in figure 2.3b. This type of torsional response mainly occurs in open, thin-walled cross-sections.

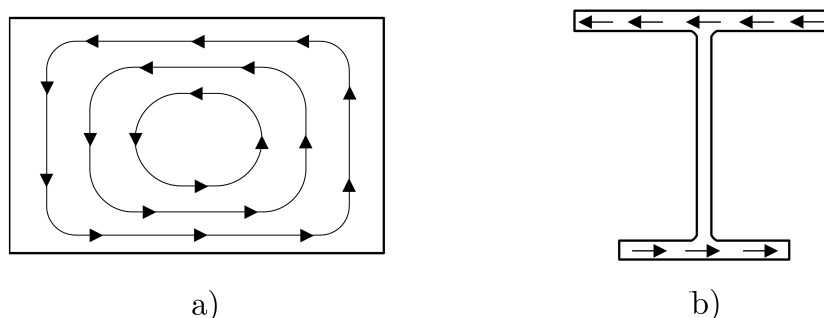


Figure 2.3: *Torsional moment resisted by shear stresses that form either a) closed or b) open trajectories*

If the entire torsional moment is resisted only by closed or only by open shear trajectories, the cross-section is said to be subjected to *pure St. Venant torsion* or *pure Vlasov torsion* respectively. A combination of St. Venant torsion and Vlasov torsion can occur, where the

torsional moment is resisted by both open and closed shear trajectories in the cross-section. This type of torsional response is referred to as *mixed torsion*. In each section of the member, the total resisting torsional moment T is defined as the sum of the St. Venant torsion and the Vlasov torsion. This is expressed in equation 2.8 [7], with the St. Venant torsion T_t and Vlasov torsion T_w defined in equations 2.8b and 2.8c respectively. Note that St. Venant torsion is related to the torsion constant I_t and the twist of the cross-section θ' , while Vlasov torsion is related to the warping constant I_w and the third derivative of the angular displacement of the cross-section θ''' .

$$T = T_t + T_w \quad (2.8a)$$

$$T_t = GI_t\theta' \quad (2.8b)$$

$$T_w = -EI_w\theta''' \quad (2.8c)$$

If the response of the cross-section is pure St Venant torsion, e.g. a solid circular section, there will be no warping deformations. For solid rectangular sections, where St. Venant torsion dominates the response, there will be small warping deformations. In open, thin-walled sections, where Vlasov torsion dominates the response, there will be significant warping deformations. This is shown principally in figure 2.4.

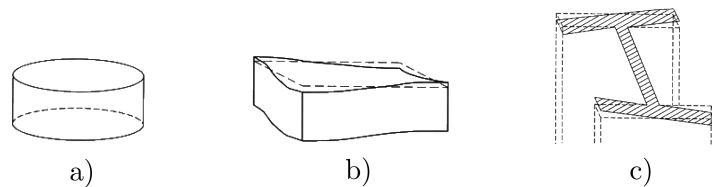


Figure 2.4: *Warping deformations for different types of cross sections; a) Circular section, no warping deformations; b) Rectangular section, small warping deformations; c) Open thin-walled section, significant warping deformations*

For practical use, a torsional parameter α is defined according to equation 2.9. This parameter is used for checking whether a certain cross section will resist torsion in St. Venant, Vlasov or mixed torsion. For small values, $|\alpha| < 0.05$, the member can be assumed to be subjected to pure Vlasov torsion. For large values, $|\alpha| > 20$, the member can be assumed to be subjected to pure St. Venant torsion. For intermediate values of α , mixed torsion must be considered [8].

$$\alpha = -\frac{GI_tL^2}{\pi^2EI_w} \quad (2.9)$$

2.3 Influence of boundary conditions on torsional response

In addition to the geometry of the cross-section, the boundary conditions greatly influence the torsional response of thin-walled members. In this section, the torsional response of a prismatic I-girder is explained using different sets of boundary conditions.

2.3.1 Unrestrained girder loaded in torsion

Consider a prismatic I-girder subjected to a torsional moment at either end as seen in figure 2.5a, with no prescribed boundary conditions. The member has a certain torsion constant I_t and warping constant I_w . According to equation 2.10, the angular displacement θ for this load case will vary linearly over the length of the member and the twist θ' will be constant. This is referred to as *uniform torsion* and is illustrated in figure 2.5b.

$$\theta(x) = \frac{Qx}{GI_t} \quad (2.10)$$

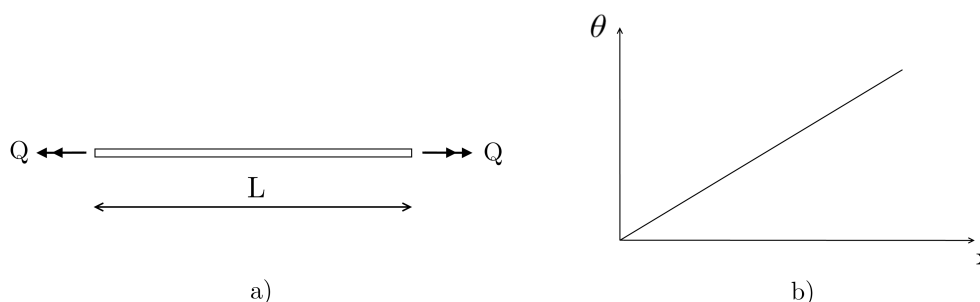


Figure 2.5: *Uniform torsion. a) Prismatic member with no external restraints against torsion or warping, subjected to a torsional moment; b) Principle digram of uniform torsional response.*

To evaluate the response, consider equation 2.8. Since the twist θ' is constant, the third derivative of the angular displacement θ''' will be equal to zero. This corresponds to that the entire torsional moment is resisted by St. Venant torsion T_t (see figure 2.7a) and that the response is governed only by the torsion constant I_t according to equation 2.8b.

2.3.2 Cantilever loaded in torsion

Now consider the same prismatic I-girder with the only difference that the torsion and warping deformations at the left end are prevented, see figure 2.6. In this load case, the rate of the angular displacement θ will not be constant over the length of the girder. This is referred to as *non-uniform torsion* and the principle torsional response is shown in figure 2.6.

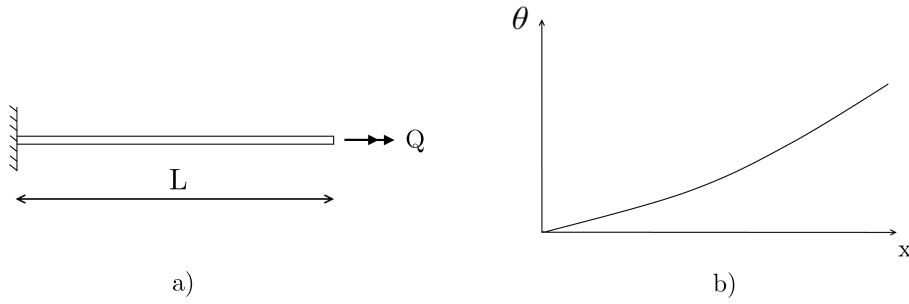


Figure 2.6: *Non-uniform torsion. a) Prismatic member with torsion and warping restrained at the left end and subjected to a torsional moment at the free end; b) Principle diagram of non-uniform torsional response.*

For the specific load case of a cantilever with length L , loaded by a concentrated torsional moment at the free end, an analytical expression for the angular displacement θ is given by equation 2.11 [8] where the *torsion bending constant* a is defined according to equation 2.12 [9].

$$\theta(x) = \frac{Q}{GI_t} \left(x - \frac{a(\sinh(\frac{L}{a}) - \sinh(\frac{L-x}{a}))}{\cosh(\frac{L}{a})} \right) \quad (2.11)$$

$$a = \sqrt{\frac{EI_w}{GI_t}} \quad (2.12)$$

By studying the expression for the angular displacement θ for this load case defined in equation 2.11, it is found that both the first derivative θ' and third derivative θ''' are non-zero. This corresponds to a combination of St. Venant torsion T_t and Vlasov torsion T_w resisting the applied torsional moment according to equation 2.8, and that the torsional response is governed by both the torsion constant I_t and the warping constant I_w . In each section of the girder, the total resisting moment must be equal to the applied torsional load Q for equilibrium to be reached. The distribution between the resisting St. Venant moment and Vlasov moment over the length of the girder for the two load cases described in this section can be seen in figure 2.7.

The cross-section of a member subjected to Vlasov torsion will exhibit out-of-plane deformations, so called warping deformations, which are shown principally in figure 2.4. When these deformations are prevented, e.g. by boundary conditions, this causes longitudinal stresses corresponding to the prevented deformation. In an I-girder, these longitudinal stresses cause flange moments M_f and warping shear forces V_w . The stresses in a doubly symmetric I-girder, caused by restrained warping, are shown in figure 2.8.

In order to quantify the forces caused by prevented warping deformations, the torsionally loaded cantilever previously studied in this section is considered. The resisting Vlasov moment consists of shear forces in the flanges, denoted V_w , which constitute a force couple with the

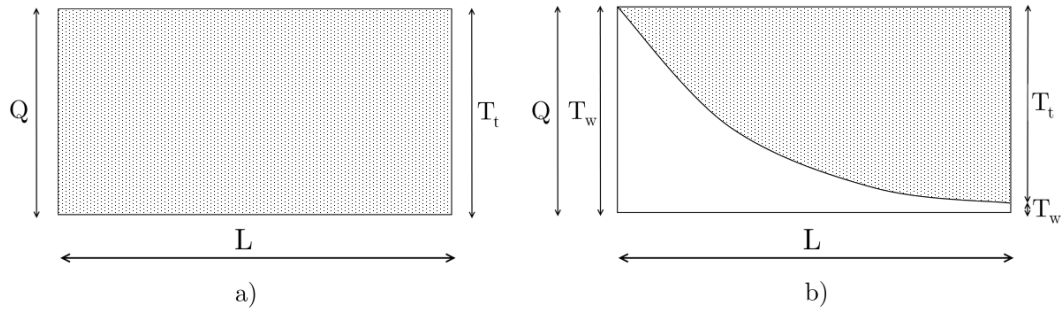


Figure 2.7: a) Distribution of the resisting moment in a member with no prescribed boundary conditions; b) Distribution of the resisting moment in a member with the left end fixed.

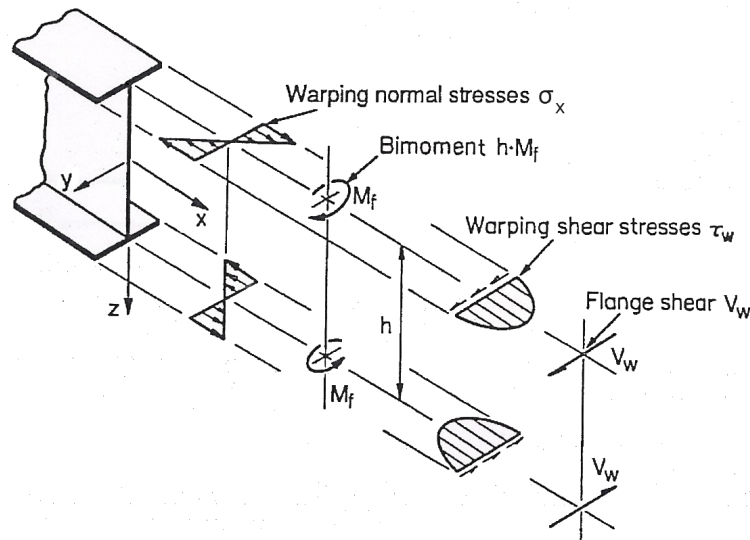


Figure 2.8: The warping shear, shear stresses and normal stresses caused by restrained warping of an I-girder loaded in torsion. Figure courtesy of New Zealand Standards [9].

depth of the girder h as lever arm. At the fixed end, warping deformations are fully prevented and the entire torsional moment Q is resisted by Vlasov torsion. The magnitude of the shear forces at the fixed end is defined according to equation 2.13a, and the magnitude at an arbitrary location along the girder can be calculated according to equation 2.13b. For a girder with constant depth, the magnitude of the shear forces is directly proportional to the magnitude of the Vlasov torsional moment, and the distribution over the length of the cantilever is illustrated in figure 2.9. By studying this distribution, it is clear that the influence of a warping restraint is high near the restraint, in this case, the fixed end. As the distance from the restraint increases, the warping stresses approach zero and the torsional behaviour approaches that of an unrestrained member.

$$V_w(x = 0) = \frac{Q}{h} \quad (2.13a)$$

$$V_w(x) = \frac{T_w(x)}{h} \quad (2.13b)$$

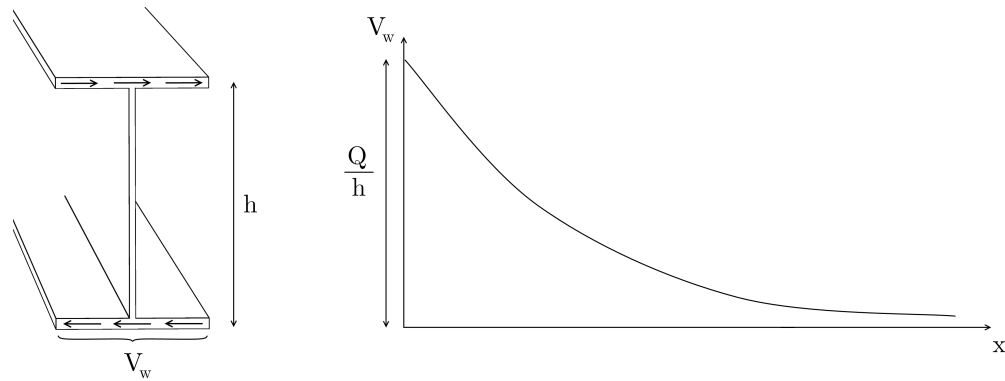


Figure 2.9: *Shear forces in flanges due to Vlasov torsion. The distribution of the shear forces has the same shape as the Vlasov moment.*

By visualising the Vlasov torsional moment as a force couple acting on the two flanges, the flanges can be seen as two separate cantilevers. These fictive ‘flange cantilevers’ are then analogous to transversally loaded cantilevers, where the warping shear force V_w is equivalent to the transversal shear force and the flange moment M_f is equivalent to the bending moment acting about the strong axis of the cantilever. From this analogy, it is concluded that the flange moment at the fixed end of the flange can be obtained by integrating the flange shear force V_w over the length of the flange L . This analogy is central in the method proposed in this report for deriving the cross-sectional constants of girders with corrugated webs, which is described in section 5.1.

3 Overview of existing approaches for lateral-torsional buckling of girders with trapezoidally corrugated webs

Previous research on the subject show that there is a considerable increase in resistance against lateral-torsional buckling for girders with trapezoidally corrugated webs compared to girders with flat webs. Sayed-Ahmed [10] states that the increase in elastic critical buckling moment is as high as 12-37 percent. Moon et al. [11] find that the increase is smaller, up to 10 percent. All existing approaches presented in this section state that the increased lateral-torsional buckling capacity is due to an increased warping constant I_w , while the moment of inertia I_z and torsion constant I_t are not influenced by the corrugation of the web [11][12][13]. In this chapter, the approaches for calculating the warping constant of girders with corrugated webs suggested by Lindner, Moon et al. and Zhang et al. are presented and critically reviewed. The notations used in this report for the geometry of the cross-section and the corrugation profile are defined in figure 3.1.

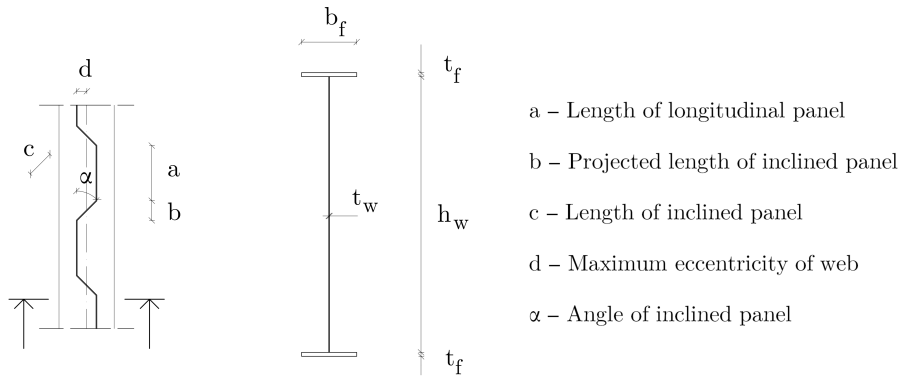


Figure 3.1: *Notations for the geometry of the cross-section and corrugation profile.*

In most of the analyses included in this report, one particular corrugation profile has been used, with the geometry specified in table 3.1. This profile is one of the most commonly used for girder webs by the steel product manufacturer Borga Steel Buildings.

Table 3.1: *Geometry of the corrugation profile used in a majority of the analyses included in this report. All dimensions in millimetres unless otherwise stated.*

a	b	c	d	α [°]
140	50	71	25	45

3.1 Approach suggested by Lindner

Lindner [12][14] proposes a method for calculating the critical moment of girders with corrugated webs based on analytical derivations, verified by experimental testing. Lindner states that

the moment of inertia about the weak axis I_z and the torsion constant I_t can be calculated using the same expressions as for girders with flat webs. The extra capacity in terms of critical lateral-torsional buckling moment obtained for girders with corrugated webs is attributed to an increased warping constant I_w^* . The critical moment is calculated using the expression stated in equation 2.6, with the torsion and warping constants I_t^* and I_w^* calculated according to equation 3.1.

$$I_t^* = I_t \quad (3.1a)$$

$$I_w^* = I_w + c_w \frac{L^2}{E\pi^2} \quad (3.1b)$$

I_t and I_w are the torsion and warping constants of a girder with flat web and c_w is defined according to equation 3.2.

$$c_w = \frac{(2d)^2 h_m^2}{8u_x(a+b)} \quad (3.2a)$$

$$u_x = \frac{h_m}{2Gat_w} + \frac{h_m^2(a+b)^3(I_{y1} + I_{y2})}{600a^2E(I_{y1}I_{y2})} \quad (3.2b)$$

I_{y1} and I_{y2} in equation 3.2b are the moment of inertia about the strong axis of the girder of the upper and lower flange respectively. For girders with equal flanges the expression for u_x can be simplified according to equation 3.3.

$$u_x = \frac{h_m}{2Gat_w} + \frac{h_m^2(a+b)^3}{25a^2Eb_f t_f^3} \quad (3.3)$$

When establishing the method, Lindner verified the expressions by performing experimental testing of girders with trapezoidally corrugated webs. These girders all had the same corrugation profile, shown in table 3.2.

Table 3.2: *Geometry of corrugation profile used by Lindner [14] when verifying his suggested method. All dimensions in millimetres unless otherwise stated. Note that this profile is similar to the one defined in table 3.1 which is the one mainly used in this project.*

a	b	c	d	α [°]
148	52	74	26	45

Lindner assumes that the torsion constant I_t^* of a girder with a corrugated web is equal to that of a girder with a flat web I_t , and that the warping constant I_w^* is higher than that of a girder with flat web I_w . It is noteworthy that, in equation 3.1b, the warping constant increases quadratically with the length of the girder L . Typically, a sectional constant should only be dependent on the geometry of the cross-section, and not on the length.

3.1.1 A proposed modified version of the approach suggested by Lindner

The authors of this report propose a method, such that the expressions originally stated by Lindner are modified, where the extra rotational stiffness provided by the corrugated web is attributed to the torsion constant I_t instead of the warping constant I_w . The modified expressions result in the same critical lateral-torsional buckling moment, using equation 2.6. This method will be referred to as the *modified Lindner method*, and is described in this section.

In equation 3.4, the term I_w is equal to the warping constant of a girder with a flat web, and the term γ accounts for the addition to the total warping constant caused by the corrugation of the web. It is recognised that c_w in γ is multiplied with the same term as the torsion constant I_t in the equation for calculating the critical buckling moment (equation 2.6). By inserting the expressions for the torsion and warping constants suggested by Lindner (defined in equation 3.1) into the expression for the critical buckling moment stated in equation 2.6, the expression for the critical buckling moment can be rewritten according to equation 3.5.

$$I_w^* = I_w + \underbrace{c_w \frac{L^2}{E\pi^2}}_{\gamma} \quad (3.4)$$

$$M_{cr} = \frac{\pi^2 EI_z}{L^2} \sqrt{\frac{I_w}{I_z} + \frac{c_w L^2}{\pi^2 EI_z} + \frac{L^2 GI_t}{\pi^2 EI_z}} = \frac{\pi^2 EI_z}{L^2} \sqrt{\frac{I_w}{I_z} + (GI_t + c_w) \cdot \frac{L^2}{\pi^2 EI_z}} \quad (3.5)$$

In the rewritten expression, the addition to the warping constant (γ in equation 3.4) can be interpreted as an addition δ to the torsion constant instead, as seen in equation 3.6a. This alternative way of calculating the sectional constants is referred to as the *modified Lindner method*, where the torsion and warping constants are denoted I'_t and I'_w respectively. Using this definition of the cross-sectional constants, neither of these constants is dependent on the girder length L . Given that lateral-torsional buckling is considered (i.e. that equation 2.6 is used), the expressions for I'_t and I'_w defined in equation 3.6 are simply a rewritten version of the expressions originally stated by Lindner [12], see equation 3.1. While the method originally stated by Lindner and the modified Lindner method provide different torsion and warping constants, the two methods will result in *exactly* the same critical buckling moment M_{cr} .

$$I'_t = I_t + \underbrace{\frac{c_w}{G}}_{\delta} \quad (3.6a)$$

$$I'_w = I_w \quad (3.6b)$$

3.2 Approach suggested by Moon et al.

Moon et al. [11] establish a method for calculating the critical buckling moment of girders with corrugated webs using the same assumptions as Lindner, i.e. that all sectional properties, except the warping constant, of a girder with corrugated web are equal to those of a prismatic girder. In contrast to the expressions for calculating the warping constant presented by Lindner [12], the expressions presented by Moon et al. are derived analytically based on the theory presented by Galambos [15]. These expressions are quite complex, but can be simplified by considering the geometry of the cross-section. By doing so, numerical formulas for warping constants of open thin-walled members can be obtained as explained by Lue et al. [16]. Using the numerical formulas provided by Lue et al., the warping constant of an open, thin-walled prismatic member can be calculated by considering the cross section to be a series of thin, interconnected plates. The cross-section is divided at discrete points, *nodes*, defining the endpoints of these plate elements. The nodes are labelled 1 to n , and the geometry of each plate element is defined by its thickness t_{ij} and length L_{ij} . The warping constant \bar{I}_w for the cross-section is calculated according to equation 3.7.

$$\bar{I}_w = \frac{1}{3} \sum (W_{ni}^2 + W_{nj}W_{ni} + W_{nj}^2)t_{ij}L_{ij} \quad (3.7)$$

The normalized unit warping W_{ni} and W_{nj} for the nodes at the ends of each element i - j are defined by equation 3.8

$$W_{ni} = \frac{1}{2A} \sum_0^n (w_{0i} + w_{0j})t_{ij}L_{ij} - w_{0i} \quad (3.8a)$$

$$W_{nj} = \frac{1}{2A} \sum_0^n (w_{0i} + w_{0j})t_{ij}L_{ij} - w_{0j} \quad (3.8b)$$

where A is the area of the cross-section, $A = \sum t_{ij}L_{ij}$, and ρ_{0i} is the distance from the centroid of each element to the shear centre of the cross-section, defined perpendicular to the plate element. The unit warping with respect to the centroid at point i and j respectively, w_{0i} and w_{0j} , are defined according to equation 3.9.

$$w_{0i} = \rho_{0ij}L_{ij} \quad (3.9a)$$

$$w_{0j} = w_{0i} + \rho_{0ij}L_{ij} \quad (3.9b)$$

Figure 3.2 and equations 3.7 through 3.10 show an example of how the warping constant is calculated for an I-girder with eccentric web, indicating how the division into thin plate elements has been performed and what nodes define each element. The normalised unit warping

for each node can be calculated according to equation 3.10, and is used in equation 3.7. For further reading, Lue et al. [16] perform a very clear step-by-step example of how the warping constant of an arbitrary open, thin-walled cross-section can be calculated.

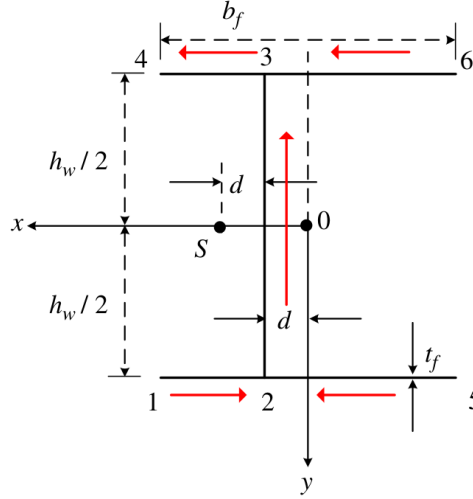


Figure 3.2: Definition of nodes and geometry used when calculating the warping constant of an I-girder with eccentric web. Figure courtesy of Moon et al. [11].

$$W_{n1} = \frac{2b_f^2 h_w t_f + b_f h_w^2 t_w}{8b_f t_f + 4h_w t_w} \quad (3.10a)$$

$$W_{n2} = \frac{2b_f^2 h_w t_f + b_f h_w^2 t_w}{8b_f t_f + 4h_w t_w} - \left(\frac{b_f}{4} - \frac{e}{2} \right) \quad (3.10b)$$

$$W_{n3} = \frac{2b_f^2 h_w t_f + b_f h_w^2 t_w}{8b_f t_f + 4h_w t_w} - \left(\frac{b_f}{4} + \frac{e}{2} \right) \quad (3.10c)$$

$$W_{n4} = \frac{2b_f^2 h_w t_f + b_f h_w^2 t_w}{8b_f t_f + 4h_w t_w} - \frac{1}{2} b_f h_w \quad (3.10d)$$

$$W_{n5} = W_{n4} \quad (3.10e)$$

$$W_{n6} = W_{n1} \quad (3.10f)$$

The method presented by Lue et al. [16] for finding the warping constant is valid for an arbitrary open, thin-walled prismatic girder. For I-shaped girders with corrugated webs, the eccentricity of the web e , which is included in equations 3.10b and 3.10c, is not constant but varies periodically. In order to overcome this, Moon et al. [11] suggest using an average eccentricity e_{avg} , calculated according to equation 3.11. By doing so, the girder is now mathematically considered to be a prismatic member with a constant web eccentricity.

$$e_{avg} = \frac{(2a + b)e_{max}}{2(a + b)} \quad (3.11)$$

Moon et al. [11] calculate the elastic critical buckling moment according to equation 3.12, which is an alternative way of writing equation 2.6

$$M_{cr} = \frac{\pi}{L} \sqrt{EI_z G_{co} I_t} \sqrt{1 + W^2} \quad (3.12)$$

where

$$W = \frac{\pi}{L} \sqrt{\frac{E \bar{I}_w}{G_{co} I_t}} \quad (3.13)$$

with \bar{I}_w defined according to equation 3.7, and where G_{co} is the *reduced shear modulus* for girders with corrugated webs. This reduced shear modulus is obtained by multiplying the regular shear modulus by a reduction factor, defined as the ratio between the projected length of the corrugated web plates in the longitudinal direction of the girder and the actual length of the web plates according to equation 3.14.

$$G_{co} = \frac{a + b}{a + c} G \quad (3.14)$$

3.2.1 Comments

It should be noted that Moon et al. suggest that the reduced shear modulus G_{co} should be applied at all instances where the shear modulus is used in equation 3.12 and 3.13, not only at the terms that relate the web. It could be argued that the reduced shear modulus should be applied only to the terms that refer to the web, and not the terms that refer to the flanges.

Moon et al. also investigate how the geometry of the corrugation influences the elastic critical buckling moment by changing the corrugation angle α . By increasing the angle between the longitudinal panels and the inclined panels of the corrugated web, the shear modulus G_{co} decreases while the warping constant \bar{I}_w increases. The reduced shear modulus decreases the gain from the corrugated web in terms of the critical buckling moment. The results presented by Moon et al. indicate that the lateral-torsional buckling resistance of girders with corrugated webs increases with an increasing angle α , with a maximum increase of approximately 10 percent for an angle α of 60° [11].

3.3 Approach suggested by Zhang et al.

Zhang et al. [13] present a method for calculating the critical buckling moment in a way similar to that presented by Moon et al. [11]. Zhang et al. also rely on the assumptions first presented by Lindner [12], stating that the moment of inertia about the weak axis I_z and the torsion constant I_t of a girder with a corrugated web can be assumed to be equal to those of a girder

with a flat web, and that the increased critical buckling moment is caused only by an increased warping constant I_w . The approach suggested by Zhang et al. [13] for obtaining the warping constant of a girder with corrugated web is based on the expression for the warping constant of a prismatic girder with a flat, eccentric web. That expression is defined in equation 3.15.

$$I_w^{ecc} = \frac{t_f b_f^3 h_m^2}{24} + \frac{t_w h_m^3 e^2}{12} \quad (3.15)$$

The first term in equation 3.15 can be identified as the expression commonly used for calculating the warping constant of a doubly symmetric I-profile, I_w , and the second term is an addition due to the eccentricity of the web. In order to account for the varying eccentricity of the corrugated web, equation 3.15 is integrated over one corrugation wavelength, q , and divided by this length as shown in equation 3.16. \hat{I}_w is the equivalent warping constant, suggested by Zhang et al., accounting for the effect of the corrugated web.

$$\hat{I}_w = \frac{1}{q} \cdot \int_0^q \frac{t_f b_f^3 h_m^2}{24} + \frac{t_w h_m^3 e(x)^2}{12} dx = I_w + \frac{t_w h_m^3 d^2}{12} \left(a + \frac{b}{3}\right) \quad (3.16)$$

3.4 Evaluation of assumptions used in existing research

In the existing research presented in this report [11][12][13] it is assumed that the contribution from the corrugated web to the torsion constant I_t is equal to that from a flat web, and that the contribution to the moment of inertia about the strong and weak axis I_y and I_z can be disregarded entirely. In order not to overlook any effects of the corrugated web, these assumptions have been critically reviewed and evaluated here in minor parametric studies. These parametric studies were conducted by studying the response of girders with corrugated webs using FE-simulations performed in ABAQUS CAE, using the models described in chapter 6, and comparing the results to values calculated analytically using models based on the aforementioned assumptions. The results from these parametric studies can be found in Appendix A.

3.4.1 Moment of inertia about the strong axis, I_y

Even though this parameter is not included in the expression for the critical buckling moment defined in equation 2.6, it is of interest to verify that the theory of the so called *accordion effect* [11], stating that a corrugated web does not contribute to the moment of inertia about the strong axis I_y , holds true for a reasonable thickness of the corrugated web. This assumption is evaluated for simply supported girders subjected to a constant bending moment about the strong axis. The girders are modelled in ABAQUS CAE as described in section 6.1 in order to obtain the longitudinal stresses in the flanges and the deflections at mid-span. These values are compared to those calculated analytically using beam theory with the assumption that the

web does not contribute to the moment of inertia about the strong axis, I_y . The analytical expression for I_y used in the calculations is stated in equation 3.17.

$$I_y = 2 \cdot \left(\frac{b_f t_f^3}{12} + b_f t_f \left(\frac{h_w}{2} \right)^2 \right) \quad (3.17)$$

The expressions for calculating the maximum stress and mid-span deflection of a girder loaded in uniform bending about the strong axis are stated in equation 3.18.

$$\sigma = \frac{M}{I_y} z_{max} \quad (3.18a)$$

$$w = \frac{ML^2}{8EI_y} \quad (3.18b)$$

The assumption regarding the contribution from the web to the moment of inertia about the strong axis I_y proved to be valid, with a maximum deviation of approximately *3 percent* between FE results and analytical calculations for girders with corrugated webs.

3.4.2 Moment of inertia about the weak axis, I_z

The moment of inertia about the weak axis I_z highly influences the lateral-torsional stability of the girder (see equation 2.6). For girders with thin, flat webs, the contribution of the web to I_z is considered to be negligible, which is also assumed to be the case for girders with corrugated webs. In order to evaluate this assumption, a simply supported girder is modelled in ABAQUS CAE, where it is loaded by a uniformly distributed load q in the weak direction of the girder as described in section 6.2. The longitudinal flange stresses and deflections at mid-span obtained from FE analyses are compared to those calculated according to equation 3.20 with I_z defined in equation 3.19.

$$I_z = 2 \cdot \frac{t_f b_f^3}{12} = \frac{t_f b_f^3}{6} \quad (3.19)$$

$$\sigma = \frac{M}{I_z} y_{max} \quad (3.20a)$$

$$w = \frac{5qL^4}{384EI_z} \quad (3.20b)$$

The assumption that the influence of the web on the moment of inertia about the weak axis I_z can be neglected proved to be valid, with a maximum deviation of *2 percent* between the results obtained from FE simulations and the analytically calculated results.

3.4.3 Torsion constant, I_t

The torsional response of an unrestrained girder is dependent only on the torsion constant I_t , which is referred to as *uniform torsion*, see section 2.3.1. According to previous research [11][12][13] the torsion constant of a girder with corrugated web is assumed to be equal to that of a girder with flat web. An I-girder has an open, thin-walled cross-section consisting of three strips, and an approximate way to calculate the torsion constant of such a section is given by equation 3.21 [17]. In this equation, a_i and b_i are the length and width of each strip, where the length always should be greater than the width in order for equation 3.21 to hold true.

$$I_t = \frac{1}{3} \sum_{i=1}^n a_i b_i^3 \quad (3.21)$$

The simplest way to evaluate the torsion constant I_t of a girder with a flat or corrugated web in an FE simulation is by modelling an unrestrained girder subjected equal and opposite torsional moments at the ends, as described in section 6.3. The expression shown in equation 3.22 is valid for uniform torsion, where θ_L is the total angular displacement of the member and Q is the applied torsional moment. In order to simulate uniform torsion, warping of the member must be unrestrained [17].

$$\theta_L = \frac{QL}{GI_t} \quad (3.22)$$

To evaluate if the assumption regarding the torsion constant I_t holds true, the total angular displacement of the member θ_L obtained from the FE analysis is compared to that calculated using equation 3.22 with I_t calculated according to equation 3.21. Using this assumption, the torsion constant was underestimated by up to *25 percent* for the girders studied, see Appendix A. This leads to the conclusion that the assumption regarding the torsion constant used in previous research is incorrect. Since this assumption is shown to be incorrect, the torsional response of girders with corrugated webs must be investigated further, which is done in chapter 4.

4 Torsional response of prismatic and non-prismatic members

The theory presented in section 2.2 is valid for open, thin-walled prismatic I-girders. In order to understand the torsional response of a girder with corrugated web, a number of FE simulations have been carried out on three types of I-girders; prismatic I-girders, prismatic I-girders with discrete warping restraints and I-girders with corrugated webs. The response of these types of girders is evaluated for different load cases in order to find similarities and differences in the torsional response between the aforementioned types of girders. The principle torsional response shown in the figures in this chapter are based on FE simulations of the different types of girders. The results from these simulations are presented in Appendix B.

4.1 Prismatic I-girder

Consider the two cases depicted in figure 4.1a; the first case considers a long, prismatic I-girder (the length of the member much larger than the depth) with free ends, loaded with equal but opposite torsional moments at the free ends such that the member is in equilibrium. The second case considers the same member, but with the left end totally fixed and the torsional moment acting only at the free end. The torsional response of these two cases is shown in figure 4.1b.

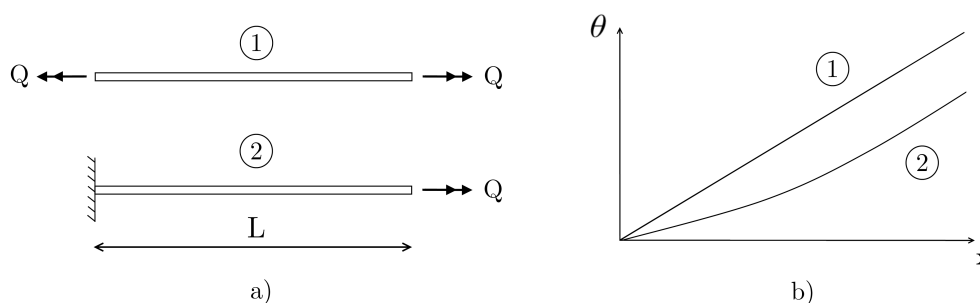


Figure 4.1: a) The two load cases used to illustrate the torsional response of prismatic members subjected to torsion; b) Principle diagram for the angular displacement for the two load cases.

As shown in figure 4.1b, the angular displacement θ varies linearly along the length of the unrestrained member (curve 1) corresponding to uniform torsion, which is described by equation 2.10. The inclination of the angular displacement graph corresponds to the twist of the cross section θ' . The member that is fixed at the left end (curve 2) has a lower twist near the fixed end than the free member (curve 1), indicating a higher rotational stiffness. This increase in stiffness is due to the prevented warping deformations, which is explained thoroughly in section 2.3. It can also be seen in figure 4.1b that the effect of the warping restraint is decreasing as the distance from the fixed end increases, and at a certain distance the effect is negligible. At

this point, the rotational stiffness of the girder only depends on the torsion constant I_t , and the twist is equal to that of the free member.

The warping stresses at the left end for these two cases can be seen in figure 4.2. The unrestrained member has no warping stresses and therefore the twist is constant over the length as seen in figure 4.1b. The fixed member has large warping stresses near the fixed end, which decrease with an increased distance from the warping restraint. As the warping stresses decrease (figure 4.2b) the twist increases (figure 4.1b), indicating that the prevented warping provides additional rotational stiffness. The response for these two load cases agrees well with common theories concerning pure and mixed torsion [8].

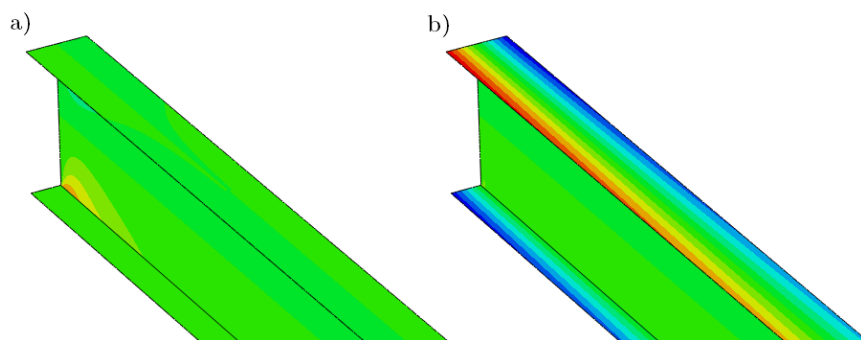


Figure 4.2: *Stresses in the longitudinal direction of the member for; a) the free member and b) the cantilever. The stresses in the web of the member which is free to warp (a) are caused by local effects from the load application.*

4.2 Prismatic I-girder with one discrete partial warping restraint

Again, consider the member without any restraints at the ends, loaded by a uniform torsional moment. A *partial warping restraint* is placed in the mid-section of the member as shown in figure 4.3a. For an I-girder, this restraint can be in the form of a web stiffener connected to the flanges, thereby partially preventing warping deformation of the flanges and providing an extra rotational stiffness to the member. This extra stiffness will locally decrease the twist of the member (θ'_2) as seen in figure 4.3b. The prevented warping deformations will also induce local longitudinal stresses in the flanges, shown in figure 4.4.

Similar to the member with one fixed end, the effect of the restrained warping decreases with the distance from the stiffener. Far away from the stiffener, the warping stresses will be very small and the twist will be approximately the same as for the unrestrained member, θ'_1 . At this point, the torsional response is once again only depending on the torsion constant I_t of the member.

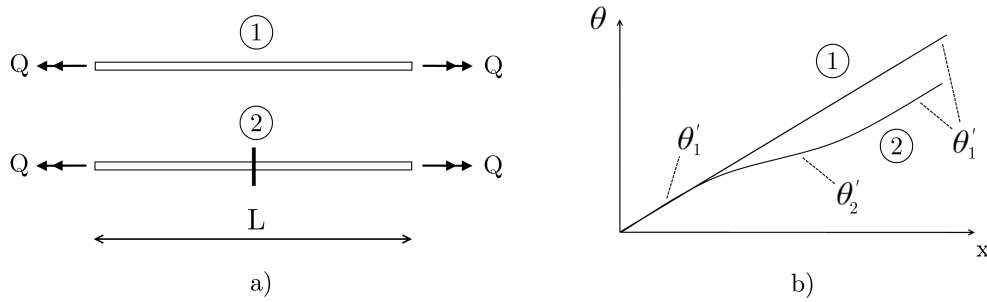


Figure 4.3: a) Illustration of the load case where two unrestrained prismatic members, without and with one single discrete warping restraint, are subjected to torsion; b) Principle diagram for the angular displacement along the members.

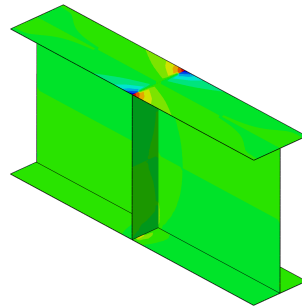


Figure 4.4: Longitudinal stresses in the flanges of in an I-girder, with one discrete partial warping restraint, subjected to torsion. These stresses are caused by the restrained warping.

4.3 Prismatic I-girder with several discrete warping restraints

Once again, consider the member without any restraints at either end, subjected to uniform torsion. In this case, web stiffeners connected to the flanges are placed close to each other with equal spacing, as shown in figure 4.5a. Figure 4.5b shows the principle torsional response of such a member and the torsional response of the same member without any web stiffeners.

The member *without* any web stiffeners has a constant twist (curve 1 in figure 4.5b), indicating uniform torsion, and the torsional response therefore only depends on the torsion constant I_t . The torsional response of the member *with* web stiffeners is represented by an oscillating curve, with a lower average inclination than that of the curve representing the torsional response of the member without web stiffeners.

Figure 4.5b indicates that the stiffeners provide extra torsional rigidity, and due to the close spacing of the stiffeners, the curve describing the angular displacement over the length of the member becomes quite smooth (curve 2). The additional stiffness provided by the stiffeners can be 'smeared out' by replacing the oscillating curve with a straight line. As explained in section 2.3.1, the torsional response of members with constant twist θ' only depends on the

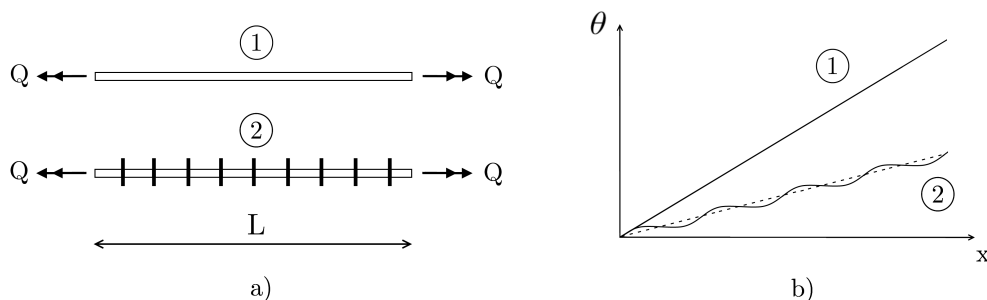


Figure 4.5: a) Load cases for the members with and without web stiffeners; b) Principle diagram for the angular displacement along the members. The dotted line represents a prismatic member with torsional stiffness equivalent to that of the member with web stiffeners.

torsion constant I_t . Replacing the oscillating curve with a straight line would be the same as attributing an increased *equivalent torsion constant* to the girder. It should be noted that this increased torsion constant is not a 'real' torsion constant. The stiffeners do not really increase the torsion constant of the girder, but they prevent warping at discrete points, causing an overall stiffer rotational behaviour of the member. This torsional response is best represented by an increased torsion constant.

4.4 I-girder with corrugated web

Consider two unrestrained members subjected to a constant torsional moment, one prismatic I-girder (member 1) and one girder with a corrugated web (member 2), depicted in figure 4.1a.

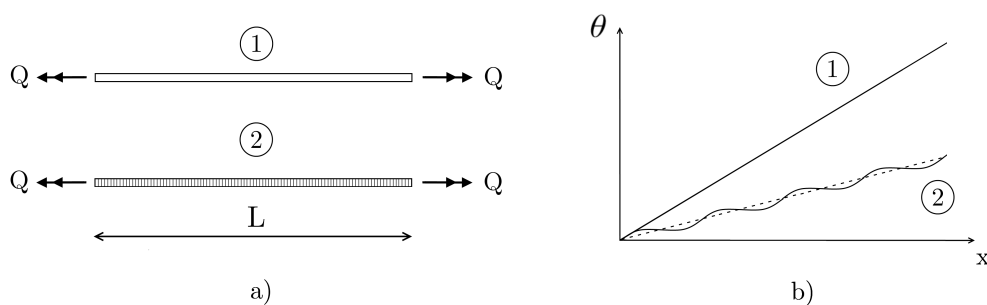


Figure 4.6: a) Load cases for the members with and without web stiffeners; b) Principle angular displacement along the members. The dotted line represents a prismatic member with torsional stiffness equivalent to that of the member with a corrugated web.

Clear similarities between the prismatic girder with several discrete warping restraints, described in section 4.3, and the girder with corrugated web can be identified. The inclined panels of the corrugated web cause longitudinal stresses (figure 4.7a) in the flanges in a similar way as the

discrete web stiffeners (figure 4.4). In the case with the prismatic member with web stiffeners, the additional resistance against the bimoment provided by the stiffeners can be quantified from the geometry of the stiffener. One stiffener can be modelled as a short member subjected to torsion due to warping of the flanges (note the flange moment in figure 2.8). In the case with the member with the corrugated web, the resistance against the bimoment is difficult to evaluate. The corrugated web is usually made from thin steel sheet, which in itself has a low torsional rigidity. However, since the inclined panels are connected to the longitudinal panels, they are anchored in the longitudinal direction, which significantly increases their stiffness. With the same reasoning as for the prismatic member with several discrete warping restraints, the additional rotational rigidity provided by the corrugated web should be accounted for by a higher equivalent torsional constant I_t^e . The main argument for this statement is that the stiffer rotational behaviour of the girder with corrugated web is obtained regardless of whether warping deformations are prevented or not, i.e. regardless of boundary conditions.

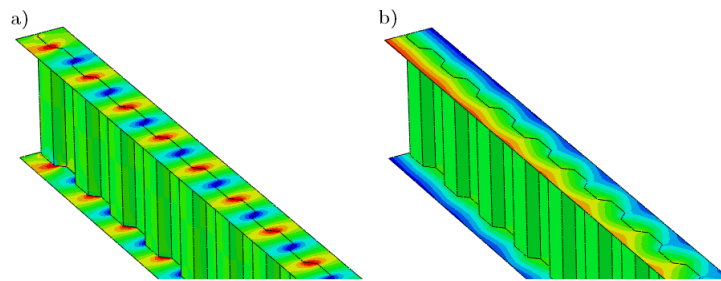


Figure 4.7: *Stresses in the longitudinal direction of a member with a corrugated web subjected to torsion for the case of; a) a free member and b) a cantilever. These stress patterns can be compared to those for prismatic girders illustrated in figure 4.2*

It should be noted that the equivalent torsion and warping constants not necessarily are the correct physical cross-sectional constants, but those which best represent the torsional behaviour of a girder with a corrugated web.

5 Derivation of method for obtaining torsion and warping constants of non-prismatic girders

This report aims at investigating what effect the corrugation of the web has on the resistance against lateral-torsional buckling. The idea is to find a method for determining the equivalent sectional constants to be used in the expression for the critical buckling moment (equation 2.6), so that the approach used for prismatic girders can be used for girders with corrugated webs as well. The parameters which must be established are the moment of inertia about the weak axis of the girder I_z , the torsion constant I_t and the warping constant I_w of the girder. An expression for calculating the moment of inertia I_z has been established and verified, see section 3.4.2. The equivalent torsion and warping constants will be evaluated by studying the response of steel girders with trapezoidally corrugated webs subjected to torsion, using FE simulations.

5.1 Method for finding equivalent torsion and warping constants, I_t^e and I_w^e

If the sectional properties governing the torsional response of a member subjected to torsion are unknown, the response must be assumed to be mixed torsion, described in section 2.2. Mixed torsional response is governed by both the torsion constant I_t and the warping constant I_w according to equation 2.8. Since, for non-prismatic girders, these two parameters are unknown, two independent relationships must be established in order to determine these parameters. The two relationships are established by studying a cantilever exposed to a torsional moment applied at the free end as shown in figure 5.1a. By using FE analysis, the angular displacement at the free end θ_L and the longitudinal stresses in the flanges at the fixed end $\sigma_{x,0}$ can be obtained. These quantities are then used to find the associated equivalent torsion and warping constants. Figure 5.1 shows the principal set-up of the member as well as the principle torsional response and angular displacement along the member. The method proposed for finding the torsion and warping constants is a combination of two existing relationships found in the literature; the first one is the analytical expression for the angular displacement of a cantilever subjected to torsion, seen in equation 5.1 [8]. The second relationship is the correlation between the flange moment M_f and the *torsion bending constant* a defined in equation 5.3 [9].

A number of observations can be made from figure 5.1. The sum of the St. Venant torsion T_t and Vlasov torsion T_w is always equal to the applied torsional moment Q , in every section of the member, as shown in figure 5.1b. At the free end, the major part of the applied moment is resisted by St. Venant torsion, with only a small amount Vlasov torsion. For long members, the Vlasov torsion will approach zero at the free end. At the fixed end, the applied load is resisted only by Vlasov torsion [8]. As seen in figure 5.1c, the twist of the member θ' is lower at the fixed end, and increases further away from the fixed end. This can be seen as an

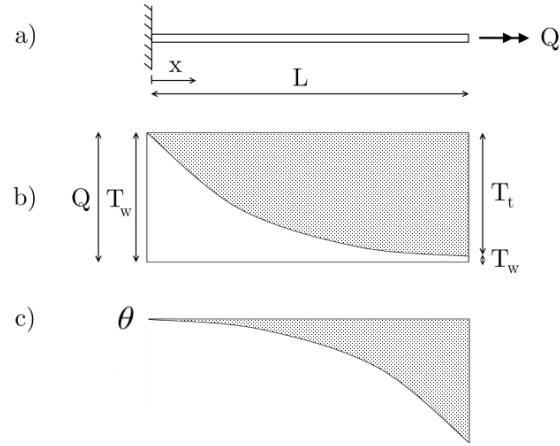


Figure 5.1: a) Cantilever subjected to a torsional moment applied at the free end causing mixed torsional response; b) Principle distribution of St. Venant and Vlasov torsion along the member; c) Angular displacement θ along the length of the member.

increased rotational stiffness near the fixed end caused by the restrained warping of the flanges, as described in section 2.3.

The first of the two relationships required to find the two unknown sectional constants is established by considering the angular displacement at the free end of the member θ_L . The angular displacement varies along the length of the member according to equation 5.1 [8], principally shown in figure 5.1c. If this expression is evaluated at the free end ($x = L$, see equation 5.2), a relationship with three unknown parameters (θ , I_t and a) is established. The angular displacement θ_L at this location will be evaluated by using FE analysis, leaving two unknown parameters.

$$\theta(x) = \frac{Q}{GI_t} \left(x - \frac{a(\sinh(\frac{L}{a}) - \sinh(\frac{L-x}{a}))}{\cosh(\frac{L}{a})} \right) \quad (5.1)$$

$$\theta(x = L) = \theta_L = \frac{Q}{GI_t} (L - a \cdot \tanh(\frac{L}{a})) \quad (5.2)$$

The torsion bending constant a is defined according to equation 5.3 [9].

$$a = \sqrt{\frac{EI_w}{GI_t}} \quad (5.3)$$

In order to find the torsion bending constant a , the nature of Vlasov torsion is considered. Vlasov torsion consists of shear forces in open trajectories as described in section 2.2. In an I-section, the shear forces in the flanges resist the Vlasov moment as a force couple, principally shown in figure 5.2a. In each flange, the Vlasov shear force V_w is defined as the Vlasov moment T_w divided by the lever arm h , which is the depth of the member. In this case, where there is an analytical, differentiable expression for the angular displacement, an expression for the Vlasov shear force can be obtained by inserting the explicit expression for the third derivative of the

angular displacement θ''' (equation 5.4b) into the equation for the Vlasov torsion (equation 5.4a). This results in the explicit expression for the Vlasov torsion shown in equation 5.4c.

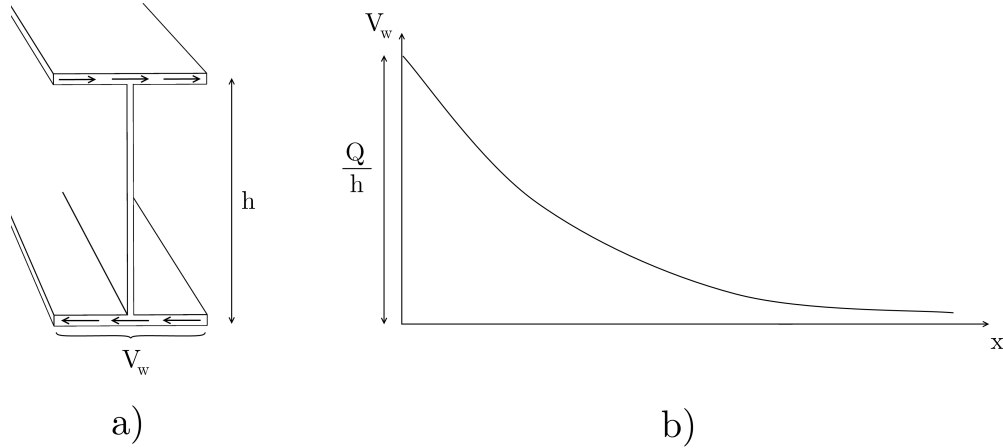


Figure 5.2: a) Vlasov shear force in flanges due to warping torsion; b) Principle distribution of the Vlasov shear force along the length of the member. The shear force has the same distribution as the Vlasov moment.

$$T_w(x) = -EI_w \theta'''(x) \quad (5.4a)$$

$$\theta'''(x) = -\frac{Q}{GI_t} \cdot \frac{\cosh(\frac{L-x}{a})}{a^2 \cosh(\frac{L}{a})} \quad (5.4b)$$

$$T_w(x) = \frac{QEI_w}{GI_t} \cdot \frac{\cosh(\frac{L-x}{a})}{a^2 \cosh(\frac{L}{a})} = \left\{ a^2 = \frac{EI_w}{GI_t} \right\} = Q \cdot \frac{\cosh(\frac{L-x}{a})}{\cosh(\frac{L}{a})} \quad (5.4c)$$

In order to find the Vlasov shear force V_w , the Vlasov moment is divided by the distance between the flanges h according to equation 5.5.

$$V_w(x) = \frac{Q}{h} \cdot \frac{\cosh(\frac{L-x}{a})}{\cosh(\frac{L}{a})} \quad (5.5)$$

At $x = 0$, the entire applied torsional moment will be resisted by Vlasov torsion causing the shear forces V_w to assume the value Q/h . At the free end the shear force will have a small but non-zero value. Analogous to a cantilever subjected to transversal load, the moment in the flange at the fixed end $M_{f,0}$ is the integral of the shear force over the length of the member, according to equation 5.6. For symmetric girders it is sufficient to consider only one of the flanges.

$$M_f(x=0) = M_{f,0} = \int_L^0 V_w(x) dx = \frac{Q}{h} \cdot a \cdot \tanh\left(\frac{L}{a}\right) \quad (5.6)$$

The flange moment at the fixed end $M_{f,0}$ can also be evaluated from the FE model. Again, consider the analogy between the flange and a cantilever subjected to a transversal load. The

flange moment at the fixed end will cause longitudinal stresses with a linear distribution over the width of the flange as shown in figure 5.3. The longitudinal flange stress at the fixed end $\sigma_{x,0}$ obtained from an FE analysis is used to calculate the flange moment at the fixed end $M_{f,0}$ according to equation 5.7.

$$M_{f,0} = \sigma_{x,0} \cdot W_f \quad (5.7)$$

W_f is the section modulus of one flange in its stiff direction. Assuming that the term $\tanh(\frac{L}{a})$ in equation 5.6 is approximately equal to 1.0 - which holds true when the ratio between the length of the member L and the torsion bending constant a is larger than 2 [9] - the expression for the flange moment shown in equation 5.6 can be rewritten according to equation 5.8.

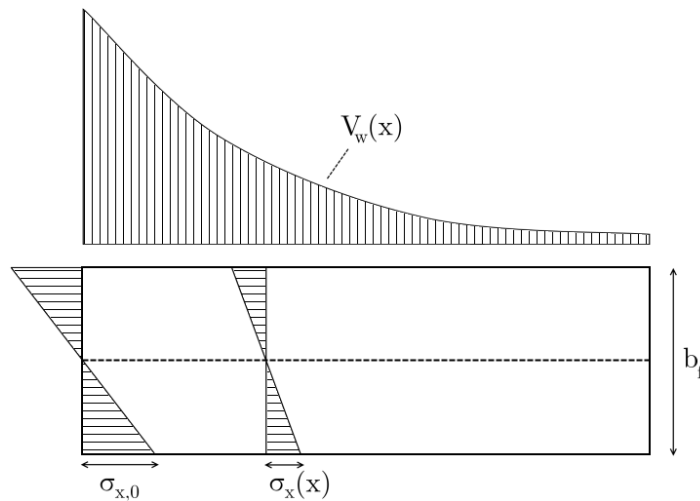


Figure 5.3: Longitudinal stresses in the flange caused by restrained warping.

$$M_{f,0} = \frac{Q}{h} \cdot a = \sigma_{x,0} \cdot W_f \Leftrightarrow a = \frac{\sigma_{x,0} \cdot W_f \cdot h}{Q} \quad (5.8)$$

With the torsion bending constant a calculated using equation 5.8, an equivalent torsion constant I_t^e can be calculated by rewriting equation 5.2 into equation 5.9, using the assumption that $\tanh(\frac{L}{a})$ is equal to 1.0. With the equivalent torsion constant I_t^e and the torsion bending constant a known, an equivalent warping constant I_w^e can be calculated by using the definition of a (equation 5.3), rewritten into equation 5.10.

$$I_t^e = \frac{Q}{\theta_L G} \cdot (L - a) \quad (5.9)$$

$$I_w^e = \frac{GI_t}{E} \cdot a^2 \quad (5.10)$$

Summary of the method proposed for obtaining the equivalent torsion and warping constants of an I-shaped girder: An FE model of a girder is established, where the girder is modelled as a cantilever subjected to a concentrated torsional moment applied at the free end. A linear static FE analysis provides values for the angular displacement at the free end of the cantilever θ_L as well as the longitudinal stresses in the flanges at the fixed end $\sigma_{x,0}$. Using the value of the longitudinal stresses, the torsion bending constant a is calculated using equation 5.11.

$$a = \frac{\sigma_{x,0} \cdot W_f \cdot h}{Q} \quad (5.11)$$

Using the calculated torsion bending constant a and the known angular displacement at the free end θ_L , the equivalent torsion constant I_t^e is calculated according to equation 5.12.

$$I_t^e = \frac{Q}{\theta_L G} \cdot (L - a) \quad (5.12)$$

By using the calculated equivalent torsion constant I_t^e and torsion bending constant a , the equivalent warping constant I_w^e is calculated according to equation 5.13.

$$I_w^e = \frac{GI_t^e}{E} \cdot a^2 \quad (5.13)$$

Using this methodology, both the equivalent torsion and warping constants I_t^e and I_w^e of the girder can be obtained by performing a single linear static FE analysis. It is important to verify, for each set-up, that the value of $\tanh(\frac{L}{a})$ is approximately equal to 1.0. This will highly influence the accuracy of the resulting equivalent sectional constants. An example of how this method is applied for a specific girder with corrugated web can be found in Appendix C. It should be noted that the presented method has been verified only for I-shaped girders with flat or corrugated webs.

5.2 Verification of the proposed method for finding equivalent cross-sectional constants, I_t^e and I_w^e

The accuracy of the equivalent torsion and warping constants I_t^e and I_w^e obtained using the method proposed in section 5.1 must be verified. The verification is performed in four different ways; in the first verification the torsion and warping constants of prismatic I-girders, obtained using the proposed method, are compared to the corresponding analytically calculated values. The next verification is performed for girders with corrugated webs, where the obtained equivalent torsion and warping constants I_t^e and I_w^e are used for calculating the critical buckling moment. This moment is compared to the corresponding moment obtained from a linear buckling analysis performed in ABAQUS CAE. In a third study, it is checked that the method is insensitive to a change of the girder length. Finally, the equivalent torsion constant I_t^e

of a girder with corrugated web, obtained using the proposed method, is compared to the torsion constant obtained from a static FE analysis of the same girder subjected to uniform torsion.

5.2.1 Torsion and warping constants of prismatic girders

This part of the verification was performed for a number of simply supported girders with flat webs which were analysed in FE simulations using the proposed cantilever method for finding the torsion and warping constants I_t and I_w (using the model described in section 6.4). These constants were compared to the corresponding constants given by LTBEAM, an analytical software treating the subject of lateral-torsional buckling of prismatic girders. The warping and torsion constants obtained using the proposed method are approximately *2 to 6 percent* lower than those calculated using LTBEAM, see Appendix D. This accuracy is considered to be sufficient for stating that the proposed method can be used for calculating the torsion and warping constants of prismatic I-shaped girders.

5.2.2 Elastic critical buckling moment for girders with corrugated web

The equivalent cross-sectional constants I_t^e and I_w^e obtained for girders with corrugated webs using the proposed method are verified by considering the critical buckling moment. With the obtained cross-sectional constants, the critical buckling moment M_{cr}^e is calculated using equation 5.14, with no contribution to I_z from the corrugated web, as explained in section 3.4.2. This moment is compared to that obtained from a linear buckling analysis of the same girder performed in ABAQUS CAE, using the model described in section 6.5. These critical buckling moments agree very well, with a maximum error of *1 percent*, see Appendix D.

$$M_{cr}^e = \frac{\pi^2 EI_z}{L^2} \sqrt{\frac{I_w^e}{I_z} + \frac{L^2 GI_t^e}{\pi^2 EI_z}} \quad (5.14)$$

5.2.3 Influence of girder length

It should be confirmed that the method proposed in this report generates the same equivalent torsion and warping constants I_t^e and I_w^e regardless of the length of the girder used for obtaining the cross-sectional constants. In order to do this, the critical buckling moment is calculated for a different length L_2 than the length L_1 used when obtaining the cross-sectional constants. The member with length L_2 was analysed in a linear buckling analysis performed using ABAQUS CAE, resulting in a critical buckling moment which agrees well with that calculated analytically using equation 5.14. The maximum difference between the two critical moments was *1 percent* as seen in Appendix D. From these results, it is concluded that the equivalent torsion and warping constants obtained using the proposed method are valid regardless of the girder length. The influence of the girder length is studied further in section 7.2.

5.2.4 Torsion constant of girders subjected to uniform torsion

In order to check the accuracy of the equivalent torsion constant I_t^e obtained using the proposed method, static torsional analyses were performed in ABAQUS CAE using the model described in section 6.3. The analyses were carried out both for prismatic girders and for girders with corrugated webs. Each girder was subjected to uniform torsion with both ends free to warp and rotate, and the equivalent torsion constant I_t^e was calculated based on the total angular displacement over the length of the beam, using equation 5.15. The equivalent torsion constant obtained using this equation was compared to that obtained using the proposed cantilever method. The two methods gave similar values with a maximum difference of 3 percent for the girders considered. The results can be seen in Appendix D.

$$I_t^e = \frac{QL}{G\theta_L} \quad (5.15)$$

6 Finite Element models

The results presented in this report are based on Finite Element analyses performed in ABAQUS CAE version 6.12-1. This chapter describes in detail how the different models have been established. All analyses have been performed using eight node shell elements with quadratic base functions and reduced integration (S8R). The elements had five integration points over their thickness and the Simpson thickness integration rule was used. The analyses were performed using linear material response with a modulus of elasticity E of 210 GPa and Poisson's ratio ν of 0.3. Unless otherwise stated, the type of analysis performed was static analysis.

It should be noted that the material thickness was applied to the shell elements in the Abaqus models from the centre of the web, flanges and stiffeners respectively, which caused a material overlap in the connections between the elements comprising the cross-section as illustrated in figure 6.1. The influence of this overlap on the results was considered to be negligible.

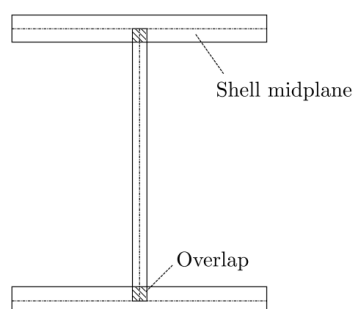


Figure 6.1: *Illustration of the material overlap in the connection between web and flange in the FE models.*

Welds between the flanges and the web were not included in any of the FE models or considered in any analytical calculations.

In order to verify that the results obtained from the FE models were accurate, a number of different simulations were performed. Since accurate analytical expressions exist for calculating stresses, deformations and critical buckling moments of prismatic members, these expressions can be used to evaluate the accuracy of the FE models. Therefore, all of the verification simulations were carried out for girders with flat webs. The geometry used and the results obtained from these verification studies are found in Appendix E except for the results of the model described in section 6.4, which are found in Appendix D. The models proved to be valid for prismatic I-girders and it is therefore assumed that they can be used for girders with corrugated webs as well.

6.1 Bending about the strong axis of a simply supported girder

When modelling bending about the strong axis, the boundary conditions simulate fork supports and were modelled as follows (see figure 6.2); at point *A*, displacements in all directions (*x*, *y* and *z*) and rotation about the longitudinal axis (*x*) were prevented. Vertical (*z*) and lateral (*y*) displacements were prevented at point *B*, as well as rotation about the longitudinal axis (*x*). In addition to this, all nodes on line *a* and line *b* were assigned a coupling condition, preventing displacement in the lateral direction (*y*) relative to point *A* and point *B* respectively. These coupling conditions are applied in order to prevent local buckling of the web caused by stress concentration at points *A* and *B*.

The girder was subjected to a uniform bending moment of 1 kNm, which was applied to the girder by adding shell edge loads normal to the flange edges, creating a force couple at each end. The load followed the nodal rotation and its magnitude was defined for the undeformed geometry.

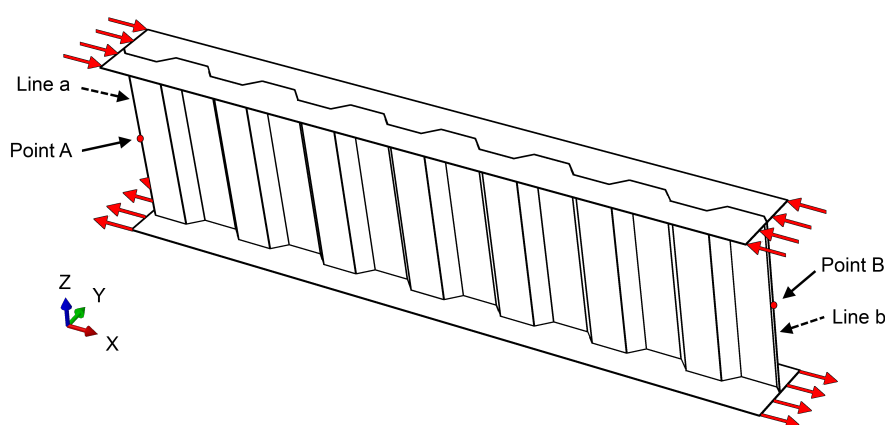


Figure 6.2: Definition of loading and boundary conditions for bending about the strong axis (*y*).

Verification of the model The mid-span deflection and the longitudinal stresses in the flanges obtained from the FE simulations for girders with flat webs were compared to the corresponding analytically calculated values. The results obtained using the FE model proved to be accurate, with a maximum difference of 4 percent for the stresses and less than 1 percent for the deflection.

6.2 Bending about the weak axis of a simply supported girder

As for bending about the strong axis, the web is assumed to give zero contribution to the bending stiffness about the weak axis. This assumption was verified by comparing the stresses

and deflections at mid-span obtained from FE simulations to the corresponding values calculated analytically. It was difficult to apply bending moments about the weak axis at the ends of the girder. Because of this, an evenly distributed lateral load of 1 kN/m was applied at the flanges. Again, the stresses and deflections at mid-span were measured in FE models and compared to analytical calculations based on the assumption that the web does not contribute to the bending stiffness about the weak axis.

The boundary conditions were, again, simulating fork supports and were applied exactly as when studying bending about the strong axis, see section 6.1. The load was applied as shell edge loads acting normal to the flanges according to figure 6.3. The load followed the nodal rotation and its magnitude was defined for the undeformed geometry.

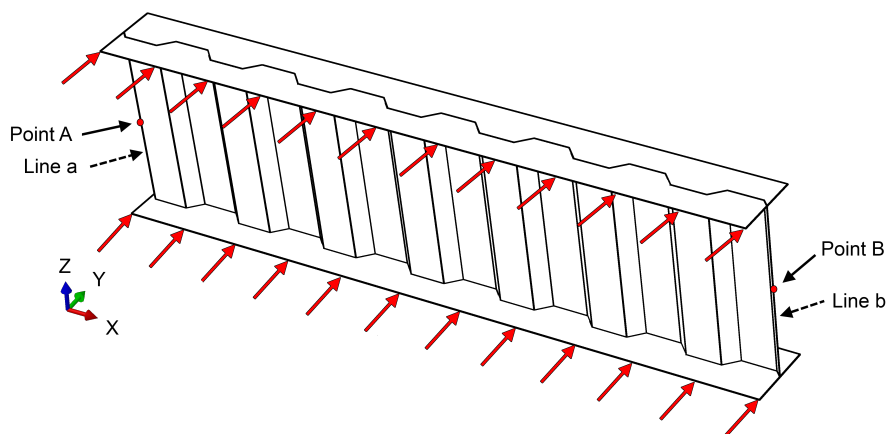


Figure 6.3: Definition of loading and boundary conditions for bending about the weak axis (z).

Verification of the model In order to verify the model, the lateral deflection and longitudinal flange stresses at mid-span were obtained from FE simulations for girders with flat webs, using this model. Again, these values were compared to the corresponding analytically calculated values. The finite element model proved accurate, with a maximum deviation of 1 percent for the stresses and less than 1 percent for the deflection.

6.3 Uniform torsion of an unrestrained girder

When calculating the torsion constant I_t (equivalent torsion constant I_t^e for girders with corrugated web), a girder without torsion or warping restraints at the ends was exposed to a constant torsional moment of 1 kNm and the angular displacement was obtained. This analysis was only performed for a few girders in order to verify that the approach used in section 5.1 is accurate when calculating the equivalent torsion constant I_t^e . By studying this load case, the assumption used in previous research [11][12][13], stating that the torsion constant of a girder with corrugated web is equal to that of a girder with a flat web, can be evaluated.

The torsional moment was applied as shell edge loads acting as shear on the flange ends as shown in figure 6.4. The load followed the nodal rotation and its magnitude was defined for

the undeformed geometry. The girder is stable in itself due to symmetry and no boundary conditions are required.

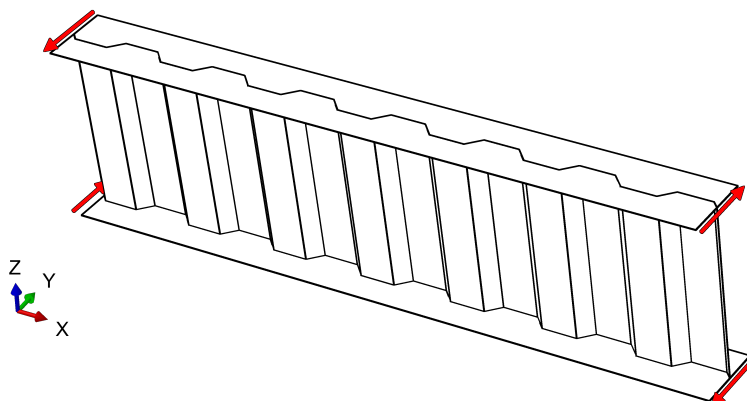


Figure 6.4: *Definition of loading conditions used when studying uniform torsion.*

Verification of the model When verifying this model for girders with flat webs, the total angular displacement over the length of the girder, obtained from FE simulations, was compared to that calculated analytically using the expression for uniform torsion, see equation 3.22. There was a maximum deviation of 5 percent for the girders included in the study.

6.4 Non-uniform torsion of a cantilever

In order to find the equivalent torsion constant I_t^e and the equivalent warping constant I_w^e , a cantilever was exposed to a concentrated torsional moment with the magnitude 1 kNm at the free end. The sectional constants were calculated from the angular displacement at the free end and the longitudinal stresses in the flanges at the fixed end, according to the method described in section 5.1.

The boundary- and loading conditions used in this model are shown in figure 6.5. Displacement was prevented in all directions (x , y , z) for the nodes on the web at the fixed end, i.e. the nodes on line a . For the nodes on lines b , the displacement in the longitudinal direction (x) was prevented. Vertical and lateral displacements were unrestrained on lines b in order to allow for strain in these directions caused by the Poisson effect following the longitudinal strains. The torsional moment at the free end was applied by adding shell edge loads acting as shear on the flange ends. The load followed the nodal rotation and its magnitude was defined for the undeformed geometry.

Verification of model In order to verify this model, the torsion constant I_t and warping constant I_w obtained using the proposed method for girders with flat webs using FE simulations are compared to those given by LTBEAM, an analytical software treating lateral-torsional buckling. The model provides results that agree reasonably well with those obtained from

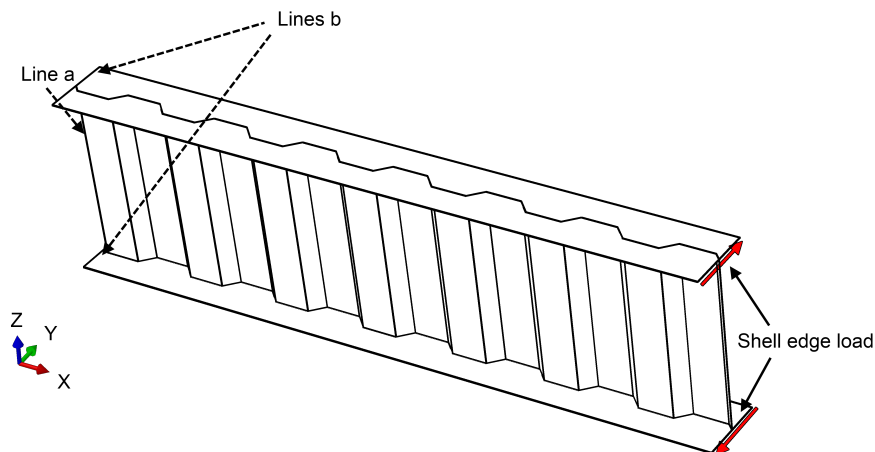


Figure 6.5: *Definition of loading and boundary conditions for the torsionally loaded cantilever.*

LTBEAM, with a maximum difference of 6 percent for the torsion constant I_t and a maximum difference of 5 percent for the warping constant I_w .

6.5 Critical lateral-torsional buckling moment of a simply supported girder

In order to find the elastic critical lateral-torsional buckling moment, linear buckling analyses were performed using the subspace eigensolver in ABAQUS CAE. The boundary- and loading conditions in these analyses were exactly the same as those used for bending about the strong axis, which are described in section 6.1. In short, the model consists of a simply supported girder with fork supports exposed to a constant bending moment about the strong axis with a magnitude of 1 kNm. The critical buckling moment is found by multiplying the eigenvalue of the first positive global lateral-torsional buckling mode by the applied unit bending moment of 1 kNm.

Verification of the model The elastic critical bending moment of girders with flat webs obtained from the FE linear buckling analyses was compared to results from LTBEAM with a maximum error of 1 percent.

Comments This type of analysis proved to be very sensitive when it comes to boundary conditions. The boundary conditions used in the models are those which best simulate the analytical fork supports, which are used when deriving the analytical expression for the critical buckling moment.

It should be noted that even if a certain set of boundary conditions produces good results in terms of stresses or deflections in a static analysis, it may still give very inaccurate results when using it in a linear buckling analysis. A model should always be verified using the appropriate analytical expression if such an expression exists.

6.6 Convergence studies

In order to find a suitable mesh density and element type to be used in the FE simulations, convergence studies were performed for two of the models - the linear buckling analysis of a simply supported girder subjected to bending and the static analysis of a cantilever subjected to torsion. These two models were selected because they were the two models used to the greatest extent in this project. They also include all types of response included in the other models (bending, torsion and warping). Both studies were conducted for a girder with corrugated web, with dimensions according to table 6.1.

Table 6.1: *The geometry of the girder used in the convergence studies. All dimensions in millimetres unless otherwise stated.*

L [m]	b_f	t_f	h_w	t_w	a	b	c	d	α [°]
9.5	200	12	700	2	140	50	71	25	45

Two different element types were used in the analyses; eight node shell elements with quadratic base function and reduced integration (S8R) and four node shell elements with linear base function and reduced integration (S4R). The results from the convergence study performed for the linear buckling model can be seen in figure 6.6 while the corresponding results for the convergence studies performed for the cantilever model are found in appendix F. The tendencies are the same for both models. S4R elements require a very dense mesh for the limit values to be reached, while S8R elements give good results for a coarser mesh. Even though S8R elements are more complex and require more computations per element, they are chosen instead of S4R elements. The critical buckling moment M_{cr} converges at an element side length of 100 mm with S8R elements. Convergence is reached for the angular displacement θ for an element side length of 40 mm using S8R elements, while an element side length of 50 mm is sufficient to reach convergence for the longitudinal flange stresses at the fixed end, $\sigma_{x,0}$. In the simulations conducted in this project, *S8R elements* with an element side length of 30 mm were used in most of the analyses. For exceptionally long girders, the element side length was increased to 50 mm in order to reduce the computation time.

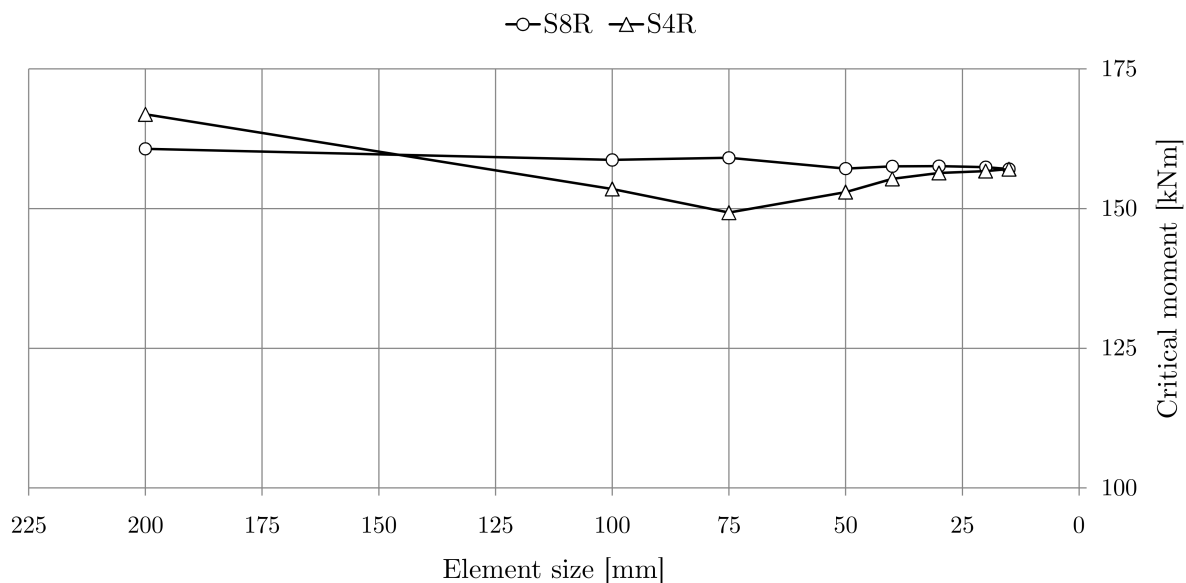


Figure 6.6: Critical buckling moment M_{cr} using different element types (S4R and S8R) with varying element size.

7 Results and discussion

In this section, the results from the different studies performed in this project are presented and discussed. The accuracy of the methods included in this report for calculating the critical buckling moment of simply supported I-shaped girders with corrugated webs is evaluated, which is done by comparing the results obtained using the different methods to results obtained using FE simulations for different geometries. More extensive data from these studies can be found in Appendices G through I.

7.1 Parametric study for evaluating existing methods

In order to verify how well the existing approaches suggested by Lindner, Zhang et al. and Moon et al. agree with results from FE simulations, a parametric study was performed. The critical buckling moments of steel girders with trapezoidally corrugated webs were calculated using these methods, and these values were compared to the critical moments obtained using FE analyses. The results are presented graphically in this section, and are presented numerically in Appendix G. Throughout this parametric study, one base geometry is used (see table 7.1), varying only one parameter at a time. The range of parameter values considered in this study is:

- Flange width, varying from 100 to 400 mm
- Flange thickness, varying from 4 to 24 mm
- Web height, varying from 300 to 1200 mm
- Web thickness, varying from 1 to 10 mm

- Girder length, varying from 5.7 to 26.6 m

Table 7.1: *The basic geometry of the girder used in the parametric study where the established approaches are compared. All dimensions in millimetres unless otherwise stated.*

L [m]	b_f	t_f	h_w	t_w	a	b	c	d	α [°]
9.5	200	12	700	2	140	50	71	25	45

Influence of flange width

When varying the flange width within the range of 100 to 400 mm, the critical buckling moment is strongly dependent on the flange width. All examined methods are reasonably accurate for calculating the critical buckling moment. Looking at figure 7.1 it is hard to distinguish any differences but, by studying the exact values (found in Appendix G), it appears that Moon et al. and Zhang et al. underestimate the critical buckling moment for girders with a small flange width.

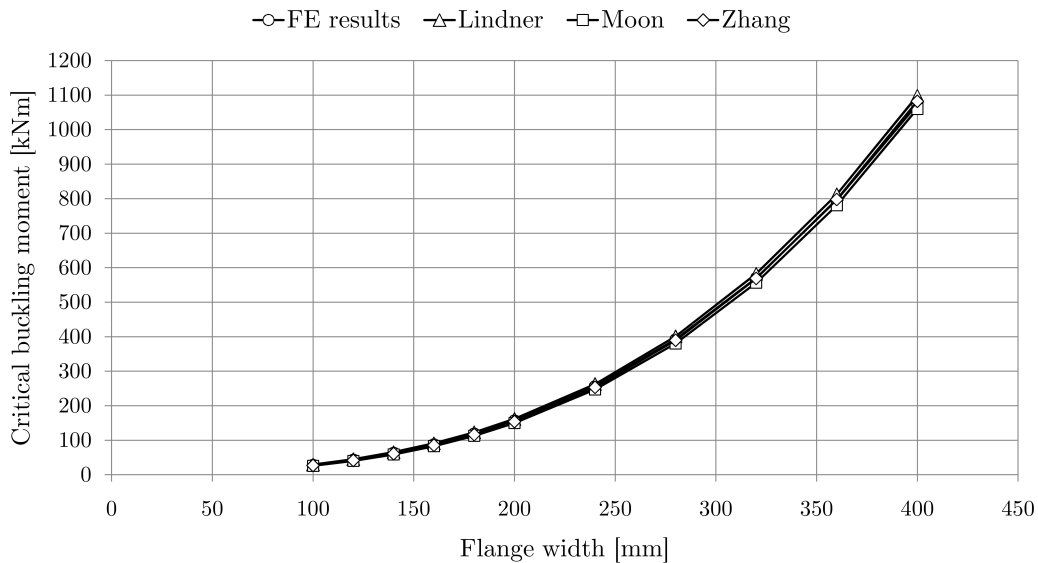


Figure 7.1: *Comparison between critical buckling moment obtained using FE simulations and the approaches suggested by Lindner, Moon et al. and Zhang et al. for varying flange width.*

Influence of flange thickness

The critical buckling moment varies approximately linearly with the flange thickness for thicknesses in the range 4 to 24 mm, as seen in figure 7.2. The methods for calculating the critical buckling moment proposed by Zhang et al. and Moon et al. are quite accurate for the range considered, while Lindner's approach overestimates the critical buckling moment of girders with thick flanges.

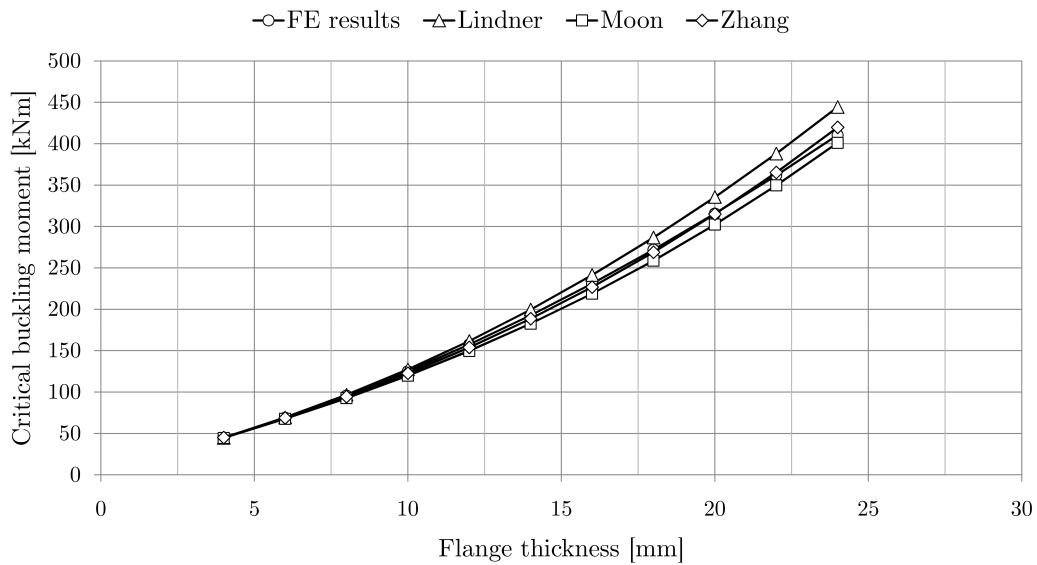


Figure 7.2: Comparison between critical buckling moment obtained using FE simulations and the approaches suggested by Lindner, Moon et al. and Zhang et al. for varying flange thickness.

Influence of web height

For web heights in the range of 300 to 1200 mm, the critical buckling moment varies approximately linearly with the web height, as seen in figure 7.3. It can be noted from the figure that all methods, and that of Moon et al. in particular, are rather inaccurate for low web heights, but give results that agree well with those obtained from FE simulations for high webs.

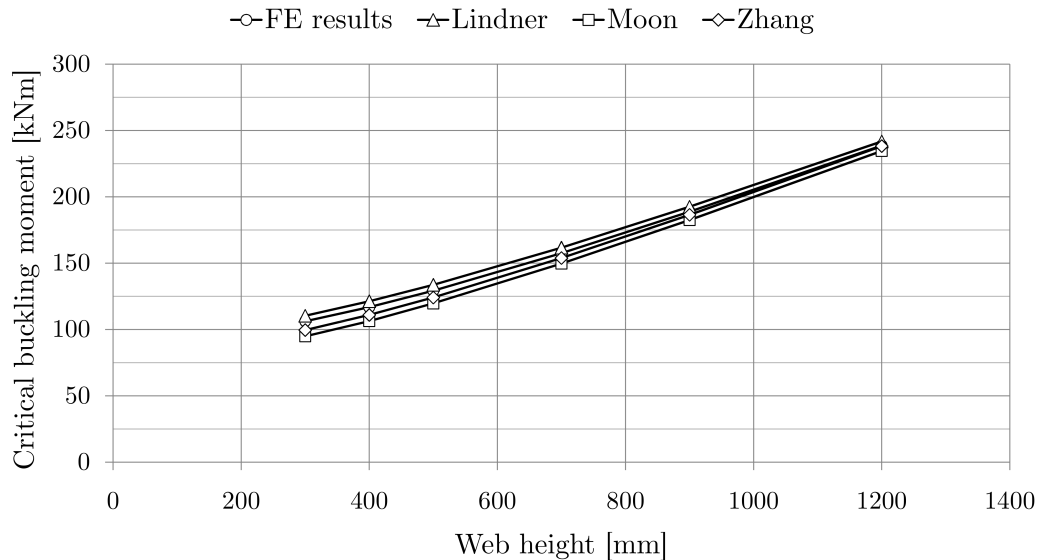


Figure 7.3: Comparison between critical buckling moment obtained using FE simulations and the approaches suggested by Lindner, Moon et al. and Zhang et al. for varying web height.

Influence of web thickness

The critical buckling moment is only slightly affected by the web thickness for the range considered in this study, 1 to 10 mm, as seen in figure 7.4. The thickness of webs with the corrugation profile used in this study is typically in the range of 1 to 4 mm. All the methods included in this study have the same tendency as the results obtained from FE simulations.

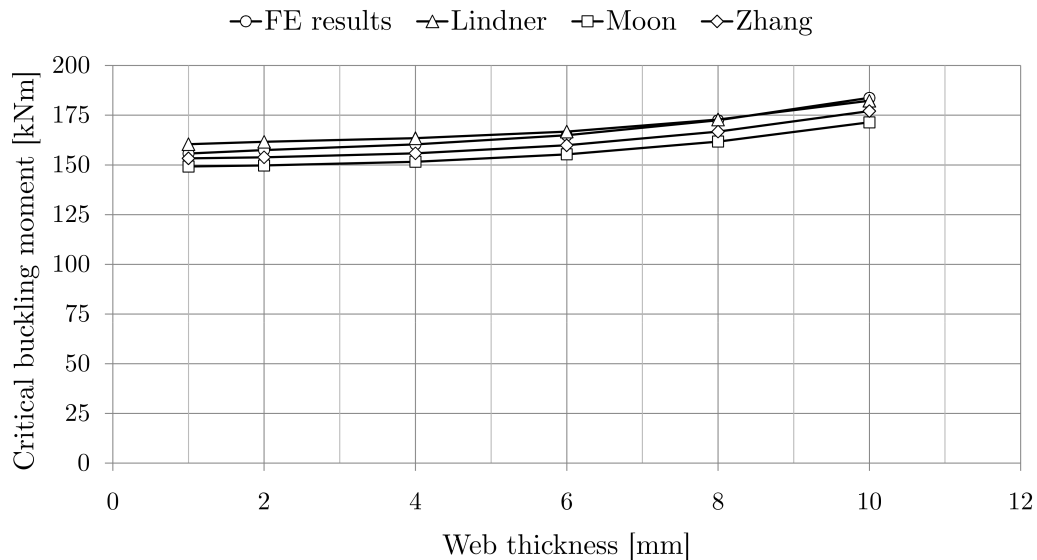


Figure 7.4: Comparison between critical buckling moment obtained using FE simulations and the approaches suggested by Lindner, Moon et al. and Zhang et al. for varying web thickness.

Influence of girder length

The critical buckling moment significantly decreases as the length of the girder increases as seen in figure 7.5. By studying the results graphically it appears that all methods considered agree very well with the results from FE simulations, but by studying the numerical results presented in Appendix G it is clear that Zhang et al. and Moon et al. underestimate the capacity of long girders - for the longest girder considered in this study, the ratio between the results obtained using the methods proposed by Zhang et al. and Moon et al. compared to the FE results is 0.91 and 0.87 respectively. The corresponding ratio when using the method proposed by Lindner was 1.04. The approaches suggested by Moon et al. and Zhang et al. attribute the extra capacity provided by the corrugated web to the warping constant independent of the girder length, while the expression for the warping constant suggested by Lindner includes the girder length as a factor. This is studied and discussed in detail in section 7.2.

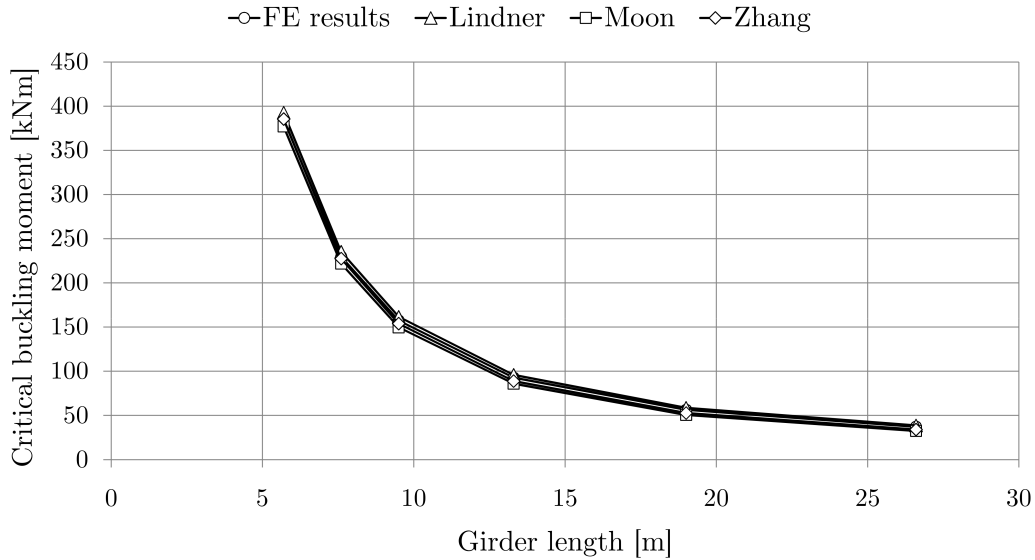


Figure 7.5: Comparison between critical buckling moment obtained using FE simulations and the approaches suggested by Lindner, Moon et al. and Zhang et al. for varying girder length.

7.2 Influence of girder length on the critical buckling moment

In chapter 4, where the torsional response of prismatic and non-prismatic girders is studied, the authors suggest that the extra rotational stiffness provided by the corrugated web should be accounted for by using an increased torsion constant I_t , a statement which is evaluated in this section. By studying equation 7.1, it can be recognised that the critical buckling moment of long girders is mainly governed by the torsion constant since I_t is multiplied by a factor L^2 . Consequently, the warping constant I_w has a stronger influence on the critical buckling moment of short girders. By studying a large range of girder lengths, the accuracy of the torsion and warping constants obtained by using the different methods can be evaluated.

$$M_{cr} = \frac{\pi^2 EI_z}{L^2} \sqrt{\frac{I_w}{I_z} + \frac{L^2 GI_t}{\pi^2 EI_z}} \quad (7.1)$$

The critical buckling moments are calculated for a large range of girder lengths using four different approaches; the method proposed in this report (section 5.1), the method proposed by Lindner (section 3.1), the method proposed by Moon et al. (section 3.2) and the method proposed by Zhang et al. (section 3.3). Three different cross-sections are considered, with geometry according to table 7.2. The critical buckling moments M_{cr} obtained using these methods are compared to the critical buckling moments M_{cr}^{FE} obtained from linear buckling analyses performed by using ABAQUS CAE. The accuracy of the different methods is illustrated by plotting the ratios between these moments. The results for profile 2 are plotted in figure 7.6. The plots for profiles 1 and 3 are found in Appendix H.

Table 7.2: *Geometry of girders with corrugated webs used in the comparative study. All dimensions in millimetres unless otherwise stated.*

ID	L [m]	b_f	t_f	h_w	t_w	a	b	c	d	α [°]
1	3.8 - 34.2	160	8	200	2	140	50	71	50	45
2	3.8 - 34.2	200	12	400	2	140	50	71	50	45
3	3.8 - 34.2	240	12	700	2	140	50	71	50	45

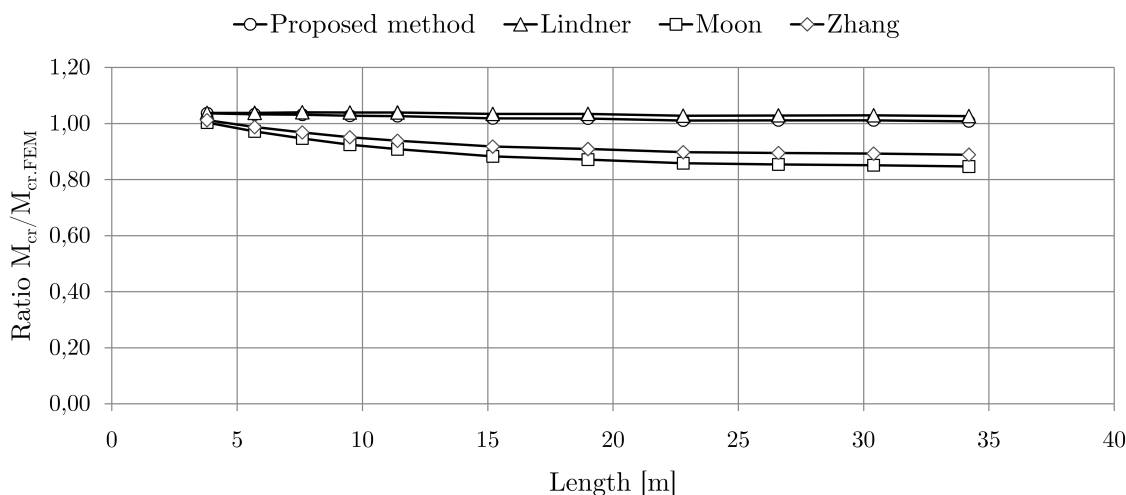


Figure 7.6: *Ratio between elastic critical buckling moment obtained using the different approaches and FE results for profile 2 in table 7.2.*

From figure 7.6 it is concluded that the results obtained using the method suggested by Lindner and the method proposed by the authors of this report agree well with the results from the FE-simulations, indicated by a ratio of approximately 1.0. The results obtained using the methods proposed by Moon et al. and Zhang et al. are acceptable for short members, but these approaches underestimate the capacity of long girders with the ratio converging to a value below one (approximately 0.85 and 0.90 respectively for profile 2 as seen in figure 7.6). As previously explained, the torsion constant I_t mainly governs the critical buckling moment of long girders. The results obtained using the methods suggested by Moon et al. and Zhang et al., where the capacity of long girders is underestimated, indicate that these methods underestimate the torsion constant.

Lindner, Moon et al. and Zhang et al. all assume that the torsion constant I_t of a girder with a corrugated web is equal to that of a girder with a flat web, and that the extra stiffness provided by the corrugated web is attributed to the warping constant I_w . These three approaches are described in sections 3.1 through 3.3. In the expression stated by Lindner, the warping constant increases quadratically with the girder length L , whereas the expressions for the warping constant stated by Moon et al. and Zhang et al. do not include the length of the girder. The results for these two methods, table 7.3 and 7.4, are very similar. The modified Lindner method, presented in section 3.1.1, produces the same critical buckling moment as the method proposed by Lindner, but in the modified method the extra lateral-torsional buckling resistance is attributed to the torsion constant instead of the warping constant. None of the

cross-sectional constants in the modified Lindner method are dependent on the girder length. The torsion and warping constants obtained using these four methods are compared to those obtained using the method proposed in this report, and the results are presented in tables 7.3 through 7.6.

Table 7.3: *Torsion and warping constants obtained by using the method proposed by Moon et al. (\bar{I}_t, \bar{I}_w) and by using the method proposed in this report (I_t^e, I_w^e) for the different cross-sections presented in table 7.2. Torsion constants given in m^4 and warping constants given in m^6 .*

ID	\bar{I}_t	\bar{I}_w	I_t^e	I_w^e	$\frac{\bar{I}_t}{I_t^e}$	$\frac{\bar{I}_w}{I_w^e}$
1	5.52E-8	5.53E-8	7.72E-8	5.54E-8	0.71	1.00
2	2.32E-7	6.45E-7	3.02E-7	6.44E-7	0.77	1.00
3	2.78E-7	3.41E-6	3.54E-7	3.38E-6	0.79	1.00

Table 7.4: *Torsion and warping constants obtained by using the method proposed by Zhang et al. (\hat{I}_t, \hat{I}_w) and by using the method proposed in this report (I_t^e, I_w^e) for the different cross-sections presented in table 7.2. Torsion constants given in m^4 and warping constants given in m^6 .*

ID	\hat{I}_t	\hat{I}_w	I_t^e	I_w^e	$\frac{\hat{I}_t}{I_t^e}$	$\frac{\hat{I}_w}{I_w^e}$
1	5.52E-8	5.53E-8	7.72E-8	5.54E-8	0.71	1.00
2	2.32E-7	6.46E-7	3.02E-7	6.44E-7	0.77	1.00
3	2.78E-7	3.42E-6	3.54E-7	3.38E-6	0.79	1.01

Table 7.5: *Torsion and warping constants obtained by using the method proposed by Lindner (I_t^*, I_w^*) and by using the method proposed in this report (I_t^e, I_w^e) for the different cross-sections presented in table 7.2. Torsion constants given in m^4 and warping constants given in m^6 .*

ID	$L[m]$	I_t^*	I_w^*	I_t^e	I_w^e	$\frac{I_t^*}{I_t^e}$	$\frac{I_w^*}{I_w^e}$
1	3.8	5.52E-8	6.70E-8	7.72E-8	5.54E-8	0.71	1.21
1	34.2	5.52E-8	1.06E-6	7.72E-8	5.54E-8	0.71	19.13
2	3.8	2.32E-7	6.86E-7	3.02E-7	6.44E-7	0.77	1.07
2	34.2	2.32E-7	4.38E-6	3.02E-7	6.44E-7	0.77	6.8
3	3.8	2.78E-7	3.45E-6	3.54E-7	3.38E-6	0.79	1.02
3	34.2	2.78E-7	8.21E-6	3.54E-7	3.38E-6	0.79	2.43

By comparing the cross-sectional constants obtained using the methods suggested by Moon et al. and Zhang et al. to those obtained using the method proposed in this report, see tables 7.3 and 7.4, it can be concluded that the torsion constants \bar{I}_t and \hat{I}_t are underestimated while the warping constants \bar{I}_w and \hat{I}_w are very similar. This verifies that, as previously explained, the methods proposed by Moon et al. and Zhang et al. underestimate the critical buckling moment of long girders. Since the expressions for calculating the *warping* constants used in these two methods appear to be accurate, these expressions should not be ruled out entirely. However, in this report, these methods will not be studied further.

Table 7.6: *Torsion and warping constants obtained by using the modified Lindner method (I'_t, I'_w) and by using the method proposed in this report (I_t^e, I_w^e) for different cross-sections presented in table 7.2. Torsion constants given in m^4 and warping constants given in m^6 .*

ID	I'_t	I'_w	I_t^e	I_w^e	$\frac{I'_t}{I_t^e}$	$\frac{I'_w}{I_w^e}$
1	7.72E-8	5.46E-8	7.72E-8	5.54E-8	1.00	0.99
2	3.14E-7	6.40E-7	3.02E-7	6.44E-7	1.04	0.99
3	3.84E-7	3.39E-7	3.54E-7	3.38E-7	1.08	1.00

The method suggested by Lindner results in critical buckling moments that agree well with results from linear buckling analyses (see figure 7.6), while the torsion and warping constants I_t^* and I_w^* differ strongly from those obtained using the method proposed in this report. The difference between the warping constants for long girders is very large which can be explained by the length factor included in the expression suggested by Lindner, see equation 3.1.

The cross-sectional constants obtained using the modified Lindner method agree well with those obtained by using the proposed method. The warping constants deviate no more than 1 percent, whereas the torsion constants deviate slightly more with a maximum deviation of 8 percent (see table 7.6). The authors conclude that the modified Lindner method results in cross-sectional constants similar to those obtained using the proposed method, which has proved to agree well with results from FE simulations of lateral-torsional buckling.

7.3 Accuracy of the modified Lindner method for arbitrary corrugation profiles

For the girders studied in section 7.2, the cross-sectional constants obtained using the modified Lindner method (described in section 3.1.1) corresponds well to the results obtained using the method proposed in this report, which have proved to agree well with FE simulations of lateral-torsional buckling. However, the same corrugation profile was used in all those simulations. The corrugation profile which was used is one of the profiles most commonly produced by Borga Steel Buildings, and is very similar to the profile used by Lindner [14]. The geometry of these two profiles is shown in table 7.7.

Table 7.7: *Geometry of two corrugation profiles; the one used by Lindner [14] when verifying the expression for calculating the warping constant of girders with corrugated webs and a profile commonly used by Borga Steel Buildings. All dimensions in millimetres unless otherwise stated.*

	a	b	c	d	α [°]
Lindner	148	52	73.5	26	45
Borga	140	50	70.7	25	45

In order to investigate whether the modified Lindner method is valid for arbitrary corrugation profiles, the critical buckling moments and equivalent cross-sectional constants were calculated for girders with three different corrugation profiles. Since the torsion constant I_t has a greater

effect on the critical buckling moment for long girders and the warping constant I_w has a larger influence when considering shorter girders, one long and one short girder were studied for each corrugation profile. The geometry of the girders can be seen in table 7.8 and the results from the study are found in table 7.9.

Table 7.8: *Cross-sections and corrugation profiles used to verify the modified Lindner method. Dimensions in millimetres unless otherwise stated.*

ID	L[m]	a	b	d_{max}	$\alpha[^\circ]$	b_f	t_f	h_w	t_w
4a	4.8	70	50	25	45	200	12	400	2
4b	24	70	50	25	45	200	12	400	2
5a	4.8	140	100	25	26.6	200	12	400	2
5b	24	140	100	25	26.6	200	12	400	2
6a	4.94	140	50	10	21.8	200	12	400	2
6b	24.32	140	50	10	21.8	200	12	400	2

Table 7.9: *Critical buckling moment and cross-sectional constants obtained using the modified Lindner method and the method proposed in this report. Torsion constants in m^4 and warping constants in m^6 , critical buckling moments in kNm .*

ID	M_{cr}^{FE}	M_{cr}^L	M_{cr}^e	$\frac{M_{cr}^L}{M_{cr}^{FE}}$	$\frac{M_{cr}^e}{M_{cr}^{FE}}$	I'_t	I'_w	I_t^e	I_w^e	$\frac{I'_t}{I_t^e}$	$\frac{I'_w}{I_w^e}$
4a	340.2	349.4	348.9	1.03	1.03	-	-	-	-	-	-
4b	40.6	41.2	40.8	1.01	1.00	3.37E-7	6.40E-7	3.30E-7	6.44E-7	1.02	0.99
5a	323.7	337.6	338.0	1.04	1.04	-	-	-	-	-	-
5b	36.4	37.1	37.0	1.02	1.02	2.68E-7	6.40E-7	2.66E-7	6.44E-7	1.01	0.99
6a	301.0	317.3	314.9	1.05	1.05	-	-	-	-	-	-
6b	33.5	35.1	34.2	1.05	1.02	2.45E-7	6.40E-7	2.30E-7	6.40E-7	1.08	1.00

It can be observed from table 7.9 that the critical buckling moments M_{cr}^L obtained using the modified Lindner method agree well with the results obtained from the linear buckling FE analyses for these different corrugation profiles. This indicates that the modified Lindner method is valid for an arbitrary geometry of the girder. The method proposed in this report also produces critical buckling moments M_{cr}^e similar to those obtained from the linear buckling analyses regardless of the corrugation profile. These results are more accurate for long members, which can be explained by the fact that the approximations included in the proposed method caused a larger error for short girders, see section 5.1. For this reason, the torsion and warping constants I_t^e and I_w^e are calculated for the long girders in table 7.8.

The equivalent sectional constants I_t^e and I_w^e obtained using the method proposed in this report have previously proved to be accurate, and are used as reference values when evaluating the sectional constants I'_t and I'_w calculated using the modified Lindner method. As seen in table 7.9, both the torsion and warping constants I'_t and I'_w are accurate for the different corrugation profiles. This indicates that the modified Lindner method is valid for calculating both the critical buckling moment and the torsion and warping constants.

Another observation that can be made from the results in table 7.9 is that the warping constant

I'_w agrees very well with that obtained using the method proposed in this report, with a maximum difference of *1 percent*. The same tendency can be seen in table 7.6 and for the girders studied in Appendix I. This indicates that the expression used in the modified Lindner method for calculating the warping constant of girders with corrugated webs, I'_w , which is the exact same expression as for girders with flat webs (equation 3.6b), is valid for an arbitrary corrugation profile. This would mean that the entire extra stiffness provided by the corrugated web should be accounted for by an increased equivalent torsion constant, while the warping constant is calculated as for a girder with flat web. This is exactly the opposite of what was stated in all the previous research reviewed in this report. Before this can be concluded, more extensive studies must be performed.

8 Conclusions

It is stated in previous research that the resistance against lateral-torsional buckling of girders with corrugated webs is higher than that of girders with flat webs. While this statement was verified in this project, it was found that this increase in resistance should be accounted for in a different way than suggested in previous research.

All previous research presented in this report is based on the assumptions that the extra stiffness provided by the corrugated web should be attributed to the warping constant I_w , and that the torsion constant I_t is equal to that of a girder with flat web. In chapter 4, it is concluded that this assumption is incorrect, and that the torsion constant should be increased due to the corrugated web.

In chapter 5, a method for calculating the equivalent torsion and warping constants of I-shaped girders is established. The validity of these cross-sectional constants was evaluated by studying the lateral-torsional buckling behaviour and the torsional response of I-shaped girders, with both flat and corrugated webs. The results from these studies show that the equivalent torsion and warping constants obtained using the proposed method are valid for any I-shaped girder with constant height.

The models proposed by Moon et al. and Zhang et al. both rely on the basic assumptions originally stated by Lindner, i.e. that the extra rotational stiffness provided by the web corrugations should be attributed to the warping constant I_w , while the torsion constant I_t is assumed to be the same as for a prismatic girder. The methods are similar in the sense that they both account for the extra stiffness provided by the corrugated web by considering a prismatic girder with an eccentric web. Moon et al. use sectorial coordinates with an *average web eccentricity*, while the expression presented by Zhang et al. considers an *average stiffness contribution* due to the web eccentricity as explained in sections 3.2 and 3.3 respectively. Since the torsion constant I_t is underestimated and the warping constant I_w is overestimated in both those methods, the critical buckling moments of long girders will be underestimated while the critical buckling moments of short girders will be overestimated. This is clear when studying the expression for the critical buckling moment seen in equation 2.6.

In the method established by Lindner, the extra rotational stiffness provided by the web corrugations is attributed to the warping constant I_w^* , while the torsion constant is assumed to be equal to that of a girder with flat web. In the expression originally stated by Lindner, the warping constant is dependent on the girder length, which is typically not the case for cross-sectional constants. A modified version of Lindner's method is proposed in this report, where the extra rotational stiffness is attributed to the torsion constant I_t' instead. This is done by rewriting the original expressions for the torsion and warping constants, yielding expressions which result in *exactly the same* critical buckling moment as the expressions originally stated by Lindner (see section 3.1). The modified Lindner method results in torsion and warping constants I_t' and I_w' which agree well with those obtained using the method proposed in this report, and seems to be valid for I-shaped girders with arbitrary corrugation profiles. For the girders studied in this project, the warping constant I_w' is approximately equal to that of a girder with a flat web, but further studies must be performed before this can be concluded.

9 Suggestions for further research

The conclusions presented in this report are not sufficient for design of girders with corrugated webs with regard to lateral-torsional buckling. Before a design process can be established, complementary research must be performed. The authors of this report suggest that the following subjects are investigated:

- Establish an expression for calculating the torsion and warping constants I_t and I_w of girders with trapezoidally corrugated webs.

It appears that the modified Lindner method provides accurate torsion and warping constants for girders with trapezoidally corrugated webs. However, in this report only a few different corrugation profiles have been considered, and while the method has produced good results for these profiles, a more extensive study with a wider range of geometries and corrugation profiles should be performed. The method proposed in this report, which is based on FE simulations, could be used as a tool for verifying the cross-sectional constants.

- Investigate the influence of initial stresses and imperfections on the critical buckling moment of girders with trapezoidally corrugated webs.

All the results presented in this report are based on elastic analyses. In order to investigate the effect from initial stresses and imperfections, as well as local stress concentrations caused by the corrugated web, plastic analyses of girders with corrugated webs must be performed. Using plastic analyses, the imperfection factor α_{LT} can be established for girders with corrugated webs. With α_{LT} known, the design moment with regard to lateral-torsional buckling, $M_{R,LT}$, can be calculated.

References

- [1] M. Al-Emrani, B. Edlund, and R. Haghani. “Girders with trapezoidally corrugated webs under patch loading”. *Nordic Steel Construction Conference*. Norwegian Steel Association and NTNU, Oslo, 2012, pp. 107–116.
- [2] European committee for standardization. *Eurocode 3 - Design of steel structures*. 2006.
- [3] S. Timoshenko and J. Gere. *Theory of elastic stability*. 2nd ed. Engineering societies monographs. McGraw-Hill Book Company, 1961.
- [4] CTICM - Centre technique de la construction métallique. *NCCI: Elastic critical moment for lateral torsional buckling*. 2005.
- [5] E. Y. Sayed-Ahmed. Lateral torsion-flexure buckling of corrugated web steel girders. *Proceedings of the Institution of Civil Engineers - Structures & Buildings* 158.1 (2004), 53–69.
- [6] B. Åkesson. *Handbook for analysis of beams subjected to torsion (Swedish Title: Handbok i analys av balkars vridning)*. Gothenburg: Chalmers University of Technology, 1969.
- [7] P. A. Seaburg and C. J. Carter. *Torsional analysis of structural steel members*. Steel design guide series 9.
- [8] B. Åkesson, H. Nylander, and B. Johansson. *Construction - Handbook for civil engineering (Swedish Title: Bygg - handbok för hus-, väg- och vattenbyggnad. Huvuddel 1A - Allmänna grunder)*. 3rd ed. Bygg. Stockholm: AB Byggmästarens förlag, 1971.
- [9] New Zealand Standards. *NZS 3404 Parts 1 and 2*. 1997.
- [10] E. Y. Sayed-Ahmed. Design aspects of steel I-girders with corrugated steel webs. *Electronic Journal of Structural Engineering* 7 (2007), 27–40.
- [11] J. Moon et al. Lateral-torsional buckling of I-girders with corrugated webs under uniform bending. *Thin-Walled Structures* 47.1 (2009), 21–30.
- [12] J. Lindner. “Lateral torsional buckling of beams with trapezoidally corrugated webs”. *Stability of steel structures*. Ed. by M Iványi. Vol. 1. Akadémiai Kiadó, Budapest, 1990, pp. 305–308.
- [13] Z. Zhang, G. Li, and F. Sun. Flexural-torsional buckling of H-beams with corrugated webs. *Advanced Materials Research* 163-167 (2011), 351–357.
- [14] J. Lindner and R. Aschinger. Torsional stiffness of girders with trapezoidal web (German Title: Zur Torsionssteifigkeit von Trapezstegträgern). *Stahlbau* 59 (1990), 113–120.
- [15] T. V. Galambos. *Structural members and frames*. Structural analysis and design. Englewood Cliffs, New Jersey: Prentice Hall, 1968.
- [16] D. M. Lue, J.-L. Liu, and C.-H. Lin. Numerical evaluation on warping constants of general cold-formed steel open sections. *Steel Structures* 7 (2007), 297–309.
- [17] H. Lundh. *Fundamental solid mechanics (Swedish Title: Grundläggande hållfasthetslära)*. Stockholm: KTH, 2000, pp. 321–345.

A Evaluation of assumptions used in previous research

This appendix contains the results from the evaluation of the assumptions used in previous research. The conclusions drawn from the results are that the assumptions regarding the moments of inertia about the strong axis and about the weak axis, I_y and I_z , are accurate, and that the torsion constant I_t is underestimated.

APPENDIX A

Girder	C1	C2	C3	C4	C5	C6	C7	C8	C9
Number of periods	25	25	25	25	25	25	40	40	40
Length [m]	9,5	9,5	9,5	9,5	9,5	9,5	15,2	15,2	15,2
h_m [mm]	700	700	700	1500	1500	1500	700	700	700
t_w [mm]	2	2	2	4	4	4	2	2	2
b_f [mm]	160	160	160	350	350	350	160	160	160
t_f [mm]	8	10	12	16	20	24	8	10	12
a [mm]	140	140	140	140	140	140	140	140	140
b [mm]	50	50	50	50	50	50	50	50	50
d_max [mm]	25	25	25	25	25	25	25	25	25
Bending moment weak [Nm]	11281	11281	11281	11281	11281	11281	28880	28880	28880
Bending moment strong [Nm]	1000	1000	1000	1000	1000	1000	1000	1000	1000
Rotational moment [Nm]	1000	1000	1000	1000	1000	1000	1000	1000	1000
Moment of inertia, strong axis [m^4]	3,14E-04	3,92E-04	4,70E-04	6,30E-03	7,88E-03	9,45E-03	3,14E-04	3,92E-04	4,70E-04
Moment of inertia, weak axis [m^4]	5,46E-06	6,83E-06	8,19E-06	1,14E-04	1,43E-04	1,72E-04	5,46E-06	6,83E-06	8,19E-06
Rotational constant [m^4]	5,65E-08	1,09E-07	1,86E-07	9,88E-07	1,90E-06	3,26E-06	5,65E-08	1,09E-07	1,86E-07
Stress strong axis, Abaqus [MPa]	1,12	0,893	0,745	0,117	0,093	0,078	1,08	0,870	0,725
Stress strong axis, analytical [MPa]	1,12	0,89	0,74	0,12	0,10	0,08	1,12	0,89	0,74
Ratio	1,00	1,00	1,00	0,98	0,98	0,98	0,97	0,97	0,97
Deflection strong axis, Abaqus [mm]	0,167	0,134	0,112	0,008	0,007	0,006	0,429	0,344	0,288
Deflection strong axis, analytical [mm]	0,171	0,137	0,114	0,009	0,007	0,006	0,439	0,351	0,292
Ratio	0,98	0,98	0,98	0,99	0,99	0,99	0,98	0,98	0,98
Stress weak axis, Abaqus [MPa]	165,5	134,3	111,9	17,4	13,9	11,6	430,1	344,2	286,8
Stress weak axis, analytical [MPa]	165,3	132,2	110,2	17,3	13,8	11,5	423,0	338,4	282,0
Ratio	1,00	1,02	1,02	1,01	1,01	1,01	1,02	1,02	1,02
Deflection weak axis, Abaqus [mm]	92,0	73,7	61,4	4,43	3,54	2,95	602,6	482,5	402,4
Deflection weak axis, analytical [mm]	92,47	73,98	61,65	4,42	3,53	2,94	606,0	484,8	404,0
Ratio	0,99	1,00	1,00	1,00	1,00	1,00	0,99	1,00	1,00

Rotation, Abaqus	1,54E+00	8,28E-01	5,00E-01	1,06E-01	5,84E-02	3,60E-02	2,43E+00	1,30E+00	7,85E-01
Rotation, analytical	2,08E+00	1,08E+00	6,32E-01	1,19E-01	6,19E-02	3,61E-02	3,33E+00	1,73E+00	1,01E+00
Ratio Abaqus free to analytical	0,74	0,76	0,79	0,89	0,94	1,00	0,73	0,75	0,78

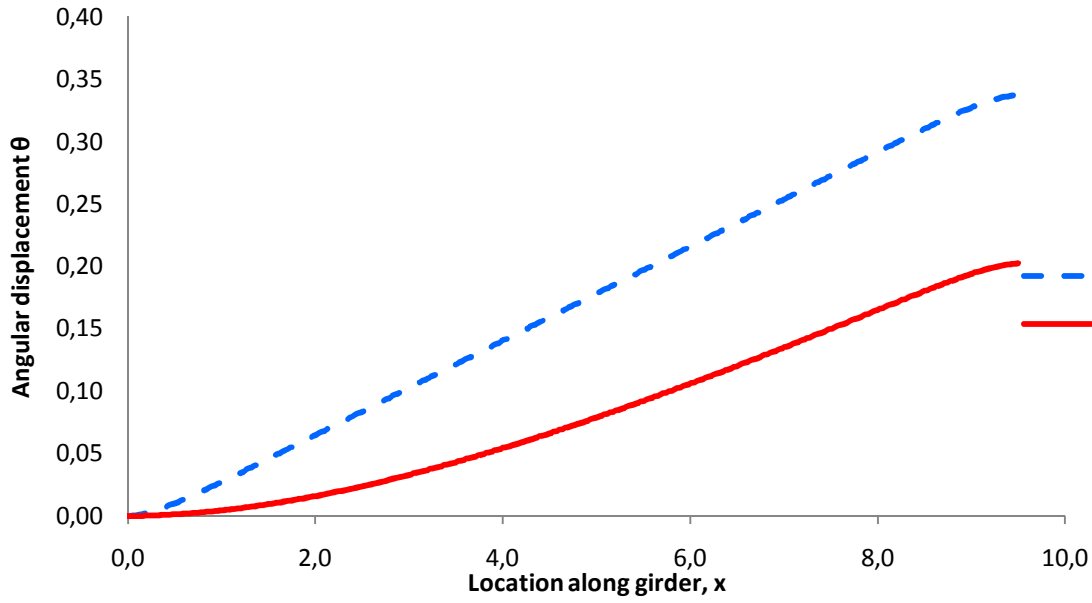
APPENDIX A

B Torsional response of I-shaped girders

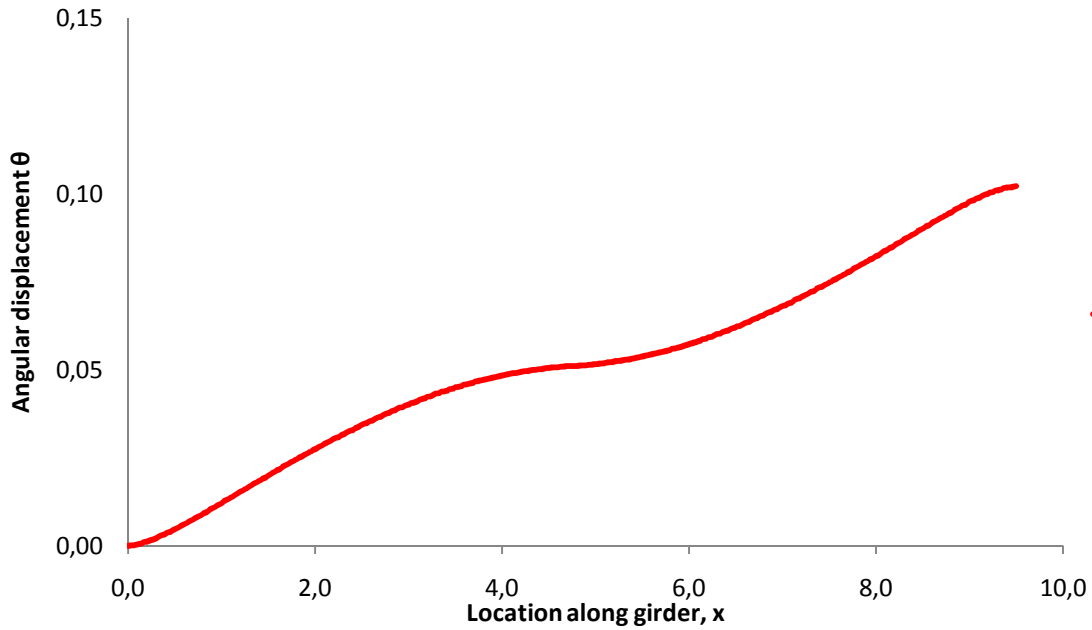
In this appendix, results from FE simulations of different I-shaped girders subjected to torsion are presented. These analyses were the basis of the principle diagrams describing the torsional response of I-shaped girders, with and without;

- Discrete partial warping restraints
- Prevented torsion and warping deformations at the left end
- Corrugated webs

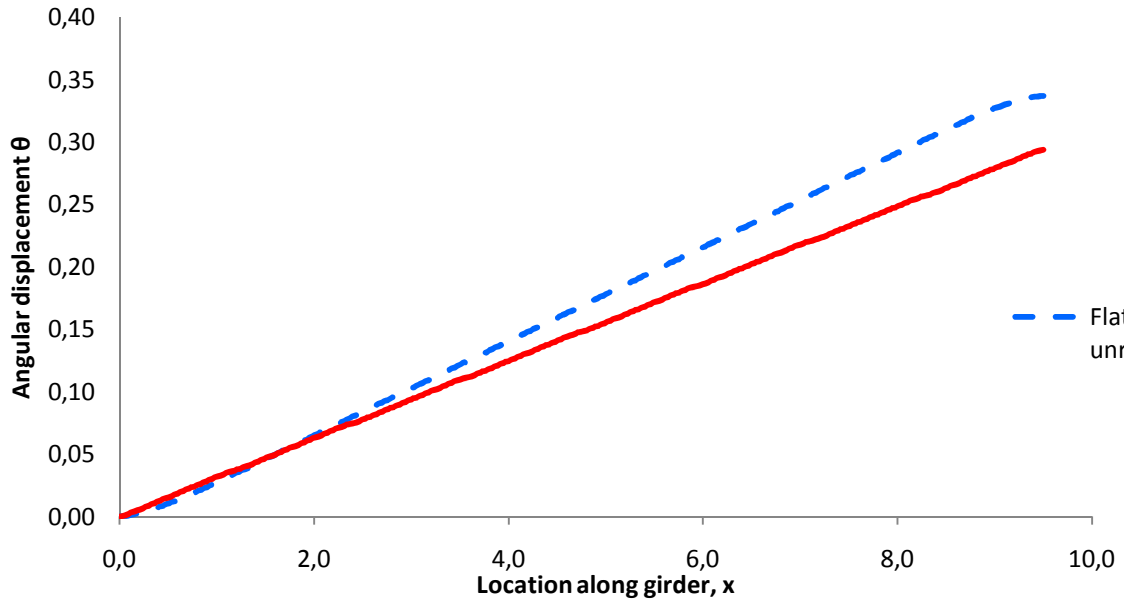
APPENDIX B



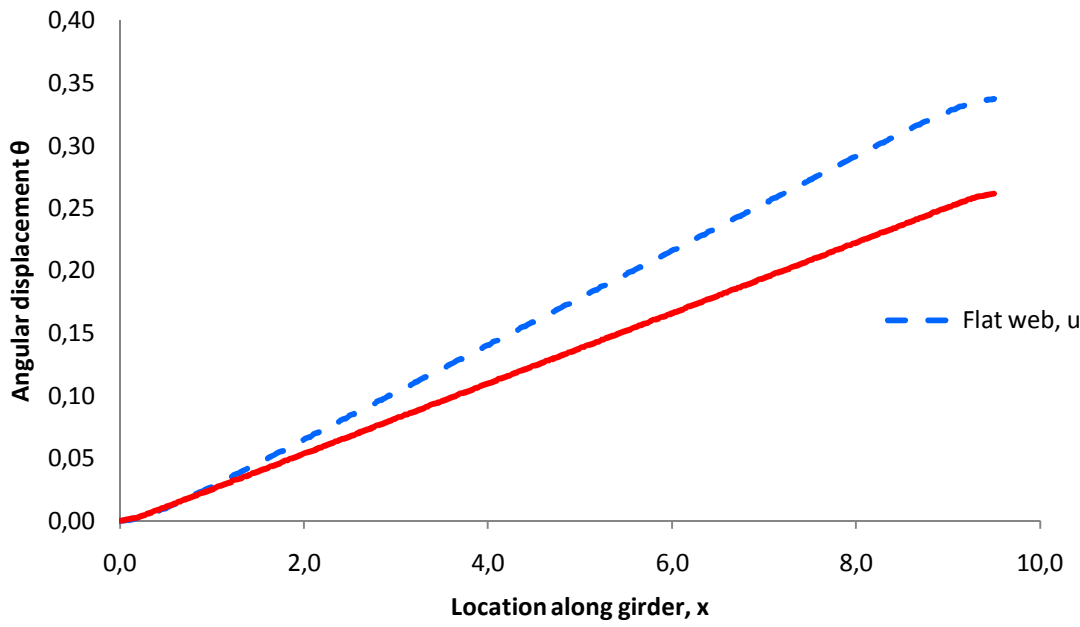
L [m]	9,5
b_f [mm]	200
t_f [mm]	12
h_w [mm]	700
t_w	8
	Flat



L [m]	9,5
b_f [mm]	200
t_f [mm]	12
h_w [mm]	700
t_w	8
t_stiff [mm]	500
	Flat



L [m]	9,5	Flat
b_f [mm]	200	
t_f [mm]	12	
h_w [mm]	700	
t_w	8	
t_stiff [mm]	10	
cc_stiff [mm]	1118	



L [m]	9,5	Flat	Corr
b_f [mm]	200	200	200
t_f [mm]	12	12	12
h_w [mm]	700	700	700
t_w	8	8	8
a [mm]	-	-	140
b [mm]	-	-	50
d_max [mm]	-	-	25

APPENDIX B

C Implementation of the proposed method

This appendix contains a short 'walk-through' of how the torsion and warping constants are calculated in a Mathcad document, using the proposed method.

APPENDIX C

Example of how the equivalent torsion and warping constants are obtained using the proposed method

Material properties

$$E := 210 \cdot \text{GPa} \quad \nu := 0.3$$

$$G := \frac{E}{2(1 + \nu)} = 80.769 \cdot \text{GPa}$$

Load

$$Q := 1000 \text{N} \cdot \text{m}$$

Geometry

$$L := 34.2 \text{m}$$

$$h_w := 200 \text{mm}$$

$$t_w := 2 \text{mm}$$

$$b_f := 160 \text{mm}$$

$$t_f := 8 \text{mm}$$

Bending resistance of one flange

$$W_f := \frac{t_f \cdot b_f^2}{6}$$

Moment of inertia about the weak axis

$$I_z := \frac{t_f \cdot b_f^3}{6} = 5.461 \times 10^{-6} \text{m}^4$$

Input from Abaqus

$$dy := 0.526422 \text{m} \quad \text{Lateral displacement of the top flange at the free end, obtained from Abaqus}$$

$$\varphi := \frac{2dy}{h_w} = 5.26422 \quad \text{Angular displacement at the free end}$$

$$\sigma_x := 200 \text{MPa} \quad \text{Maximum longitudinal stress in the flanges at the fixed end, obtained from Abaqus}$$

Moment in flange

$$M_f := \sigma_x \cdot W_f = 6.827 \cdot \text{kN} \cdot \text{m} \quad \text{Flange moment at the fixed end}$$

$$a := \frac{M_f \cdot h_w}{Q} = 1.365 \text{m} \quad \text{Torsion bending constant}$$

$$I_t := \frac{Q}{G \cdot \varphi} \cdot (L - a) = 7.72241 \times 10^{-8} \text{m}^4 \quad I_w := \frac{G \cdot I_t}{E} \cdot a^2 = 5.53677 \times 10^{-8} \cdot \text{m}^6$$

Control of L/a-ratio

$$\tanh\left(\frac{L}{a}\right) = 1$$

APPENDIX C

D Verification of the proposed method

In this appendix, the accuracy of the proposed method is evaluated. The accuracy is performed in four steps;

- The torsion and warping constants obtained for girders with flat webs are compared to analytical values.
- The critical buckling moment calculated using the torsion and warping constant obtained using the proposed method is compared to the critical buckling moment from a linear buckling FE analysis of the same girder.
- The critical buckling moment is calculated, using the same torsion and warping constants as in the second step, but for a different length L_2 . The critical buckling moment is compared to that obtained from a linear buckling FE analysis of the girder with length L_2 .
- Finally, the torsion constant obtained using the proposed method is compared to that obtained from a static FE analysis of a the same girder subjected to uniform torsion, with no torsion or warping restraints at the boundaries.

APPENDIX D

Girder:	F1	F2	F3	F4
L [m]	10	8	12	15
b_f [mm]	180	200	150	200
t_f [mm]	12	20	10	15
h_w [mm]	700	900	500	700
t_w [mm]	8	8	6	8
a [mm]	-	-	-	-
b [mm]	-	-	-	-
d_max [mm]	-	-	-	-
φ [rad]	0,26344	0,05516	0,90036	0,27059
σ [Pa]	7,60E+07	2,97E+07	1,41E+08	4,90E+07
I_t Abaqus [m ⁴]	3,08E-07	1,44E-06	1,29E-07	5,30E-07
I_t LTBeam [m ⁴]	3,21E-07	1,52E-06	1,32E-07	5,50E-07
Ratio	0,96	0,94	0,97	0,96
I_w Abaqus [m ⁶]	1,41E-06	5,17E-06	3,46E-07	2,39E-06
I_w LTBeam [m ⁶]	1,48E-06	5,43E-06	3,52E-07	2,45E-06
Ratio	0,95	0,95	0,98	0,97

This is the first step of the verification of the method, where the torsion and warping constants are obtained for four different girders with flat webs. These constants are then compared to those calculated using the analytical software LTBeam.

Girder	C101	C102	C103	C104	C105
L1 [m]	9,5	9,5	9,5	15,2	15,2
L2 [m]	19	13,3	15,2	11,4	7,6
h_w [mm]	700	500	700	700	700
b_f [mm]	180	180	180	200	200
t_f [mm]	12	12	12	12	10
t_w [mm]	2	2	6	2	2
a [mm]	140	140	140	140	140
b [mm]	50	50	50	50	50
c [mm]	70,7	70,7	70,7	70,7	70,7
φ [rad]	0,27121	0,31816	0,22992	0,46226	0,72089
σ [Pa]	8,14E+07	8,20E+07	7,38E+07	7,39E+07	1,04E+08
I_t [m ⁴]	2,65E-07	2,66E-07	3,31E-07	2,96E-07	1,78E-07
I_w [m ⁶]	1,39E-06	7,23E-07	1,43E-06	1,95E-06	1,61E-06
M_cr_L1 [Nm]	119533	101039	126302	77120	58687
M_cr_L1 (FE) [Nm]	119400	99706	126360	76447	58593
Ratio	1,00	1,01	1,00	1,01	1,00
M_cr_L2 [Nm]	44368	64009	64345	118524	185756
M_cr_L2 (FE) [Nm]	44520	63646	64248	117410	185450
Ratio	1,00	1,01	1,00	1,01	1,00

General:	E [Pa]	2,10E+11
	G [Pa]	8,08E+10

This is the second and third step of the verification, where the critical buckling moment is calculated using the expression for the critical buckling moment with the torsion and warping constants obtained from the proposed method.

The torsion and warping constants is obtained for a girder of length L1, and are then used to calculate the critical buckling moments of two girders with the same 'cross-section', with length L1 and L2 respectively. These buckling moments are then compared to those obtained from linear buckling analyses in ABAQUS.

Shear modulus G 8,077E+10
 Torsional moment 1000

Comparison of I_t from proposed method to I_t obtained from a girder in uniform torsion

Girder	C101	C102	C103	C104	C105	106	107	C108
L [m]	9,5	9,5	9,5	9,5	19	19	19	19
b _f [mm]	200	240	280	320	350	350	350	350
t _f [mm]	12	12	12	12	12	12	12	24
h _w [mm]	700	700	700	700	500	700	900	900
t _w [mm]	2	2	2	2	2	2	2	2
a [mm]	140	140	140	140	140	140	140	140
b [mm]	50	50	50	50	50	50	50	50
d _{max} [mm]	25	25	25	25	25	25	25	25
Total rotation [rad]	0,41189	0,3517	0,3083	0,2755	0,4917	0,4936	0,49593	0,0739
I _t pure twist [m ⁴]	2,86E-07	3,34E-07	3,82E-07	4,27E-07	4,78E-07	4,77E-07	4,74E-07	3,18E-06
I _t cantilever [m ⁴]	2,93E-07	3,44E-07	3,91E-07	4,38E-07	4,85E-07	4,83E-07	4,81E-07	3,29E-06
Ratio	0,97	0,97	0,97	0,97	0,99	0,99	0,99	0,97

This is the fourth and final step of the verification, where the torsion constant obtained using the proposed method is compared to the torsion constant obtained from the simulation of the unrestrained girder.

APPENDIX D

E Verifications of FE models

In this appendix, the accuracy of the Finite Element models, described in chapter 6, are evaluated for girders with flat webs. They are verified by comparing to analytically calculated values of;

- Stresses
- Deflections
- Angular displacement
- Critical buckling moment

APPENDIX E

Girder	F1	F2	F3
Length [m]	10	8	14
h_m [mm]	700	708	700
t_w [mm]	8	8	8
b_f [mm]	180	160	180
t_f [mm]	12	8	12
Bending moment weak [Nm]	12500	8000	24500
Bending moment strong [Nm]	1000	1000	1000
Rotational moment [Nm]	1000	1000	1000
Moment of inertia, strong axis [m ⁴]	7,58E-04	5,57E-04	7,58E-04
Moment of inertia, weak axis [m ⁴]	1,17E-05	5,46E-06	1,17E-05
Rotational constant [m ⁴]	3,27E-07	1,75E-07	3,27E-07
Stress strong axis, Abaqus [MPa]	0,470	0,628	0,445
Stress strong axis, analytical [MPa]	0,46	0,64	0,46
Ratio	1,02	0,99	0,96
Deflection strong axis, Abaqus [mm]	0,079	0,068	0,154
Deflection strong axis, analytical [mm]	0,079	0,068	0,154
Ratio	1,00	1,00	1,00
Stress weak axis, Abaqus [MPa]	96,2	116,6	188,6
Stress weak axis, analytical [MPa]	96,5	117,2	189,0
Ratio	1,00	0,99	1,00
Deflection weak axis, Abaqus [mm]	53,1	46,29	203,8
Deflection weak axis, analytical [mm]	53,2	46,5	204,2
Ratio	1,00	1,00	1,00
Rotation, Abaqus (Free to warp)	0,40	0,57	0,55
Rotation, analytical	0,38	0,56	0,53
Ratio Abaqus free to analytical	1,05	1,01	1,04
Critical buckling load, Abaqus [Nm]	114670	79987	70935
Critical buckling load, LTBeam [Nm]	115950	80402	71143
Ratio	0,99	0,99	1,00

APPENDIX E

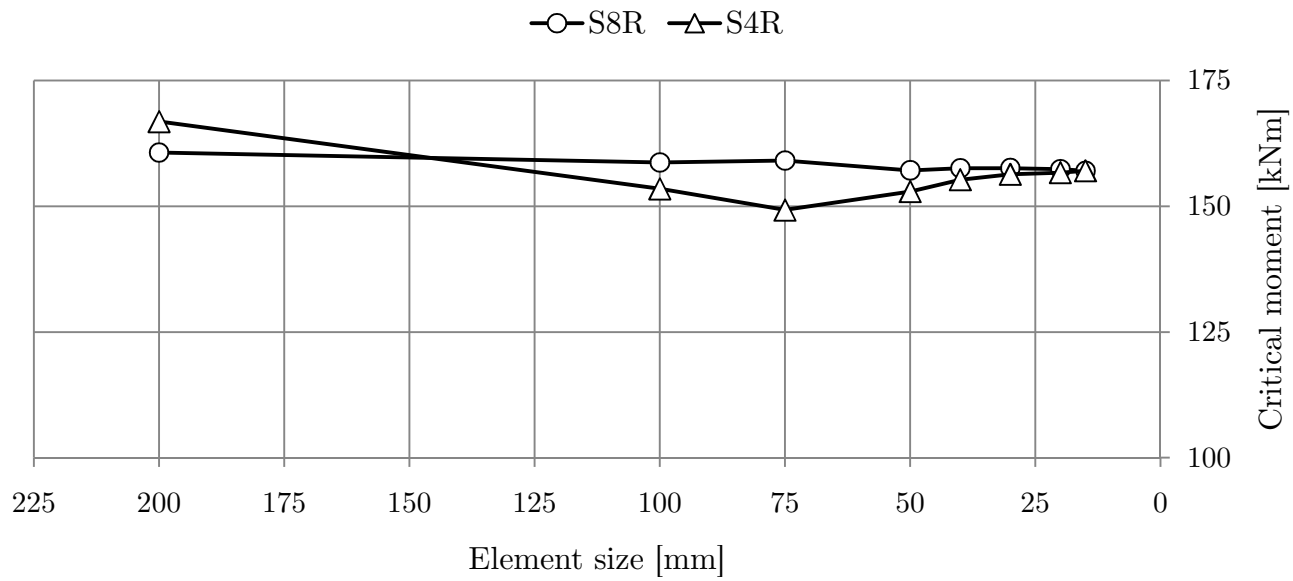
F Convergence studies

This is the convergence studies, where it is verified that the mesh densities and element types used are appropriate. Convergence of the results is checked for the linear buckling model and for the cantilever model.

APPENDIX F

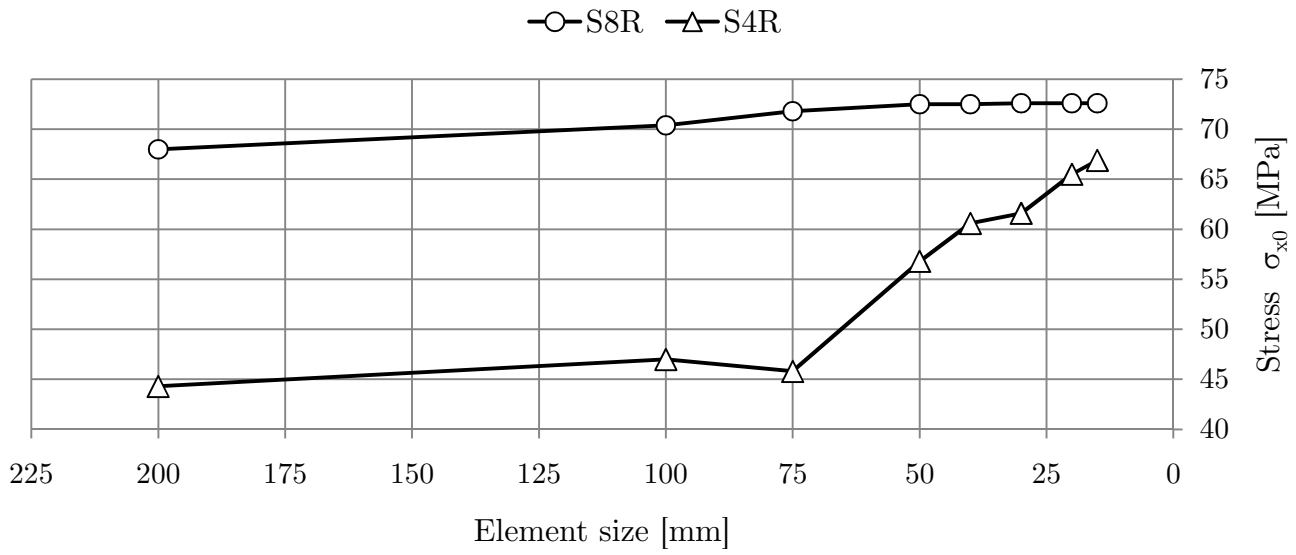
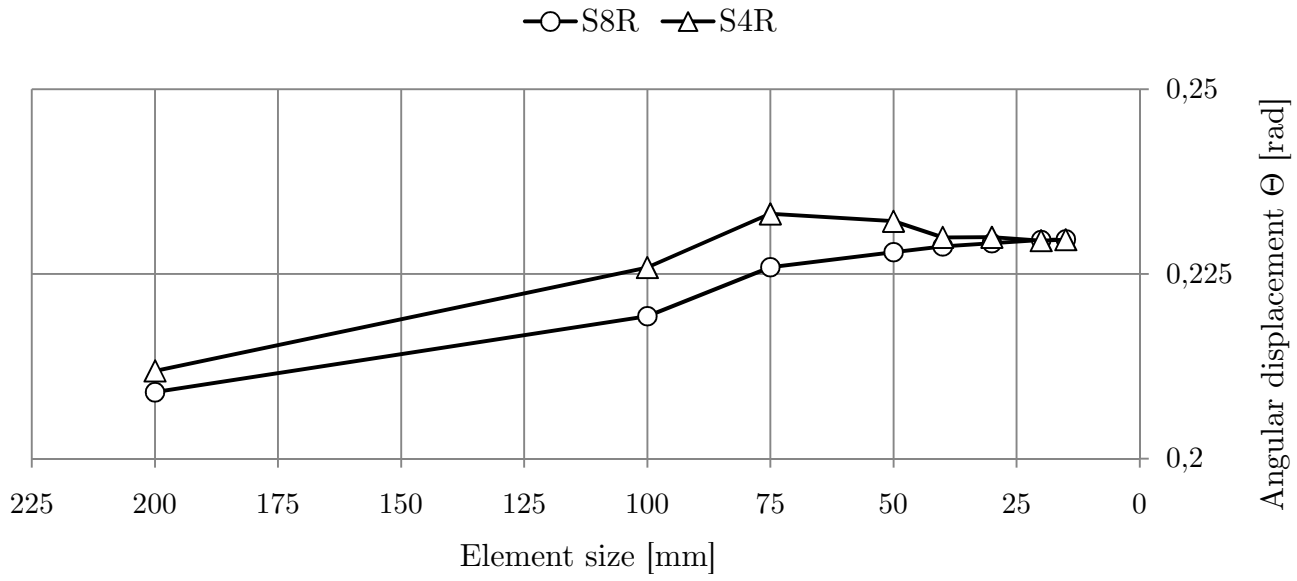
Convergence study for the linear buckling model

	Geometry							
	L [m]	b_f [mm]	t_f [mm]	h_w [mm]	t_w [mm]	a [mm]	b [mm]	d [mm]
	9,5	200	12	700	2	140	50	25
Element size [mm]	200	100	75	50	40	30	20	15
Elements per longitudinal panel	1	1	2	3	4	5	7	8
Elements per inclined panel	2	2	2	2	2	2	4	4
Critical buckling moment, S8R [kNm]	160,7	158,71	159,09	157,16	157,57	157,61	157,41	157,08
Critical buckling moment, S4R [kNm]	166,87	153,51	149,28	152,96	155,32	156,38	156,72	157,08



Convergence study for the cantilever model

	Geometry							
	L [m]	b_f [mm]	t_f [mm]	h_w [mm]	t_w [mm]	a [mm]	b [mm]	d [mm]
	9,5	200	12	700	2	140	50	25
Element size [mm]	200	100	75	50	40	30	20	15
Elements per longitudinal panel	1	1	2	3	4	5	7	8
Elements per inclined panel	2	2	2	2	2	2	4	4
Angle θ , S8R [rad]	0,20899	2,19E-01	2,26E-01	2,28E-01	2,29E-01	2,29E-01	2,30E-01	2,30E-01
Angle θ , S4R rad[]	0,21187	2,26E-01	2,33E-01	2,32E-01	2,30E-01	2,30E-01	2,29E-01	2,30E-01
Stress σ_{x0} , S8R [MPa]	68	70,4	71,8	72,5	72,5	72,6	72,6	72,6
Stress σ_{x0} , S4R [MPa]	44,3	47	45,8	56,8	60,6	61,6	65,5	66,9



APPENDIX F

G Parametric study

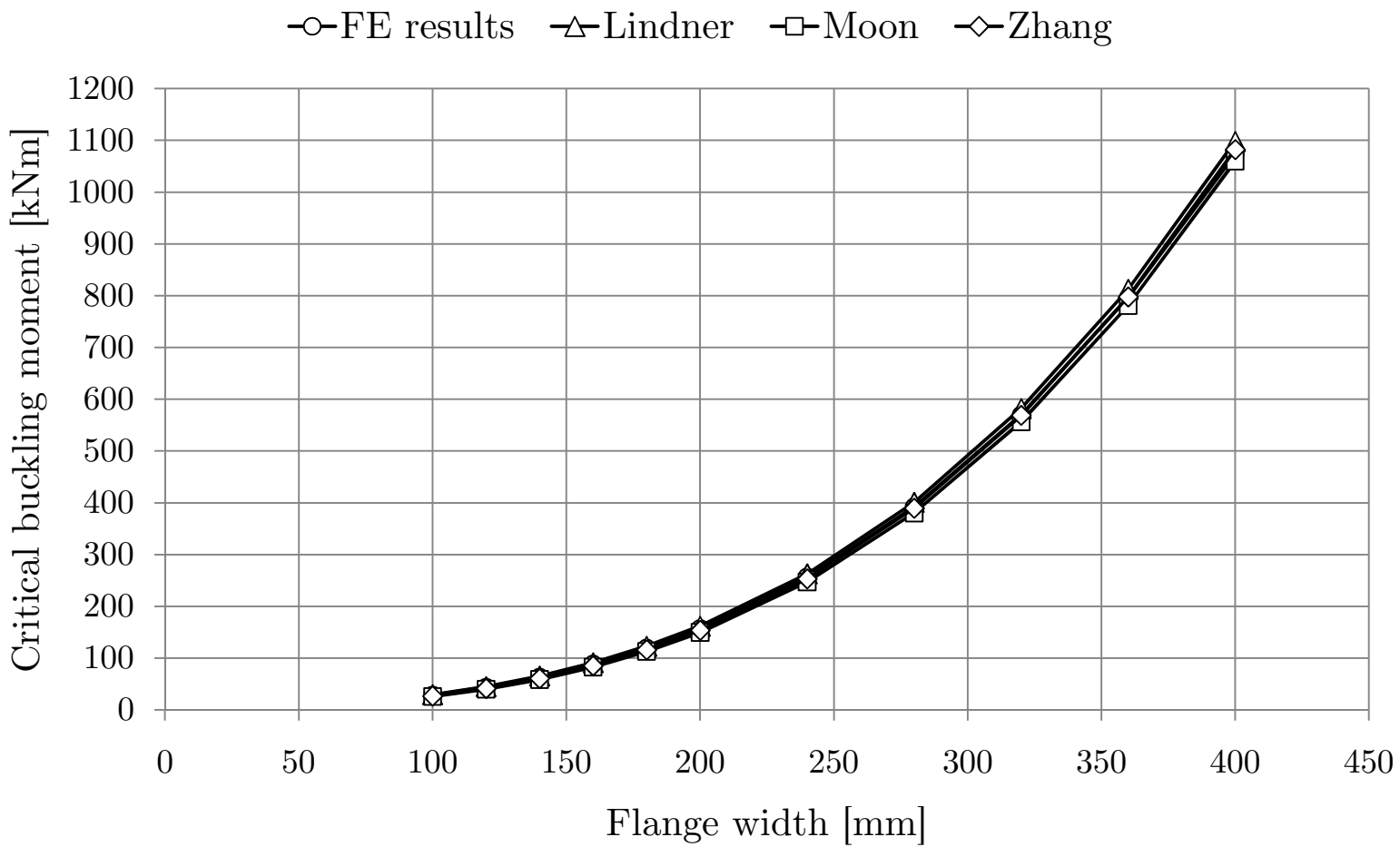
In this appendix, a parametric study is presented where influence of different geometrical parameters on the critical buckling moment is evaluated, as well as the accuracy of the different methods considered in this report. The parameters that are varied are;

- Flange width
- Flange thickness
- Web height
- Web thickness
- Girder length

APPENDIX G

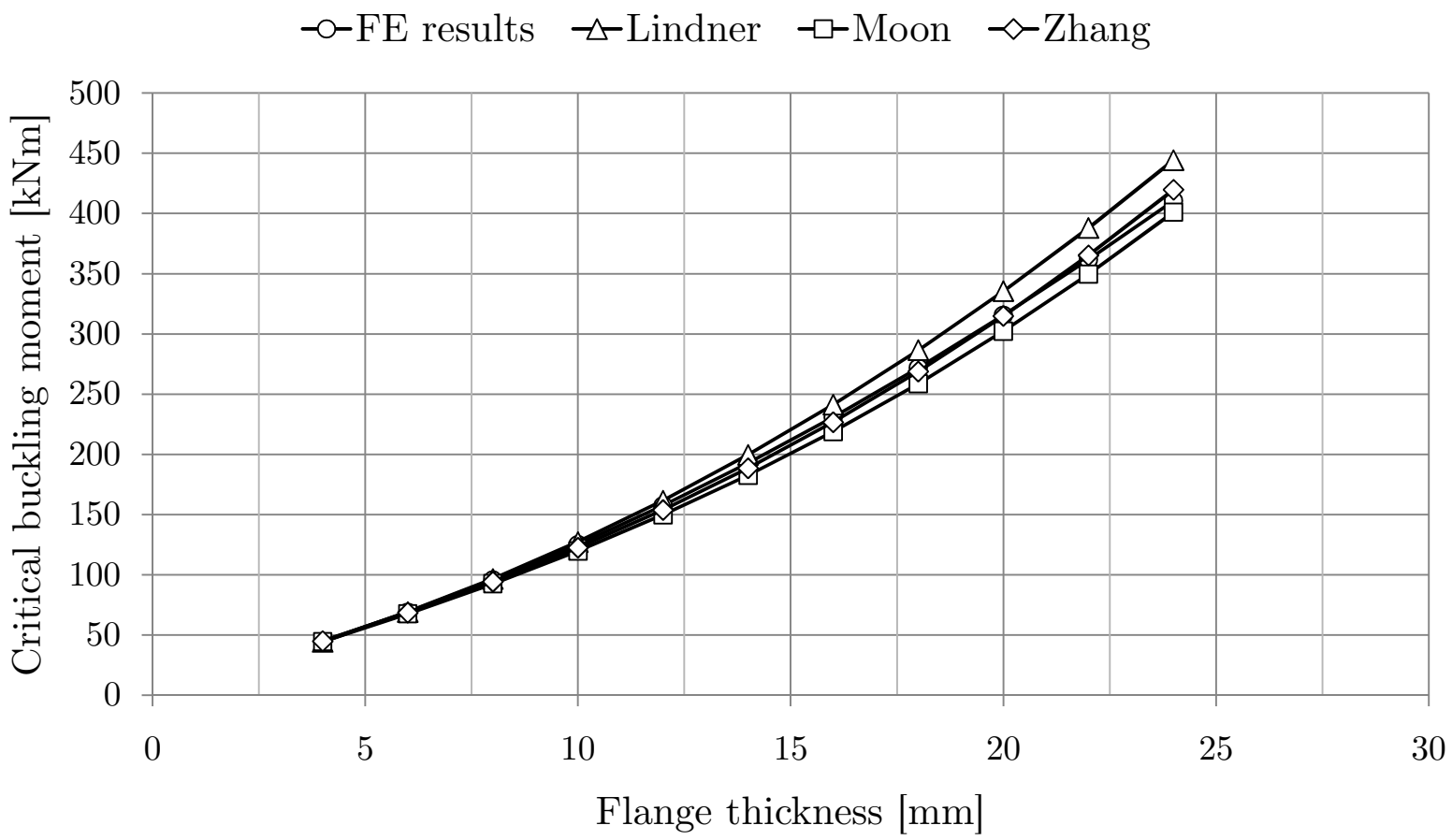
Varying flange width

Girder	C001	C002	C003	C004	C005	C006	C007	C008	C009	C010	C011
L [m]	9,5	9,5	9,5	9,5	9,5	9,5	9,5	9,5	9,5	9,5	9,5
b_f [mm]	100	120	140	160	180	200	240	280	320	360	400
t_f [mm]	12	12	12	12	12	12	12	12	12	12	12
h_w [mm]	700	700	700	700	700	700	700	700	700	700	700
t_w [mm]	2	2	2	2	2	2	2	2	2	2	2
a [mm]	140	140	140	140	140	140	140	140	140	140	140
b [mm]	50	50	50	50	50	50	50	50	50	50	50
d_max [mm]	25	25	25	25	25	25	25	25	25	25	25
M_cr_FEM [kNm]	28,559	43,726	63,705	88,469	119,31	157,45	256,83	392,42	569,94	795,91	1073,2
M_cr_Lindner [kNm]	30	45	65	91	123	162	263	401	582	812	1098
Ratio	1,04	1,03	1,03	1,03	1,03	1,03	1,02	1,02	1,02	1,02	1,02
M_cr_Moon [kNm]	26	40	59	83	113	150	247	380	556	781	1060
Ratio	0,91	0,92	0,92	0,94	0,95	0,95	0,96	0,97	0,98	0,98	0,99
M_cr_Zhang [kNm]	27	41	61	85	116	154	253	389	569	798	1082
Ratio	0,94	0,95	0,95	0,96	0,97	0,98	0,99	0,99	1,00	1,00	1,01



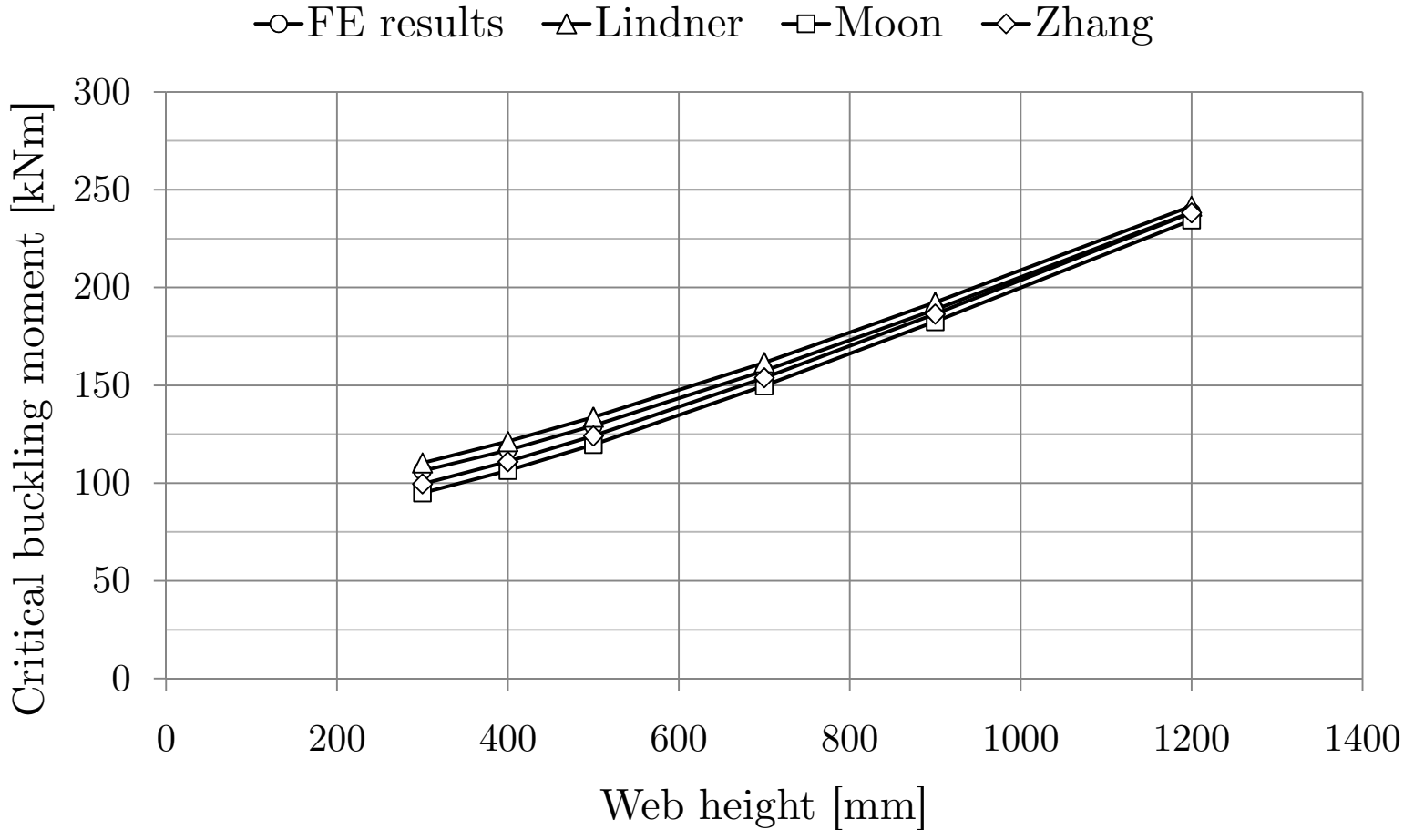
Varying flange thickness

Girder	C101	C102	C103	C104	C105	C106	C107	C108	C109	C110	C111
L [m]	9,5	9,5	9,5	9,5	9,5	9,5	9,5	9,5	9,5	9,5	9,5
b_f [mm]	200	200	200	200	200	200	200	200	200	200	200
t_f [mm]	4	6	8	10	12	14	16	18	20	22	24
h_w [mm]	700	700	700	700	700	700	700	700	700	700	700
t_w [mm]	2	2	2	2	2	2	2	2	2	2	2
a [mm]	140	140	140	140	140	140	140	140	140	140	140
b [mm]	50	50	50	50	50	50	50	50	50	50	50
d_max [mm]	25	25	25	25	25	25	25	25	25	25	25
M_cr_FEM [kNm]	44,561	68,929	95,66	125,11	157,45	192,72	230,88	271,84	315,51	361,75	410,48
M_cr_Lindner [kNm]	44	69	97	127	162	200	241	287	336	388	444
Ratio	1,00	1,00	1,01	1,02	1,03	1,04	1,05	1,05	1,06	1,07	1,08
M_cr_Moon [kNm]	45	68	93	120	150	183	219	259	302	350	401
Ratio	1,00	0,98	0,97	0,96	0,95	0,95	0,95	0,95	0,96	0,97	0,98
M_cr_Zhang [kNm]	45	69	94	123	154	189	227	269	315	365	420
Ratio	1,01	1,00	0,99	0,98	0,98	0,98	0,98	0,99	1,00	1,01	1,02



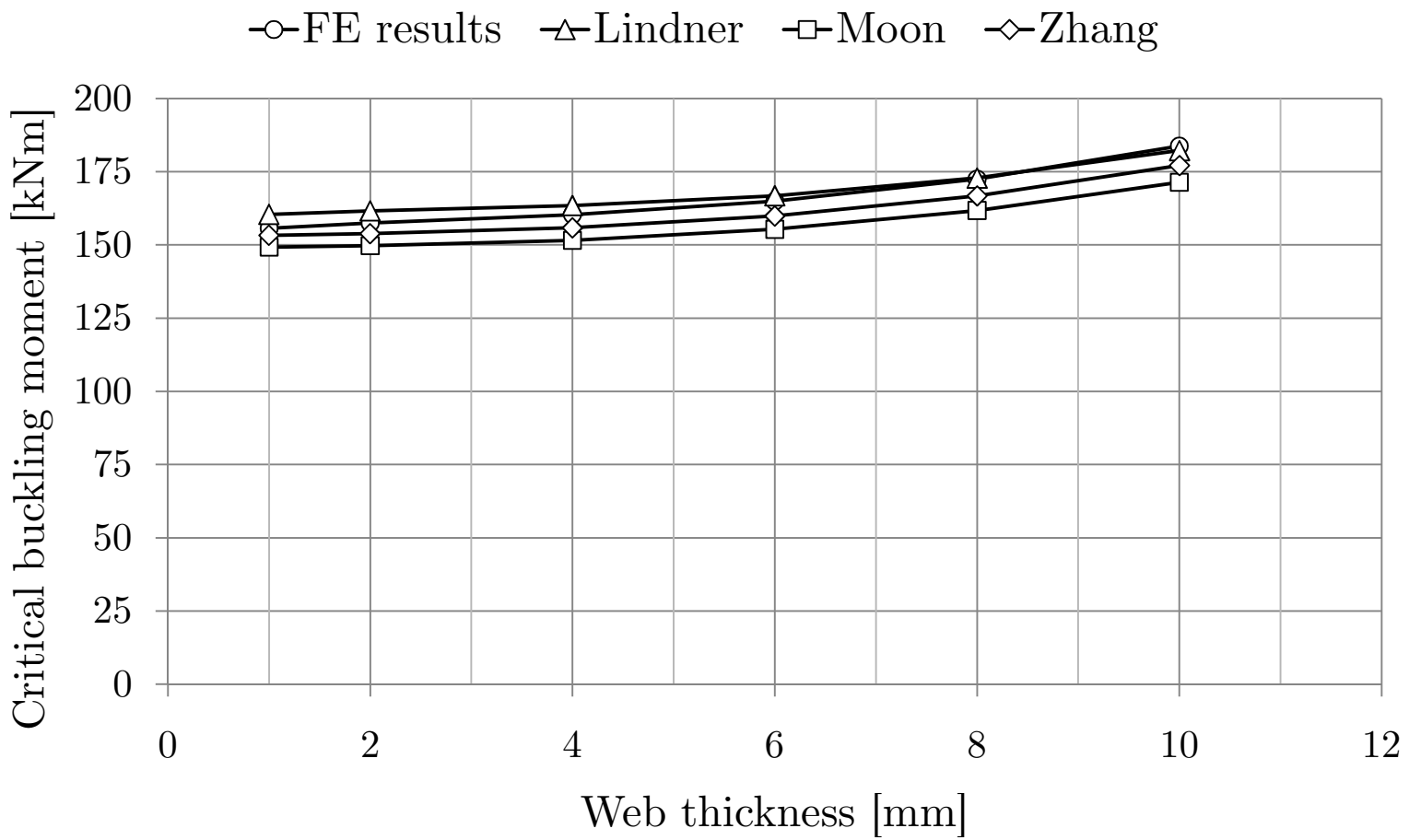
Varying web height

Girder	C201	C202	C203	C204	C205	C206
L [m]	9,5	9,5	9,5	9,5	9,5	9,5
b_f [mm]	200	200	200	200	200	200
t_f [mm]	12	12	12	12	12	12
h_w [mm]	300	400	500	700	900	1200
t_w [mm]	2	2	2	2	2	2
a [mm]	140	140	140	140	140	140
b [mm]	50	50	50	50	50	50
d_max [mm]	25	25	25	25	25	25
M_cr_FEM [kNm]	106,19	116,83	129,28	157,45	188,74	238,52
M_cr_Lindner [kNm]	110	121	134	162	192	242
Ratio	1,04	1,04	1,03	1,03	1,02	1,01
M_cr_Moon [kNm]	95	106	120	150	182,527	235
Ratio	0,89	0,91	0,93	0,95	0,97	0,98
M_cr_Zhang [kNm]	100	111	124	154	186	238
Ratio	0,94	0,95	0,96	0,98	0,99	1,00



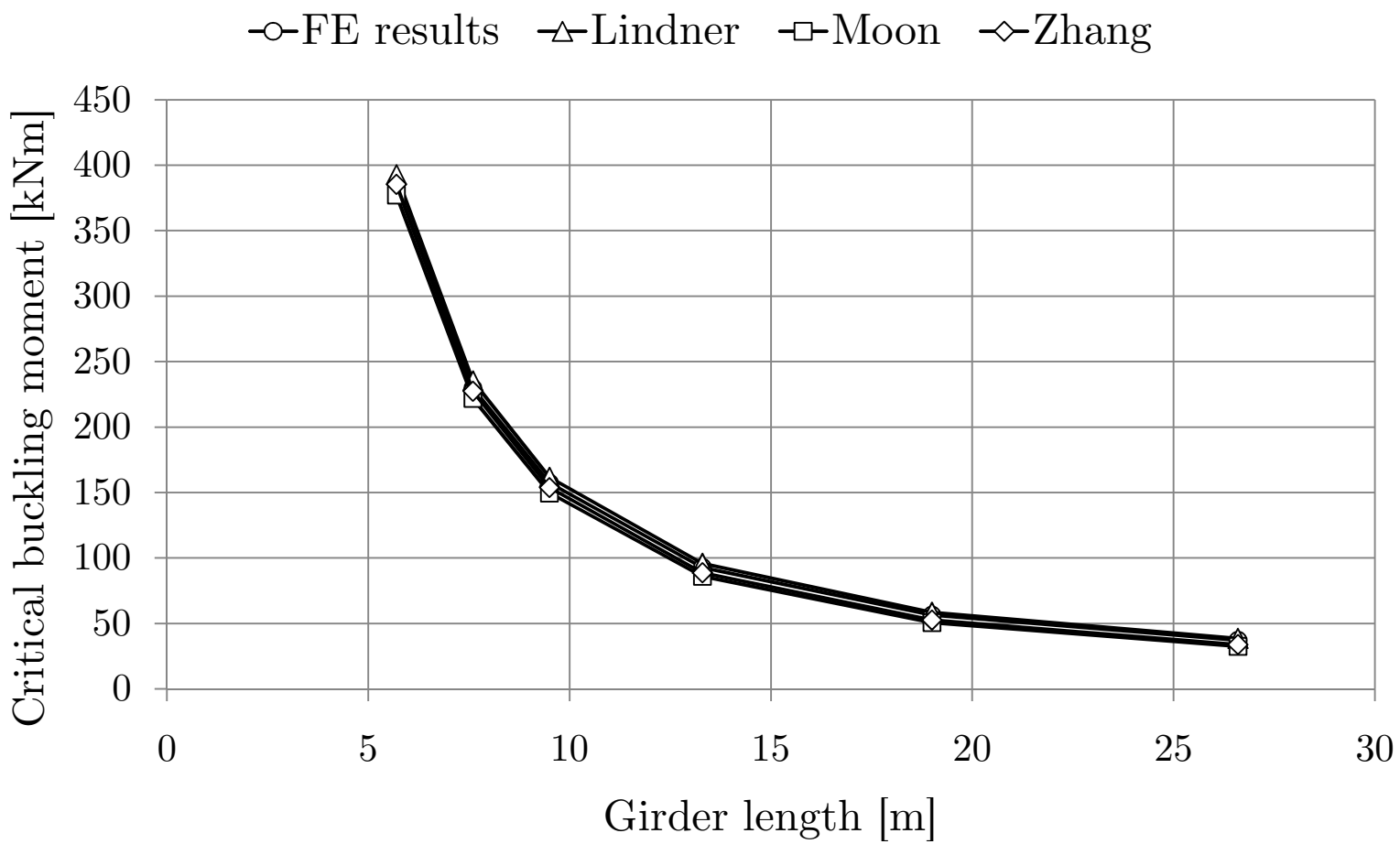
Varying web thickness

Girder	C301	C302	C303	C304	C305	C306
L [m]	9,5	9,5	9,5	9,5	9,5	9,5
b_f [mm]	200	200	200	200	200	200
t_f [mm]	12	12	12	12	12	12
h_w [mm]	700	700	700	700	700	700
t_w [mm]	1	2	4	6	8	10
a [mm]	140	140	140	140	140	140
b [mm]	50	50	50	50	50	50
d_max [mm]	25	25	25	25	25	25
M_cr_FEM [kNm]	155,7	157,45	160,34	164,91	172,46	183,74
M_cr_Lindner [kNm]	160	162	163	167	173	182
Ratio	1,03	1,03	1,02	1,01	1,00	0,99
M_cr_Moon [kNm]	149	150	152	155	162	171
Ratio	0,96	0,95	0,95	0,94	0,94	0,93
M_cr_Zhang [kNm]	153	154	156	160	167	177
Ratio	0,98	0,98	0,97	0,97	0,97	0,96



Varying length

Girder	C401	C402	C403	C404	C405	C406
L [m]	5,7	7,6	9,5	13,3	19	26,6
b_f [mm]	200	200	200	200	200	200
t_f [mm]	12	12	12	12	12	12
h_w [mm]	700	700	700	700	700	700
t_w [mm]	2	2	2	2	2	2
a [mm]	140	140	140	140	140	140
b [mm]	50	50	50	50	50	50
d_max [mm]	25	25	25	25	25	25
M_cr_FEM [kNm]	384,94	229,7	157,45	92,816	56,439	37,194
M_cr_Lindner [kNm]	393	235	162	96	59	39
Ratio	1,02	1,02	1,03	1,03	1,04	1,04
M_cr_Moon [kNm]	377	222	150	86	50,6559	32
Ratio	0,98	0,97	0,95	0,93	0,90	0,87
M_cr_Zhang [kNm]	385	227	154	89	53	34
Ratio	1,00	0,99	0,98	0,96	0,93	0,91



APPENDIX G

H Influence of girder length on the critical buckling moment

The accuracy of the different methods proposed in this report is evaluated for 3 different cross-section, for a wide range of girder lengths. A Mathcad document is also appended, with examples of how the sectional constants and critical buckling moments are calculated for the different methods.

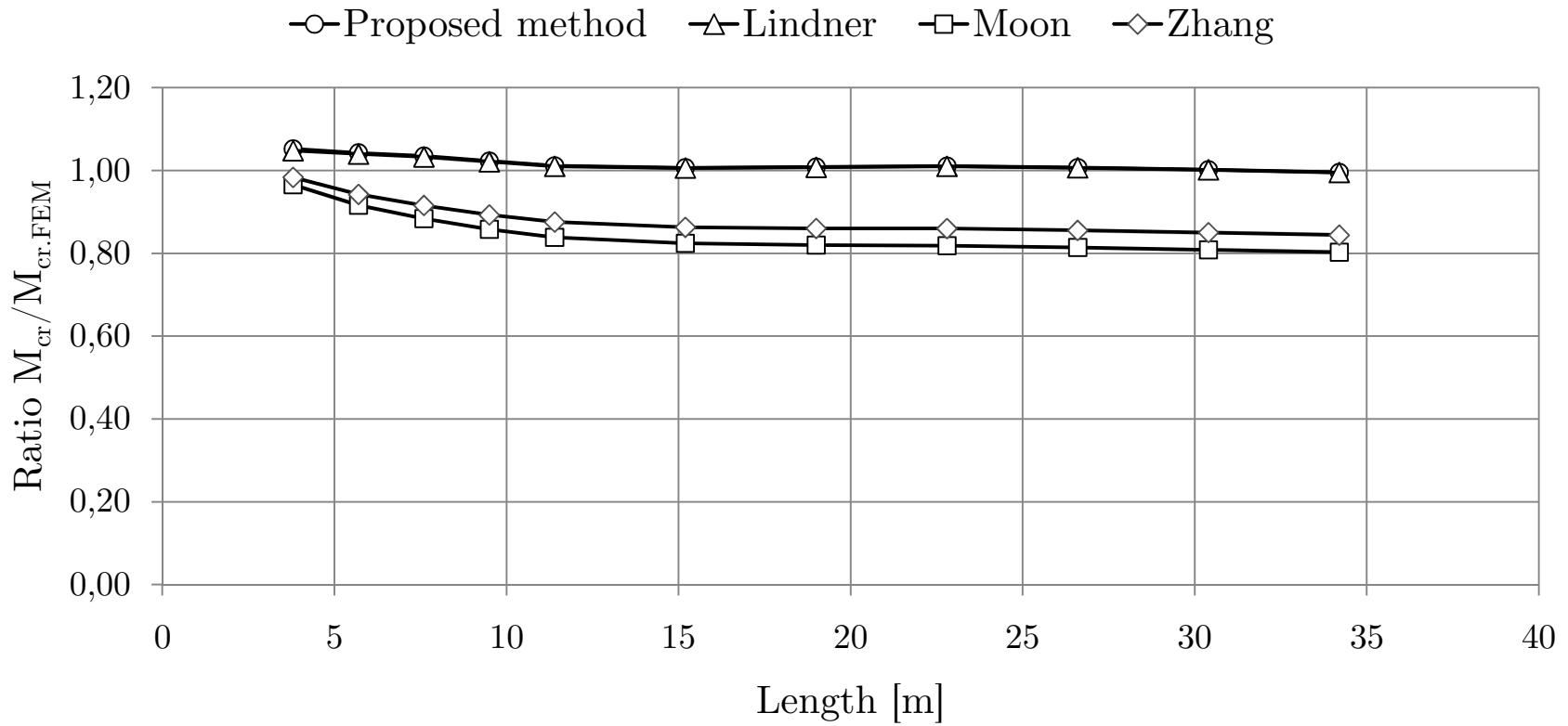
It is clear that the methods proposed by Moon et al. and Zhang et al. underestimate the capacity of long girders.

APPENDIX H

Web height 200 mm

L [m]	3,8	5,7	7,6	9,5	11,4	15,2	19	22,8	26,6	30,4	34,2
Corrugation periods	10	15	20	25	30	40	50	60	70	80	90
b_f [mm]	160	160	160	160	160	160	160	160	160	160	160
t_f [mm]	8	8	8	8	8	8	8	8	8	8	8
h_w [mm]	200	200	200	200	200	200	200	200	200	200	200
t_w [mm]	2	2	2	2	2	2	2	2	2	2	2
a [mm]	140	140	140	140	140	140	140	140	140	140	140
b [mm]	50	50	50	50	50	50	50	50	50	50	50
d_max [mm]	25	25	25	25	25	25	25	25	25	25	25
φ [rad]	-	-	-	-	-	-	-	-	-	-	5,26422
σ [Pa]	-	-	-	-	-	-	-	-	-	-	2,00E+08
M_cr_FEM [Nm]	1,00E+05	5,59E+04	3,88E+04	3,00E+04	2,46E+04	1,80E+04	1,42E+04	1,17E+04	1,00E+04	8,81E+03	7,86E+03
I_t [m^4]	7,72E-08										
I_w [m^6]	5,54E-08										
M_cr [Nm]	1,05E+05	5,83E+04	4,01E+04	3,07E+04	2,49E+04	1,82E+04	1,43E+04	1,19E+04	1,01E+04	8,83E+03	7,83E+03
Ratio	1,05	1,04	1,03	1,02	1,01	1,01	1,01	1,01	1,01	1,00	1,00
I_t_Lindner [m^4]	5,52E-08										
I_w_Lindner [m^6]	6,70E-08	8,25E-08	1,04E-07	1,321E-7	1,66E-07	2,53E-07	3,65E-07	5,01E-07	6,621E-7	8,48E-07	1,06E-06
M_cr_Lindner [Nm]	1,05E+05	5,82E+04	4,01E+04	3,06E+04	2,49E+04	1,82E+04	1,43E+04	1,19E+04	1,01E+04	8,82E+03	7,83E+03
Ratio	1,05	1,04	1,03	1,02	1,01	1,01	1,01	1,01	1,01	1,00	1,00
I_t_Moon [m^4]	5,52E-08										
I_w_Moon [m^6]	5,53E-08										
M_cr_Moon [Nm]	9,68E+04	5,13E+04	3,43E+04	2,57E+04	2,07E+04	1,49E+04	1,17E+04	9,61E+03	8,18E+03	7,12E+03	6,31E+03
Ratio	0,97	0,92	0,88	0,86	0,84	0,82	0,82	0,82	0,81	0,81	0,80

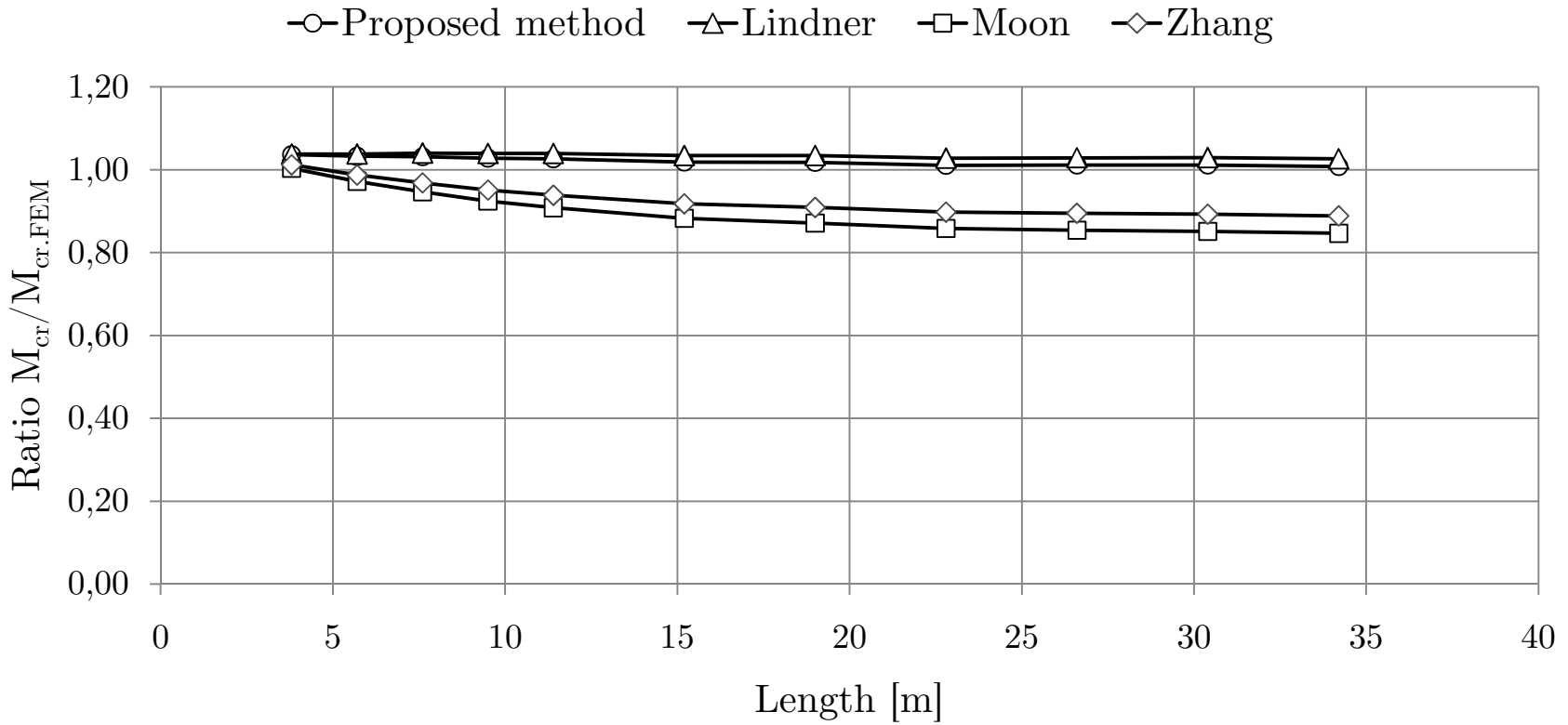
I_t _Zhang [m ⁴]	5,52E-08										
I_w _Zhang [m ⁶]	5,53E-08										
M_{cr} _Zhang [Nm]	9,86E+04	5,27E+04	3,55E+04	2,68E+04	2,16E+04	1,56E+04	1,22E+04	1,01E+04	8,59E+03	7,49E+03	6,64E+03
Ratio	0,98	0,94	0,92	0,89	0,88	0,86	0,86	0,86	0,86	0,85	0,84



Web height 400 mm

L [m]	3,8	5,7	7,6	9,5	11,4	15,2	19	22,8	26,6	30,4	34,2
Corrugation periods	10	15	20	25	30	40	50	60	70	80	90
b_f [mm]	200	200	200	200	200	200	200	200	200	200	200
t_f [mm]	12	12	12	12	12	12	12	12	12	12	12
h_w [mm]	400	400	400	400	400	400	400	400	400	400	400
t_w [mm]	2	2	2	2	2	2	2	2	2	2	2
a [mm]	140	140	140	140	140	140	140	140	140	140	140
b [mm]	50	50	50	50	50	50	50	50	50	50	50
d_max [mm]	25	25	25	25	25	25	25	25	25	25	25
φ [rad]	-	-	-	-	-	-	-	-	-	-	1,30615
σ [Pa]	-	-	-	-	-	-	-	-	-	-	7,36E+07
M_cr_FEM [Nm]	5,00E+05	2,50E+05	1,60E+05	1,17E+05	9,16E+04	6,46E+04	4,99E+04	4,10E+04	3,47E+04	3,01E+04	2,67E+04
I_t [m^4]	3,02E-07										
I_w [m^6]	6,44E-07										
M_cr [Nm]	5,18E+05	2,58E+05	1,65E+05	1,20E+05	9,40E+04	6,58E+04	5,08E+04	4,15E+04	3,51E+04	3,04E+04	2,69E+04
Ratio	1,04	1,03	1,03	1,03	1,03	1,02	1,02	1,01	1,01	1,01	1,01
I_t_Lindner [m^4]	2,32E-07										
I_w_Lindner [m^6]	6,86E-07	7,44E-07	8,25E-07	9,29E-07	1,06E-06	1,38E-06	1,79E-06	2,30E-06	2,90E-06	3,60E-06	4,38E-06
M_cr_Lindner [Nm]	5,19E+05	2,60E+05	1,67E+05	1,21E+05	9,52E+04	6,68E+04	5,16E+04	4,22E+04	3,57E+04	3,10E+04	2,74E+04
Ratio	1,04	1,04	1,04	1,04	1,04	1,03	1,03	1,03	1,03	1,03	1,03
I_t_Moon [m^4]	2,32E-07										
I_w_Moon [m^6]	6,45E-07										
M_cr_Moon [Nm]	5,01E+05	2,43E+05	1,52E+05	1,08E+05	8,32E+04	5,70E+04	4,35E+04	3,52E+04	2,96E+04	2,56E+04	2,26E+04
Ratio	1,00	0,97	0,95	0,92	0,91	0,88	0,87	0,86	0,85	0,85	0,85

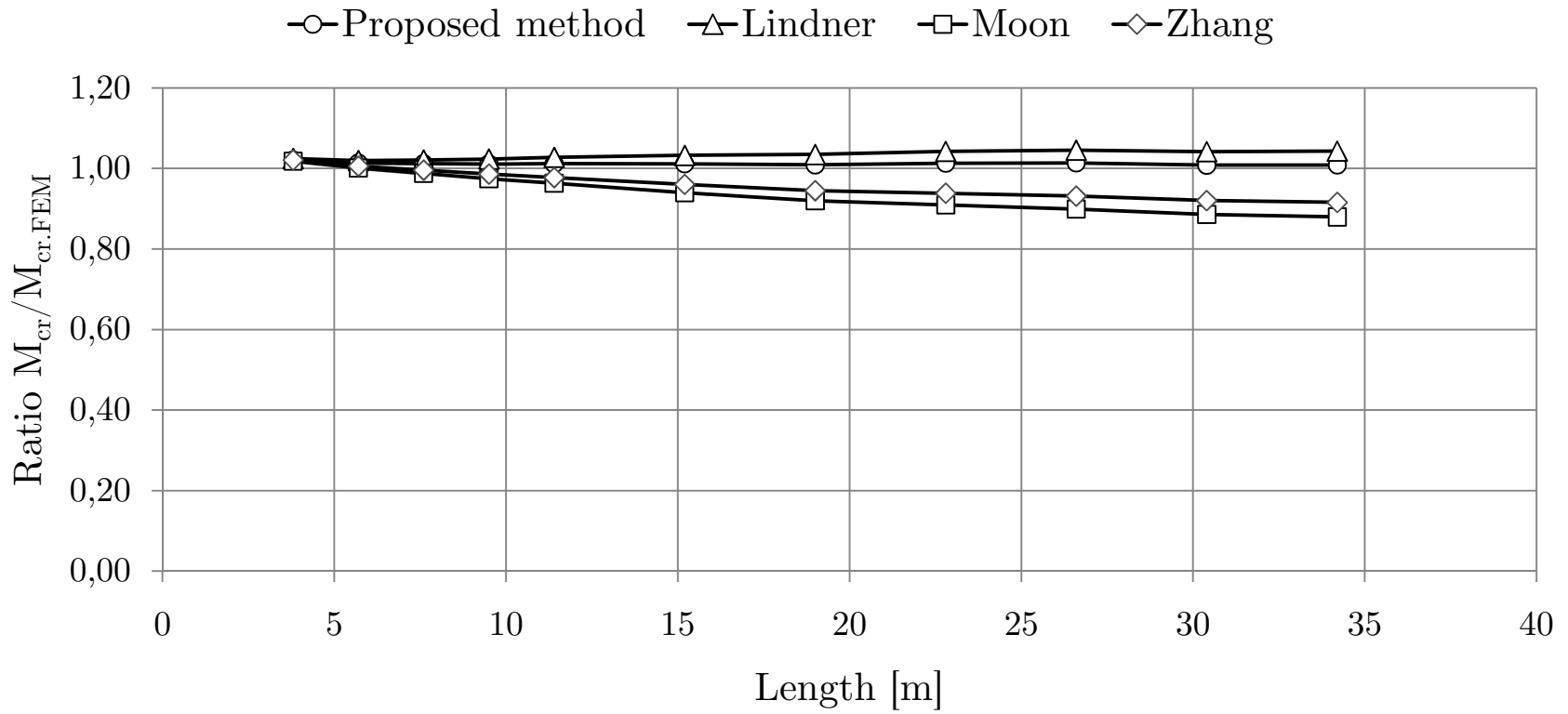
I_t_Zhang [m^4]	2,32E-07	2,32E-08	2,32E-09	2,32E-10	2,32E-11	2,32E-12	2,32E-13	2,32E-14	2,32E-15	2,32E-16	2,32E-17
I_w_Zhang [m^6]	6,46E-07	6,46E-08	6,46E-09	6,46E-10	6,46E-11	6,46E-12	6,46E-13	6,46E-14	6,46E-15	6,46E-16	6,46E-17
M_cr_Zhang [Nm]	5,06E+05	2,47E+05	1,55E+05	1,11E+05	8,60E+04	5,93E+04	4,54E+04	3,68E+04	3,11E+04	2,69E+04	2,37E+04
Ratio	1,01	0,99	0,97	0,95	0,94	0,92	0,91	0,90	0,89	0,89	0,89



Web height 700 mm

L [m]	3,8	5,7	7,6	9,5	11,4	15,2	19	22,8	26,6	30,4	34,2
Corrugation periods	10	15	20	25	30	40	50	60	70	80	90
b_f [mm]	240	240	240	240	240	240	240	240	240	240	240
t_f [mm]	12	12	12	12	12	12	12	12	12	12	12
h_w [mm]	700	700	700	700	700	700	700	700	700	700	700
t_w [mm]	2	2	2	2	2	2	2	2	2	2	2
a [mm]	140	140	140	140	140	140	140	140	140	140	140
b [mm]	50	50	50	50	50	50	50	50	50	50	50
d_max [mm]	25	25	25	25	25	25	25	25	25	25	25
φ [rad]	-	-	-	-	-	-	-	-	-	-	1,02154
σ [Pa]	-	-	-	-	-	-	-	-	-	-	6,18E+07
M_cr_FEM [Nm]	1,40E+06	6,47E+05	3,81E+05	2,57E+05	1,88E+05	1,20E+05	8,65E+04	6,72E+04	5,51E+04	4,70E+04	4,08E+04
I_t [m^4]	3,54E-07										
I_w [m^6]	3,38E-06										
M_cr [Nm]	1,43E+06	6,56E+05	3,86E+05	2,60E+05	1,91E+05	1,21E+05	8,73E+04	6,81E+04	5,58E+04	4,74E+04	4,12E+04
Ratio	1,02	1,01	1,01	1,01	1,01	1,01	1,01	1,01	1,01	1,01	1,01
I_t_Lindner [m^4]	2,78E-07										
I_w_Lindner [m^6]	3,45E-06	3,52E-06	3,625E-6	3,76E-06	3,92E-06	4,34E-06	4,34E-06	5,53E-06	6,31E-06	7,20E-06	8,21E-06
M_cr_Lindner [Nm]	1,43E+06	6,60E+05	3,89E+05	2,63E+05	1,94E+05	1,23E+05	8,95E+04	7,01E+04	5,76E+04	4,89E+04	4,26E+04
Ratio	1,02	1,02	1,02	1,02	1,03	1,03	1,03	1,04	1,05	1,04	1,04
I_t_Moon [m^4]	2,78E-07										
I_w_Moon [m^6]	3,41E-06										
M_cr_Moon [Nm]	1,42E+06	6,48E+05	3,76E+05	2,50E+05	1,82E+05	1,12E+05	7,96E+04	6,11E+04	4,95E+04	4,16E+04	3,59E+04
Ratio	1,02	1,00	0,99	0,97	0,96	0,94	0,92	0,91	0,90	0,89	0,88

I_t_Zhang [m^4]	2,78E-07	2,78E-08	2,78E-09	2,78E-10	2,78E-11	2,78E-12	2,78E-13	2,78E-14	2,78E-15	2,78E-16	2,78E-17
I_w_Zhang [m^6]	3,42E-06	3,42E-07	3,42E-08	3,42E-09	3,42E-10	3,42E-11	3,42E-12	3,42E-13	3,42E-14	3,42E-15	3,42E-16
M_cr_Zhang [Nm]	1,43E+06	6,51E+05	3,79E+05	2,53E+05	1,84E+05	1,15E+05	8,17E+04	6,31E+04	5,13E+04	4,32E+04	3,74E+04
Ratio	1,02	1,01	1,00	0,99	0,98	0,96	0,94	0,94	0,93	0,92	0,92



Comparison of warping and torsion constants given by the proposed method and by the methods presented in previous research

Web height 200 mm

I _t mod Lindner [m ⁴]	7,72E-08
I _t [m ⁴]	7,72E-08
Ratio	1,00

I _t Moon [m ⁴]	5,52E-08
I _t [m ⁴]	7,72E-08
Ratio	0,71

I _t Zhang [m ⁴]	5,52E-08
I _t [m ⁴]	7,72E-08
Ratio	0,71

I _w mod Lindner [m ⁶]	5,46E-08
I _w [m ⁶]	5,54E-08
Ratio	0,99

I _w Moon [m ⁶]	5,53E-08
I _w [m ⁶]	5,54E-08
Ratio	1,00

I _w Zhang [m ⁶]	5,53E-08
I _w [m ⁶]	5,54E-08
Ratio	1,00

Web height 400 mm

I _t mod Lindner [m ⁴]	3,14E-07
I _t [m ⁴]	3,02E-07
Ratio	1,04

I _t Moon [m ⁴]	2,32E-07
I _t [m ⁴]	3,02E-07
Ratio	0,77

I _t Zhang [m ⁴]	2,32E-07
I _t [m ⁴]	3,02E-07
Ratio	0,77

I _w mod Lindner [m ⁶]	6,40E-07
I _w [m ⁶]	6,44E-07
Ratio	0,99

I _w Moon [m ⁶]	6,45E-07
I _w [m ⁶]	6,44E-07
Ratio	1,00

I _w Zhang [m ⁶]	6,46E-07
I _w [m ⁶]	6,44E-07
Ratio	1,00

Web height 700 mm

I _t mod Lindner [m ⁴]	3,84E-07
I _t [m ⁴]	3,54E-07
Ratio	1,08

I _t Moon [m ⁴]	2,78E-07
I _t [m ⁴]	3,54E-07
Ratio	0,79

I _t Zhang [m ⁴]	2,78E-07
I _t [m ⁴]	3,54E-07
Ratio	0,78

I _w mod Lindner [m ⁶]	3,39E-06
I _w [m ⁶]	3,38E-06
Ratio	1,00

I _w Moon [m ⁶]	3,41E-06
I _w [m ⁶]	3,38E-06
Ratio	1,01

I _w Zhang [m ⁶]	3,42E-06
I _w [m ⁶]	3,38E-06
Ratio	1,01

APPENDIX H

Example of how the critical buckling moments as well as torsion and warping constants are calculated using the different methods. This is performed for profile 1 defined in table 7.2.

General properties

Material properties

$$E := 210 \cdot \text{GPa} \quad \nu := 0.3$$

$$G := \frac{E}{2(1 + \nu)} = 80.769 \cdot \text{GPa}$$

$$f_y := 355 \text{MPa}$$

Load

$$Q := 1000 \text{N} \cdot \text{m}$$

**Cross-sectional constants for the approach suggested in this report, $L = 34.2$ m,
 $h_w = 200$ mm**

Geometry

$$L := 34.2\text{m}$$

$$h_w := 200\text{mm}$$

$$t_w := 2\text{mm}$$

$$b_f := 160\text{mm}$$

$$t_f := 8\text{mm}$$

$$r := \frac{b_f}{t_f} = 20$$

Bending resistance flange

$$W_f := \frac{t_f \cdot b_f^2}{6}$$

Moment of inertia weak axis

$$I_z := \frac{t_f \cdot b_f^3}{6} = 5.461 \times 10^{-6} \text{m}^4$$

Input from Abaqus

$$dy := 0.526422\text{m} \quad \varphi := \frac{2dy}{h_w} = 5.26422$$

$$\sigma_x := 200\text{MPa}$$

Moment in flange

$$M_f := \sigma_x \cdot W_f = 6.827 \cdot \text{kN} \cdot \text{m}$$

$$a := \frac{M_f \cdot h_w}{Q} = 1.365\text{m}$$

$$I_{t,FE} := \frac{Q}{G \cdot \varphi} \cdot (L - a) = 7.72241 \times 10^{-8} \text{m}^4 \quad I_{w,FE} := \frac{G \cdot I_{t,FE}}{E} \cdot a^2 = 5.53677 \times 10^{-8} \cdot \text{m}^6$$

Control of L/a-ratio

$$\tanh\left(\frac{L}{a}\right) = 1$$

Cross-sectional constants according to Moon, $h_w = 200\text{mm}$

Corrugation profile

$a := 140\text{mm}$

$b := 50\text{mm}$

$d_{\max} := 25\text{mm}$

$c := \sqrt{(2 \cdot d_{\max})^2 + b^2} = 70.7 \cdot \text{mm}$

$\overrightarrow{q} := (2a + 2b) = 0.38 \text{ m}$

One period of the corrugation

$d_{\text{avg}} := \frac{(2a + b)d_{\max}}{2(a + b)} = 21.711 \cdot \text{mm}$

Calculating warping and torsional constants

$$W_n := \begin{bmatrix} \frac{2 \cdot b_f^2 h_w \cdot t_f + b_f \cdot h_w^2 \cdot t_w}{8 \cdot b_f \cdot t_f + 4 \cdot h_w \cdot t_w} \\ \frac{2b_f^2 \cdot h_w \cdot t_f + b_f \cdot h_w^2 \cdot t_w}{8b_f \cdot t_f + 4 \cdot h_w \cdot t_w} - \left(\frac{b_f}{4} - \frac{d_{\text{avg}}}{2} \right) \cdot h_w \\ \frac{2b_f^2 \cdot h_w \cdot t_f + b_f \cdot h_w^2 \cdot t_w}{8b_f \cdot t_f + 4 \cdot h_w \cdot t_w} - \left(\frac{b_f}{4} + \frac{d_{\text{avg}}}{2} \right) \cdot h_w \\ \frac{2 \cdot b_f^2 h_w \cdot t_f + b_f \cdot h_w^2 \cdot t_w}{8 \cdot b_f \cdot t_f + 4 \cdot h_w \cdot t_w} - \frac{1}{2} \cdot b_f \cdot h_w \\ \frac{2 \cdot b_f^2 h_w \cdot t_f + b_f \cdot h_w^2 \cdot t_w}{8 \cdot b_f \cdot t_f + 4 \cdot h_w \cdot t_w} - \frac{1}{2} \cdot b_f \cdot h_w \\ \frac{2 \cdot b_f^2 h_w \cdot t_f + b_f \cdot h_w^2 \cdot t_w}{8 \cdot b_f \cdot t_f + 4 \cdot h_w \cdot t_w} \end{bmatrix} \quad L_n := \begin{pmatrix} \frac{b_f}{2} - d_{\text{avg}} \\ h_w + t_f \\ \frac{b_f}{2} - d_{\text{avg}} \\ \frac{b_f}{2} + d_{\text{avg}} \\ \frac{b_f}{2} + d_{\text{avg}} \end{pmatrix} \quad t_n := \begin{pmatrix} t_f \\ t_w \\ t_f \\ t_f \\ t_f \end{pmatrix}$$

$$C_w := \frac{1}{3} \cdot \left[\left[(W_{n_1})^2 + W_{n_1} \cdot W_{n_2} + (W_{n_2})^2 \right] \cdot L_{n_1} \cdot t_{n_1} + \left[(W_{n_2})^2 + W_{n_2} \cdot W_{n_3} + (W_{n_3})^2 \right] \cdot L_{n_2} \cdot t_{n_2} \dots \right. \\ \left. + \left[(W_{n_3})^2 + W_{n_3} \cdot W_{n_4} + (W_{n_4})^2 \right] \cdot L_{n_3} \cdot t_{n_3} + \left[(W_{n_4})^2 + W_{n_4} \cdot W_{n_5} + (W_{n_5})^2 \right] \cdot L_{n_4} \cdot t_{n_4} \dots \right. \\ \left. + \left[(W_{n_5})^2 + W_{n_5} \cdot W_{n_6} + (W_{n_6})^2 \right] \cdot L_{n_5} \cdot t_{n_5} \right]$$

$I_{w.M} := C_w = 5.527 \times 10^{-8} \text{ m}^6$

$I_{t.M} := \frac{1}{3} \cdot (h_w \cdot t_w^3 + 2 \cdot b_f \cdot t_f^3) = 5.515 \times 10^{-8} \text{ m}^4$

Modified shear modulus due to web corrugation

$\eta := \frac{a + b}{a + c} = 0.902$

$G_{co} := \eta \cdot G = 72.83 \cdot \text{GPa}$

Critical lateral-torsional buckling moment for the different approaches, $h_w = 200\text{mm}$

Defining the lengths of the girders in the parametric study

$$L_{ww} := \begin{pmatrix} 3.8 \\ 5.7 \\ 7.6 \\ 9.5 \\ 11.4 \\ 15.2 \\ 19 \\ 22.8 \\ 26.6 \\ 30.4 \\ 34.2 \end{pmatrix} \text{ m}$$

$$I_{t,FE} = 7.722 \times 10^{-8} \text{ m}^4$$

$$I_{w,FE} = 5.537 \times 10^{-8} \text{ m}^6$$

Critical moment for the approach suggested in this report

$$M_{cr,FE} := \left(\frac{\pi^2 \cdot E \cdot I_z}{L^2} \cdot \sqrt{\frac{I_{w,FE}}{I_z} + \frac{L^2 \cdot G \cdot I_{t,FE}}{\pi^2 \cdot E \cdot I_z}} \right) = \begin{array}{|c|c|} \hline & 1 \\ \hline 1 & 105.446 \\ \hline 2 & 58.34 \\ \hline 3 & 40.146 \\ \hline 4 & 30.688 \\ \hline 5 & 24.903 \\ \hline 6 & 18.164 \\ \hline 7 & 14.337 \\ \hline 8 & 11.858 \\ \hline 9 & 10.118 \\ \hline 10 & 8.827 \\ \hline 11 & 7.83 \\ \hline \end{array} \cdot \text{kN} \cdot \text{m}$$

Critical moment for the approach suggested by Moon

$$W := \frac{\pi}{L} \cdot \sqrt{\frac{E \cdot I_{w,M}}{G_{co} \cdot I_{t,M}}}$$

$$M_{cr,M} := \left(\frac{\pi}{L} \cdot \sqrt{E \cdot I_z \cdot G_{co} \cdot I_{t,M} \cdot \sqrt{1 + W^2}} \right) = \text{ kN} \cdot \text{ m}$$

	1
1	96.781
2	51.26
3	34.289
4	25.747
5	20.654
6	14.868
7	11.657
8	9.605
9	8.176
10	7.121
11	6.31

Lindner and modified Lindner

$$I_{y1} := \frac{b_f \cdot t_f^3}{12}$$

Second moment of area for the top flange, strong axis

$$I_{y2} := I_{y1}$$

Second moment of area for the bottom flange, strong axis

$$I_t := \frac{1}{3} \cdot \left(h_w \cdot t_w^3 + 2 \cdot b_f \cdot t_f^3 \right) = 5.515 \times 10^{-8} \text{ m}^4$$

$$I_w := \frac{t_f \cdot b_f^3 \cdot h_w^2}{24}$$

Expression for a girder with flat web

$$\beta := \left[\frac{h_w}{2 \cdot G \cdot a \cdot t_w} + \frac{h_w^2 \cdot (a + b)^3 \cdot (I_{y1} + I_{y2})}{600 \cdot a^2 \cdot E \cdot (I_{y1} \cdot I_{y2})} \right]$$

$$c_w := \frac{(2 \cdot d_{max})^2 \cdot h_w^2}{8 \cdot \beta \cdot (a + b)}$$

$$I_{w.L} := I_w + c_w \cdot \frac{L^2}{E \cdot \pi^2} = \begin{array}{|c|c|} \hline & 1 \\ \hline 1 & 6.701 \cdot 10^{-8} \\ \hline 2 & 8.251 \cdot 10^{-8} \\ \hline 3 & 1.042 \cdot 10^{-7} \\ \hline 4 & 1.321 \cdot 10^{-7} \\ \hline 5 & 1.662 \cdot 10^{-7} \\ \hline 6 & 2.53 \cdot 10^{-7} \\ \hline 7 & 3.646 \cdot 10^{-7} \\ \hline 8 & 5.01 \cdot 10^{-7} \\ \hline 9 & 6.621 \cdot 10^{-7} \\ \hline 10 & 8.481 \cdot 10^{-7} \\ \hline 11 & 1.059 \cdot 10^{-6} \\ \hline \end{array} \text{m}^6$$

$$M_{cr.L} := \left[\frac{\pi^2 \cdot E \cdot I_z}{L^2} \cdot \sqrt{\frac{I_w}{I_z} + \frac{L^2}{\pi^2 \cdot E \cdot I_z} \cdot (c_w + G \cdot I_t)} \right] = \begin{array}{|c|c|} \hline & 1 \\ \hline 1 & 105.03 \\ \hline 2 & 58.185 \\ \hline 3 & 40.071 \\ \hline 4 & 30.645 \\ \hline 5 & 24.876 \\ \hline 6 & 18.15 \\ \hline 7 & 14.328 \\ \hline 8 & 11.852 \\ \hline 9 & 10.114 \\ \hline 10 & 8.823 \\ \hline 11 & 7.827 \\ \hline \end{array} \cdot \text{kN} \cdot \text{m}$$

$$I_{t.L.mod} := \left(I_t + \frac{c_w}{G} \right) = 7.718 \times 10^{-8} \text{m}^4$$

$$I_{w.L.mod} := I_w = 5.461 \times 10^{-8} \text{m}^6$$

Zhang et al.

$$I_t = 5.515 \times 10^{-8} \text{ m}^4$$

$$I_{w,Z} := \left[\frac{t_f \cdot b_f^3 \cdot h_w^2}{24} + \frac{t_w \cdot h_w^3 \cdot (2d_{\max})^2}{12} \cdot \frac{a + \frac{b}{3}}{2q} \right] = 5.53 \times 10^{-8} \text{ m}^6$$

$$M_{cr,Z} := \left[\frac{\pi^2 \cdot E \cdot I_z}{L^2} \cdot \left(\sqrt{\frac{I_{w,Z}}{I_z} + \frac{L^2 \cdot G \cdot I_t}{\pi^2 \cdot E \cdot I_z}} \right) \right] = \text{Table} \cdot \text{kN} \cdot \text{m}$$

	1
1	98.557
2	52.734
3	35.521
4	26.794
5	21.558
6	15.573
7	12.232
8	10.089
9	8.593
10	7.488
11	6.637

APPENDIX H

I Different corrugation profiles evaluated using the modified Lindner method

In this appendix, the accuracy of the modified Lindner method is evaluated for different corrugation profiles.

APPENDIX I

Corrugation profile	4b	5b	6b	4a	5a	6a
L [m]	24	24	24,32	9,5	9,5	9,6
b_f [mm]	200	200	200	200	200	200
t_f [mm]	12	12	12	12	12	12
h_w [mm]	400	400	400	400	400	400
t_w [mm]	2	2	2	2	2	2
a [mm]	70	140	140	70	140	140
b [mm]	50	100	50	50	100	50
d_max [mm]	25	25	10	25	25	10
φ [rad]	0,816	1,001	1,163	-	-	-
σ [Pa]	7,04E+07	7,84E+07	8,40E+07	-	-	-
M_cr_FEM [Nm]	4,06E+04	3,64E+04	3,35E+04	1,19E+05	1,09E+05	1,06E+05
I_t [m^4]	3,30E-07	2,66E-07	2,30E-07	-	-	-
I_w [m^6]	6,44E-07	6,44E-07	6,40E-07	-	-	-
M_cr [Nm]	4,08E+04	3,70E+04	3,42E+04	1,22E+05	1,14E+05	1,11E+05
Ratio	1,01	1,02	1,02	1,02	1,04	1,04
I_t_Lindner [m^4]	3,37E-07	2,68E-07	2,45E-07	-	-	-
I_w_Lindner [m^6]	6,40E-07	6,40E-07	6,40E-07	-	-	-
M_cr_Lindner [Nm]	4,12E+04	3,71E+04	3,51E+04	1,22E+05	1,14E+05	1,13E+05
Ratio	1,02	1,02	1,05	1,03	1,04	1,06
I_t_Lindner [m^4]	3,37E-07	2,68E-07	2,45E-07			
I_t [m^4]	3,30E-07	2,66E-07	2,30E-07			
Ratio	1,02	1,01	1,06			
I_w_Lindner [m^6]	6,40E-07	6,40E-07	6,40E-07			
I_w [m^6]	6,44E-07	6,44E-07	6,40E-07			
Ratio	0,99	0,99	1,00			

Same geometry as the three girders to the left, only shorter. The critical buckling moment according to the proposed method M_{cr} and the critical buckling moment calculated using the modified Lindner method $M_{cr_Lindner}$ are based on the torsion and warping constants derived for the longer girders.